A Mechatronic System for Achieving Optimum Alignment of Lower Limb Prosthesis

by

Kian Sek TEE

Submitted in accordance with the requirements
for the degree of Doctor of Philosophy

The University of Leeds
School of Mechanical Engineering

November 2011

The candidate confirms that the work submitted is his own and that appropriate credit has been given where reference has been made to the work of others.

Abstract

Misalignment in the lower limb prosthesis can cause great discomfort in the stump-socket interface and disturbance to gait function. In the long run, it could deteriorate the musculoskeletal system. In practice, the assessment still depends heavily on the verbal feedback of an amputee and experiences of a prosthetist. Moreover it is inconsistent amongst the prosthetists.

Prosthetic alignment involves the adjustment of the prosthetic components relative to the gait quality. Some methods were proposed, including symmetry index, variation in a step-to-step transition, stability within the zone of integrated balance, matching roll-over shape (ROS) to an ideal ROS and etc. It is not clear if the optimum alignment could be achieved. These methods exhibit a few limitations, i.e. limited use of gait variables in a single comparison and non-uniform results when different gait variables are applied. There is a need to provide an objective assessment method that processes high dimensional gait variables and presents them in a simple form. In addition, it could be impractical and expensive clinically to spend excessive time on a patient. An ambulatory gait measurement system could achieve this objective to a certain extent.

This research investigates a potential engineering solution that is able to provide an assistive and objective assessment of the lower limb prosthetic alignment that provides optimal gait quality.

The effort includes a development of a low-cost ambulatory gait measurement system which could be reliably used during indoor and outdoor trials. Human walking trials using the designed ambulatory system are designed and performed to justify the proposed solution. A novel gait analysis method using Principle Component Analysis and Self-Organizing Feature Map is proposed to process high dimensional gait data into a simple plot and a decision guide. The proposed methodology could help to collect sufficient gait data during indoor and outdoor gaits and could provide an objective gait assessment during the application of lower limb prosthetic alignments.

Acknowledgement

I would like to thank the people who have helped me through my study and supported me all the way along the project.

Special thanks to Dr. D. Moser and Prof. S. Zahedi from Chas A Blatchford & Sons Ltd., whom have shown me the door of biomechanics especially lower limb prosthetics. Great thanks to my supervisor, Dr. A. Dehghani for guiding me with great patience throughout the period of the study.

I would like to thank my colleagues especially Mohammed Awad and Mojtapa Khazravi. Many thanks to all technical staffs in the School of Mechanical Engineering for their advices and supports, especially David Readman and Tony Wiese.

My greatest gratitude must forward to my financial support, University Tun Hussein Onn Malaysia.

I must thank my family especially my parent for continual love and support. Last but not least, my thanks to my beloved wife, Soon Chin Fhong and my daughter, Chloe Tee, for sharing the happiness and hardship together.

Content

List of Abbreviations

2D	2 Dimension
3D	3 Dimension
A/D	Analog to Digital
AK	Above Knee
AP	Anterior Posterior
ASYM	Asymmetry
BCOM	Body Centre of Mass
BK	Below Knee
BMB	Bisector of Medial Brim
BMU	Best Matching Unit
CA	Cronbach's Alpha
CAD	Computer Aided Design
CW	Clockwise
CCW	Counter Clockwise
COM	Centre of Mass
COP	Centre of Pressure
CSV	Comma-Separated Values
D/A	Digital to Analog
dof	Degree of Freedom
FO	Foot Off
FS	Foot Strike
FSR	Force Sensitive Resistor
GC	Gait Cycle
GCI	Gait Cycle Index
GRF	Ground Reaction Force
vGRF	Vertical Ground Reaction Force
HC	Heel Contact
HPF	High Pass Filter
HS	Heel Strike
IC	Initial Contact

IMU	Inertial Measurement Unit
ISw	Initial Swing
L.A.S.A.R.	Laser Assisted Static Alignment Reference
LiNo GC	Linear Interpolated Normalized Gait Cycle
LPF	Low Pass Filter
LR	Load Response
KAF	Knee, Ankle and Foot
MEMS	Micro-Electro-Mechanical Systems
MISO	Master In Slave Out
ML	Medial Lateral
MOSI	Master Out Slave In
MSt	Mid Stance
MSw	Mid Swing
PC	Principle Component
PCA	Principle Component Analysis
PCB	Printed Circuit Board
PSw	Pre-Swing
RHR	Right Hand Rule
RMS	Root Mean Square
ROS	Roll Over Shape
RSD	Relative Standard Deviation
SCLK	Serial Clock
RVCG	Rotational Vibratory Coriolis Gyroscope
s	Standard Deviation
SD	Secure Digital
SE	Standard Error
SOFM	Self-Organizing Feature Map
SPI	Serial Peripheral Interface
SS	Slave Select
TF	Transfemoral
TO	Toe Off
TSA	Total Sway Activity
TSt	Terminal Stance
TSw	Terminal Swing

TT	Transtibial
WBI	Weight-bearing Imbalance
ZPLP	Zero Phase Low Pass Filter

List of Figures

List of Tables

CHAPTER 1
INTRODUCTION

1.1 Background

Misalignment in lower limb prostheses could cause serious skin issues and damages to the musculoskeletal system if not corrected. Undesired pressure distribution in the stump/socket interface [1-7] would result in great discomfort, and continuous mechanical abrasion will eventually cause tissue breakdown, bruise, irritation, stump pain and skin problems. Stump skin damages are serious and should be avoided. Furthermore, heavy and consistent dependency on the sound limb would cause undesired pressure distribution to the rest of musculoskeletal system [8] and hence increase in the prevalence of degenerative changes in the lumbar spines and knee.

Currently, there is no agreement amongst practitioners and researchers regarding the parameters and objective methodologies of gait performance assessment to identify the optimum alignment for lower limb prosthesis. Some researchers believe that symmetry [3, 9] is the key in searching for the optimum alignment. They tried to look for the symmetry between the sound leg and the prosthetic leg. Others [10] believe that the assessment should look into the variation in between steps. Meanwhile, another group of researchers believes in stability and minimum energy expedition [11-13]. Recently some researchers [14, 15] have proposed that matching roll over shape (ROS) as close as possible to an ideal ROS shape of the foot is the key to a priori alignment. Somehow none of the researchers have claimed confidently that they have found the key of the optimum alignments. Above all, Zahedi [1] proved that the amputees are highly capable to adapt themselves to a broad range of optimum alignments in level walking. He also suggested a set of alignment definitions for both transtibial and transfemoral

prosthesis. Later, Sin [16] re-examined the accepted range and found that a non-level walking test could constraint the acceptable range into a smaller set.

Instrumental gait analysis is crucial for providing a scientific view of walking performance with reported error margins. These instruments provide measurements in temporal, kinematic or kinetic properties of the gait. A gait analysis laboratory may consist of commercial gait measurement instruments such as a vision motion capture system to acquire temporal and kinematic gait data, while using a force plate to measure the ground reaction force within a step. Examples of a vision motion capture system and a force plate are Vicon and Kistler respectively. The commercial motion capture systems provide reliable measurement consistency and accuracy which are reported in their datasheets. In practice, they are expensive and stationary in a confined room.

On the other hand, an ambulatory gait measurement system provides a choice for portable and continuous gait measurements outside a gait laboratory. A number of sensory units that feature light-weight and small in size could be used for direct measurements. A Micro-Electro-Mechanical System (MEMS) type Inertial Measurement Unit (IMU) is light-weight and small in size, relatively cheap, reliable and accurate. An IMU could measure kinematic properties of the limb segments in multiple axes. Commercial MEMS IMUs from Xsens, MEMSense, MicroStrain, MotionNode etc. for example, give a broad range of selections such as types and number of transducers (accelerometer, gyroscope and magnetometer) incorporated, number of degree of freedom (dof) per transducer, signal choices (USB, SPI, I2C, RS232 or analogue voltage) as well as the calibration and analytical software. Off-the-shelf IMUs for gait measurement are rather expensive as compared to their electronic components. An example of MEMS IMU is the integration of ADXL335 (3-axis accelerometer, Analog Devices, Inc.) and IDG500 (2-axis gyroscope, InvenSence, Inc.). However, skilled circuitry development to assemble these ICs is required. The IMU needs to be calibrated before applying it for motion data acquisition.

Controversy on the lower limb alignment might be due to disagreements in gait-alignments assessments. The disagreements could be categorized in two major groups. Firstly the algorithms of assessment and secondly choices of measured gait parameters. Many algorithms are suggested, including symmetry index, variation in a step-to-step transition and ROS as explained above. However limited choices of

gait parameters are suggested to be weighted via these algorithms since these algorithms are mathematically incapable to handle high dimensional data at once. Nowadays, gait data are easily available in high dimensions. It may be an irrational sense just to limit to a number of choices. Since walking is a series of voluntary controlled motions, the gait data should map to a distribution with a centre tendency. The gait data are postulated to form the gait patterns as the results of alignments and other restrictions. Next, the challenge would be to present the multi-dimensional data in a simple form that displays the centre tendency. In practice, a prosthetist spends limited time in monitoring the patient's gait. Short gait monitoring time might possibly result in insufficient observation as the patient leaves the clinic. It is envisaged that an ambulatory system instead of a stationary system would provide a longer observation and collect sufficient gait data.

1.2 Motivation

Some methods were proposed, including symmetry index [5, 9, 16, 17], variation in a step-to-step transition [10, 18], stability within zone of integrated balance [11] and matching roll-ever shape (ROS) to an ideal ROS [14, 15] (see arguments of these methods in Chapter 2). These reported methods for lower limb prosthetic alignment assessment still exhibit a few limitations as listed.

1. The first limitation is the limited use of gait variables in a single comparison. For example, a symmetry index would compare the stride speed of the left leg and the right leg. In another example, variations of thigh moments in a step-to-step transition are calculated and plotted to justify the quality of an alignment.
2. The second limitation is the non-uniform sensitivity of the methods when different gait variables are applied. Non uniform results could be produced when different gait variables are applied in the reported methods. This is especially true for the symmetry index and variation in a step-to-step transition. The above methods do not consider compound gait variables at a time. If there are n-sets of gait parameters, there could be n-sets of unequal assessment results. Certain gait parameters are sensitive to the changes of the alignment while certain are not.

3. The third limitation is inadequate observation time during an alignment session. From the prescription point of view, it could be impractical and costly in clinical practices to spend excessive time on a patient. Gait observation during a schedule gait trial could be insufficient to provide adequate gait data for analysis. The amputee would adapt to a new gait pattern over the long run upon any alignment updates. An ambulatory gait measurement system which could continuously collect sufficient amount of gait data out of the clinic could achieve this objective to a certain extent.

It is arguable that the lower limb prosthetic assignment and its assessment must be limited to a pre-scheduled clinical session and must be confined within a certain types of gait variables and must investigate the sensitivity of certain gait variables with regard to the alignment. To date, a typical instrumental gait measurement would easily generate many gait variables. Simple plots and statistical analysis focused on a limited number of gait variables may be insufficient to reveal the 'true' gait quality. It could be a waste of information by discarding part of the gait variables without proper justification. Since human walking involves a high synchronization of falling and supporting of the body controlled by the lower limbs, repeated gait variables measured from predefined body segments could possibly reveal crucial gait patterns due to the alignment. There is a need to provide an objective assessment method for the application of lower limb prosthetic alignment, that acquires sufficient amount of gait data and processes high dimensional gait variables and presents them in a simple form.

1.3 Aims and Objectives

1.3.1 Aims

1. To design a low cost portable mechatronic system that is able to monitor gait in lower limb segments during normal walking.
2. To propose a simple gait analysis solution as an objective assessment during lower limb prosthetic alignments.

1.3.2 Objectives

1. To develop an ambulatory system for gait data collection. The system should be portable and low cost.
2. To calibrate the ambulatory system including the datalogger and the sensors. The efforts should specify the system and provide margin of errors.
3. To collect gait data using the ambulatory system under several walking restrictions.
4. To propose a procedure of gait data processing. The procedure involves multi-stages of signal processing and conditioning.
5. To propose a simple presentation of gait data that could provide essential visual aids and guides during lower limb prosthetic alignments.

1.4 The Scope of this Research

The project could cover many stages of research and development phases before reaching a clinically proven solution. However, at this early stage, this project is intended to provide a potential solution to the problem and is limited into these scopes.

1. To develop a low-cost ambulatory gait measurement system that could be used indoors and outdoors.
2. To propose a novel assessment method that consider a compound set of gait variables
3. To use healthy subjects to validate the proposed solution

1.5 Contributions of this research

As a contribution to the body of knowledge, part of the thesis are published in peer-reviewed conferences. The development of the ambulatory system as reported in Chapter 3 is published in *The 2011 International Conference of Mechanical Engineering, July 6-8*, London, UK, 2011. Different techniques of static calibration of an triaxial accelerometer and the comparison of these techniques as reported in Chapter 4 are published in:

- *The Eighth IASTED International Conference on Biomedical Engineering, February 16 – 18*, Innsbruck, Austria, 2011.

- *The 2011 International Conference of Mechanical Engineering, July 6-8*, London, UK, 2011.

From the same chapter, the dynamic calibration of a gyroscope using a simple pendulous rig and a statistical method is published in *The 14th International Conference on Climbing and Walking Robots and the Support Technologies for Mobile Machines (CLAWAR2011), September 6-8*, Paris, France, 2011. Further works and findings from the research will be published in peer-reviewed journals. The citations of the publications are listed in Appendix D.

Further contributions of this research work can be summarized as:

1. Proposing the development consideration of an ambulatory system. This includes the embedded system design and the recommendation of IMU sensory axes conversion according to the body axes at predefined body landmarks.
2. Revising and comparing several IMU static calibration methods. The comparison reveals the advantages and disadvantages of each method. An innovative procedure using 6/12 known positions and the iterative mathematical solution proves to be useful and easy to apply.
3. Proposing an innovative dynamic calibration for a gyroscope using a pendulous system.
4. Proposing a validation method for IMU dynamic performance using a pendulous system. The IMU actual outputs are compared with the theoretical models formulated from the principle of circular motions.
5. Proposing a novel set of cross-designed experiments to investigate the effect of a crucial alignment factor (ankles) and the walking level to the gait quality.
6. Proposing an innovative procedure to systematically process the collected gait data into a structure of normalized and linear interpolated gait cycles.
7. Proposing a novel gait assessment algorithm that provides a visual aid and a decision guide using PCA and SOFM. The solution is envisaged to serve as an easy-to-use gait assessment tool for the prosthetists during dynamic alignment or more generally, for normal and pathological gait analysis.

1.6 Organization of the Thesis

The thesis is divided into seven chapters. Chapter 2 reviews the problem background of the research. A general knowledge on human waking and biomechanics is reviewed. This includes essential definitions regarding walking and crucial concepts for gait analysis. The review also investigates specially on the issues regarding lower limb prosthetic alignments. These issues include the importance and the need for the alignments, reviews on many alignment methodologies, tools and their arguments. Lastly, contribution of this research to the body of knowledge are mentioned.

Chapter 3 presents the design and development of an ambulatory system which consists of a customized embedded datalogger, five units of inertial measurement units (IMUs) and straps to hold the devices.

Chapter 4 describes the procedures for both static calibration and dynamic calibration of an IMU. The accelerometers are calibrated using several static calibration techniques and these techniques are compared. A pendulous system is recommended for the dynamic calibration. A frequency distribution method is proposed to calibrate the gyroscope. Finally dynamic performances of an IMU are verified by comparing its theoretical models and the actual measurements in the pendulous system.

Chapter 5 reports the procedures of human walking trials and their results. The experiments are cross-designed using two walking restriction factors that influence the gait. The factors are the ankle and the walking level. The experiments received an ethical approval from the Research Support Unit of the University of Leeds and consents from the participants. The procedure for gait feature extraction is demonstrated. It includes multi-stages of signal processing and conditioning techniques, gait events identification, gait features selection and extraction out of processed gait data. The reliability of the ambulatory system (see Chapter 3) is justified using a statistical method called test-retest reliability.

Chapter 6 proposes a potential objective assessment for the lower limb alignments. Correlation and dimensionality are emphasized to be the issues in multi-variants gait data processing. The proposed solution applies Principle Component Analysis (PCA) and Self-Organizing Feature Map (SOFM) to resolve the above issues. The algorithms generates visual aids and guides that map the gait

patterns in low dimensional plots. By means of a 2D or 3D plot, both PCA and trained SOFM are able to show clear clusters of gait performances under different walking restrictions. A trained SOFM could determine the class of a gait pattern in future applications.

Chapter 7 summarizes the work reported in this thesis, highlights the main findings and outlines future works.

CHAPTER 2
LITERATURE REVIEW

2.1 Introduction

This chapter reviews the background knowledge regarding the study of human locomotion and lower limb prosthetic alignments. In a broader view, the review would give a general understanding about the studies of human locomotion and their relevant discoveries. In specific, the review would provide a deeper understanding regarding the researches in the lower limb prosthetic alignments and their relevant discoveries. Lastly, the contributions of this research to the body of knowledge are mentioned.

The review starts with fundamental concepts and terminologies in the study of human locomotion. They include formal definitions of walking, anatomical geometry, motions in lower limbs in kinematic and kinetic terms. These definitions form the background knowledge necessary for gait analysis. All studies in human locomotion cannot leave without gait data collection with reliable gait measurement instruments. A review of these instruments and their limitations are provided.

Next, a few human walking models are reported. Each model emphasizes on different key variants that determine gait quality. The classical human walking model, the six determinants, has gone through several challenges and is seriously questioned. However, it still describes well about human walking. The model, dynamic walking, utilizes the law of conservation of energy to model the walking actions. Meanwhile, the model, rocker based inverted pendulum, utilizes the geometry of roll-over shape (ROS) to anticipate the virtual leg length. Optimal values of ROS radius and virtual leg length are suggested.

It is a great clinical concern to provide optimal prosthetic alignments. The concerns include both dermatological and musculoskeletal reasons. The alignment must at least provide a certain extent of proper gait function and comfort. Key

methodologies and their arguments regarding the lower limb prosthetic alignments are reviewed.

2.2 Basic Concepts

2.2.1 Definition of Walking

Inman [19] defines locomotion as a rhythmic displacement of body parts in forward progression, either walking or running. Different to walking, the period of double limb support during running disappears and both limbs are at not on the ground for a brief period. Perry [20] describes walking as a repetitious pattern of reciprocal floor contact by lower limbs to move the body forward in a stable manner. Above all, Whittle [21] provides specific tasks of walking as quoted "…accomplish four things:

1. Each leg in turn must be able to support the body weight without collapsing.
2. Balance must be maintained, either statically or dynamically, during single leg stance.
3. The swinging leg must be able to advance to a position where it can take over the supporting role.
4. Sufficient power must be provided to make the necessary limb movements and to advance the trunk. "

2.2.2 Anatomical Geometry

Human body could be described geometrically [21] as shown in Figure 2.1. Three orthogonal planes could be virtually seen crossing the body into three perspective views. A sagittal plane divides the human body in bilateral views. A frontal plane divides the human body in the front and back views. A transverse plane divides the human body in the top and bottom views. There are a number terms that are frequently used to describe the geometry of a human body. 'Medial' means the midline of the body where the big toe is on the medial side of the foot. 'Anterior' and 'Posterior' means toward the front or toward the back of the body respectively. 'Inferior' and 'Superior' means toward the bottom or toward top of the body respectively. 'Lateral' means away from the median plane. 'Distal' means away

from the centre of body. Proximal means towards the centre of the body. Detail human anatomical descriptions could be found in most kinesiology textbooks.

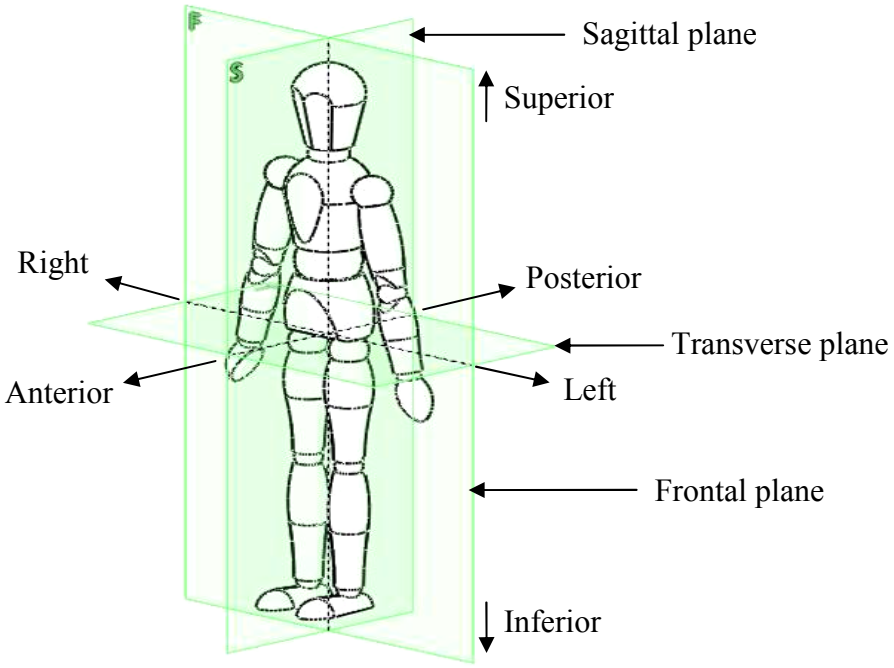

Figure 2.1: Human geometry. Redrawn from [21]

2.2.3 Motions of Lower Limbs

Voluntary lower limb motions are mostly joint-segment rotations and are specifically named as shown in Figure 2.2. The paired motions are the resultant contraction of the agonist-antagonist muscles. In the frontal plane view, abduction is the movement away from the medial while adduction does the opposite. In the sagittal plane view, the hip flexion is the raise of thigh toward the body while the hip extension does the opposite. The knee extension is the movement to extend or straighten the shank while knee flexion defines the action of knee bending. A few crucial foot motions are recognized. For ankle and foot as shown in Figure 2.3, in the sagittal plane, dorsiflexion describes the revolute action of the foot pivoted at the ankle that bends the foot toward the shank while plantarflexion does the opposite. Eversion is the rotation of the foot about the ankle that the sole turns away from the median plane while inversion does the opposite. Foot abduction and adduction could be observed as the complex joint-segment rotations that rotate the insole away and toward the median plane respectively. Furthermore, Kirtley [22]

provides a better understanding by relating corresponding key agonist-antagonist muscles for each pair of motions, as shown in Table 2.1.

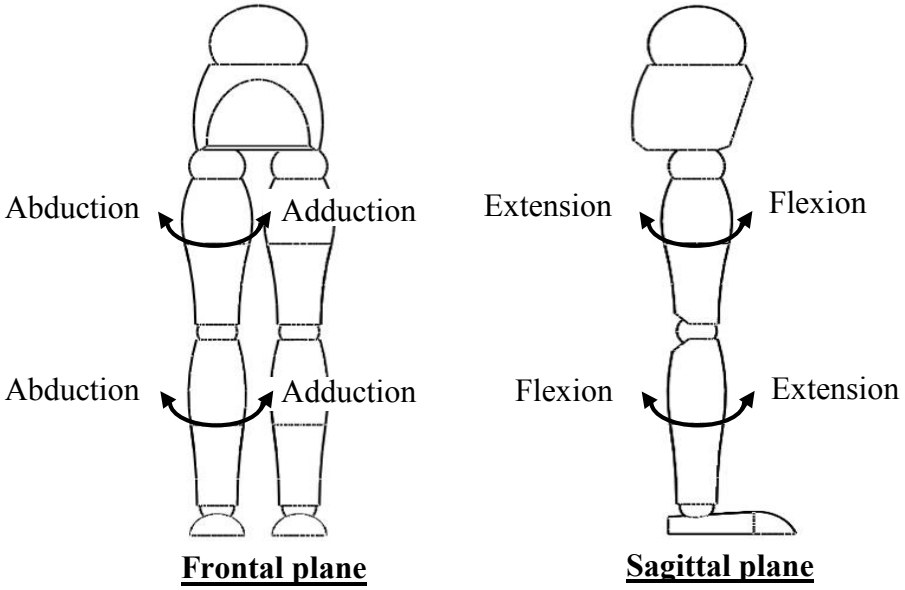

Figure 2.2: Lower limbs motions [21]

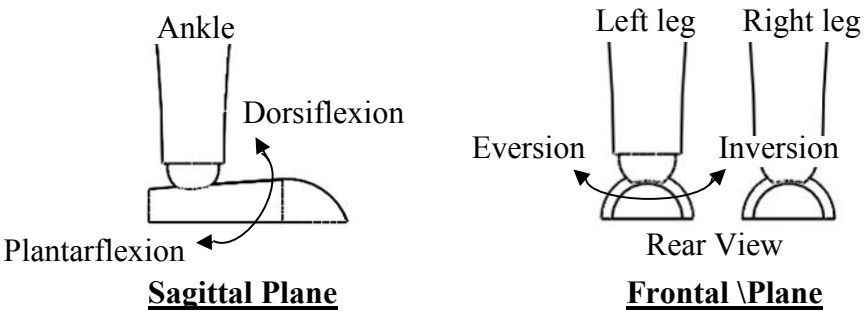

Figure 2.3: Ankle and foot motions. Modified from [21]

Table 2.1: Lower limbs motions and agonist-antagonist muscles. Quoted from [22]

Joint	Motion	Key muscles
Hip	Flexion/Adduction/Medial rotation	Iliopsoas
	Extension/Abduction/Lateral rotation	Gluteus maximus, medius
Knee	Extension	Quadriceps
	Flexion	Hamstrings
Ankle/Foot	Dorsiflexion	Tibialis anterior
	Plantarflexion	Gastrocnemius, soleus
	Inversion	Tibialis posterior
	Eversion	Peroneal

2.2.4 Kinematic and Kinetic Parameters

Kinematic and kinetic parameters are normally applied during gait analysis. These parameters are well-explained in literatures [23, 24] and textbooks [20-22, 25, 26] relating to human biomechanics or gait analysis. A few key concepts and terminologies are elaborated below. More detail could be found in most textbooks regarding kinesiology and human biomechanics.

2.2.4.1 Step, Stride, Cadence, Velocity

Step is defined as the length in meters between ipsilateral leg and contralateral leg, starting from the heel of ipsilateral leg to the heel of contralateral leg. A Stride consists of two Steps (left Step and right Step) or is defined as the length in meters between the heels of ipsilateral leg to consecutive ipsilateral leg. Both Step and Stride are illustrated in Figure 2.4.

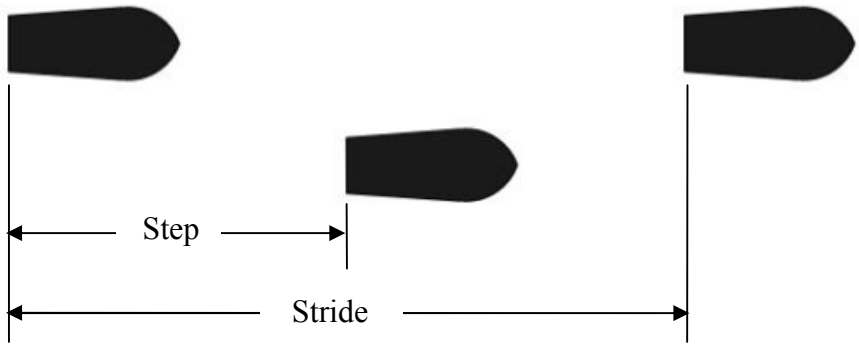

Figure 2.4: Definition of step and stride. Redraw from [20]

Cadence is defined as the number of steps per unit of time, normally at *steps per minute (steps/m)*. It is the rate of paces. Since a stride comprises of two steps, half of Cadence (0.5 x Cadence) could be expressed as the number of strides per minute (*strides per minute*). Velocity is defined as Stride length per Stride time, normally in *meter per second (m/s)*. It is the rate of linear displacement of the human walking. Cadence (*steps/m*), Stride (*meter*) and Velocity (*m/s*) are interrelated. Given any two parameters, it is possible to calculate the rest using equation (2.1) and equation (2.2).

$$\boldsymbol{Velocity = \frac{Cadence \times Stride}{120}} \qquad \textbf{[22]} \qquad \textbf{(2.1)}$$

$$\boldsymbol{Stride = \frac{120 \times Velocity}{Cadence}} \qquad \textbf{[22]} \qquad \textbf{(2.2)}$$

2.2.4.2 Angular Properties

Anatomically, human body consists of multiple joints and segments, rotating about their axis. For lower limbs (shown in Figure 2.5), Winter [27] defined the hip angle as the difference between the trunk and the thigh, the knee angle as the difference between the thigh and the shank, the ankle angle as the difference between the foot and the shank. Based on these definitions, the angular displacement can be measured and computed. Angular velocity and angular acceleration are the first and the second derivatives of the angular displacement respectively. Healthy joints consist of more than one degree-of-freedom, considering the type of joints in the leg. The hip joint is a ball and socket joint; the knee joint is not pivoted at a fixed revolute point while the foot comprises of multiple-linked bones and joints. A major concern of prescribing a lower limb prosthesis and the alignment is the capability of motions at the AP plane.

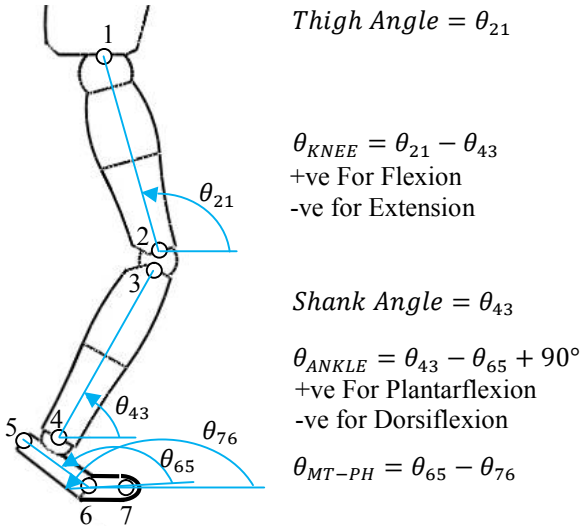

Figure 2.5: Definitions of the limb segment angles. Redrawn from [28]

2.2.4.3 Centre of Mass, Centre of Pressure and Ground Reaction Force

Centre of Mass (COM) is a virtual mechanics concept [29] of a concentrated mass located at a specific geometrical position. The concept allows the calculation of forces and moments at the concentrated mass. Each body segment could be treated as an enclosed geometrical mass where COM of that segment could be computed. The body COM (BCOM) [19] is fluctuating around within the pelvic during walking. BCOM trajectory along the line of progression forms a smooth sinusoidal waveform. The lowest is at double limb stance and the highest at single limb stance. The trajectory also changes smoothly as the body sways medial-laterally. COP is a position defined at the insole contact point of ground reaction force (GRF). Using a force plate, it is at the centre of forces. GFR is a reaction force [20-22, 25, 26] generated by the body mass during foot collision onto the ground through the insole centre of pressure (COP). It could be further decomposed into three orthogonal components, i.e. the vertical ground reaction force (vGRF), the anterior posterior (AP) force and the medial lateral (ML) force. These force vectors could be measured using a multi-axial force plate. They are important parameters in studying normal and pathological gait. For general plane motion, applying equations of motion [28, 29] as listed in equations (2.3), (2.4) and (2.5) at the COM of a selected body segment, forces and moments could be computed if kinematic information and the segment inertia of moment are known or vice versa.

$$\sum \boldsymbol{F_x = ma_x} \qquad \textbf{[28, 29]} \qquad \textbf{(2.3)}$$

$$\sum \boldsymbol{F_y = ma_y} \qquad \textbf{[28, 29]} \qquad \textbf{(2.4)}$$

$$\sum \boldsymbol{M = I_o \alpha} \qquad \textbf{[28, 29]} \qquad \textbf{(2.5)}$$

2.2.5 Gait Definitions

Gait definitions explained in this section are suitable for walking since the main interest is to understand human walking which could be applicable to the study of the able-bodied locomotion and the amputee locomotion. Other styles of locomotion such as running is not described and defined in the thesis.

Walking consists of series of repeated gait cycles. A gait cycle is divided into two distinctive phases, called Stance phase and Swing phase as illustrated in Figure 2.6. The Stance phase is defined as the duration where the foot is in contact with the ground while the Swing phase is defined as the duration where the foot is in air. A number of gait events within a gait cycle are defined. Definitions recommended by influential researchers such as Inman [19], Perry [20] and Whittle [21] coined different terms but agreed mostly in the context explained. These gait events as shown in Figure 2.6 are recommended by Perry. A gait cycle is categorized sequentially as Initial Contact (IC), Loading Response (LR), Mid Stance (MSt), Terminal Stance (TSt), Preswing (PSw), Initial Swing (ISw), Mid Swing (MSw) and Terminal Swing (TSw). In some literatures, the event of foot collision with the ground is named as Heel Contact (HC) [30] or Heel Strike (HS) [31-34] or in a more general term, Foot Strike (FS) [19] since a patient could possibly have no heel at all. It is important to identify the border line that differentiates between Stance phase and Swing phase. From Swing phase to Stance phase, the gait event named as Heel Contact (HC) or Heel Strike (HS) or Foot Strike (FS) is applied. From Stance phase to Swing phase, the gait event named as Toe-Off (TO) [21] or Foot Off (FO) [19] is used.

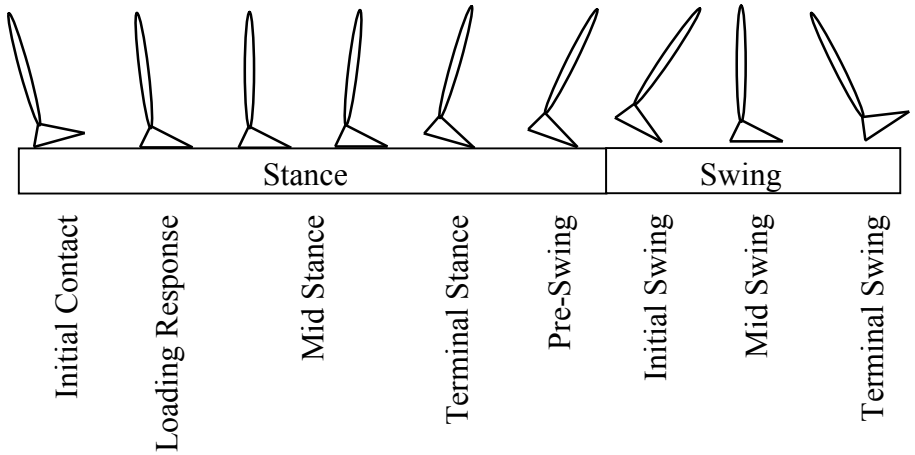

Figure 2.6: Definition of stance and swing phases. Modified from [20]

Walking could be explained according to their tasks or periods within a GC. One of the example is demonstrated by Perry, i.e. Double Limb Stance and Single Limb Stance as shown in Figure 2.7. Double Limb Support occupies a brief period of a GC when both legs are on the ground, starting for heel strike and ended when

the trailing leg leaves the ground. Single Limb Support occupies a longer period of stance phase when the body is vaulting over a single leg like a pendulum.

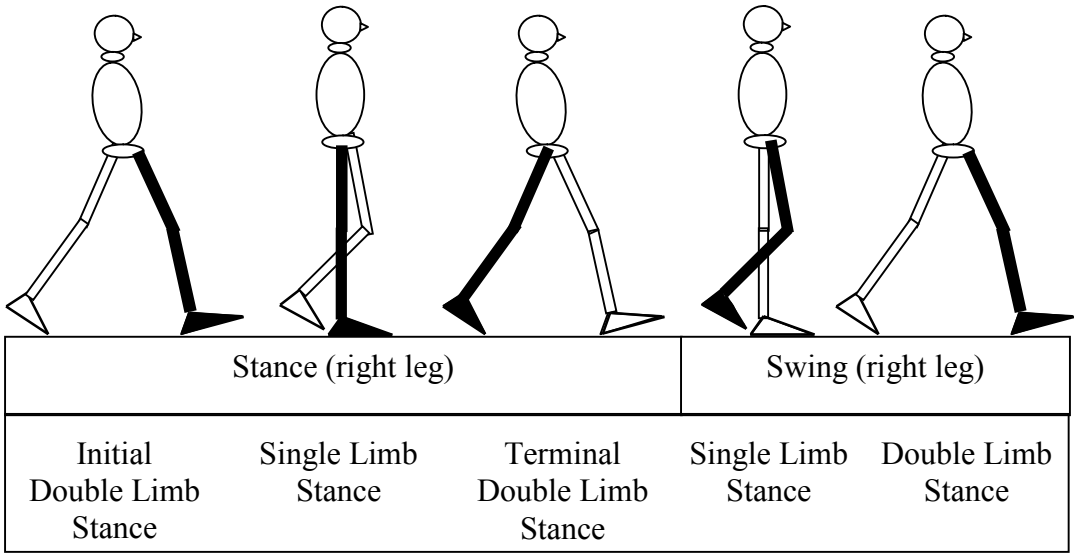

Figure 2.7: Double Limb Stance and Single Limb Stance. Redraw from [20]

Normalized gait cycles are useful during gait analysis. The variation of GCs (any measured gait data) could be observed qualitatively via a plot or analyzed statistically. Using a plot, GCs are plotted overlapping each other. The variation could be seen as the gap amongst the lines. Examples of such plots are reported in many literatures such as [19-21, 28, 32, 34]. General statistical results could be drawn at critical gait events or during the gait tasks or the periods. Reported results for normal human locomotion using gait definitions are shown in Table 2.2. Stance phase consists of approximately 60% of a GC while Swing phase 40%. Further breakdown descriptions in tasks, Initial Double Stance would occupy 10%; Single Limb Support would occupy 40%; Terminal Double Stance would occupy 10% out of a GC.

Table 2.2: Task durations in percentages of gait cycle. Redrawn from [20]

Floor Contact Periods			
Stance			60%
	Initial Double Stance	10%	
	Single Limb Support	40%	
	Terminal Double Stance	10%	
Swing			40%

In an even detail breakdown, Kaufman and Sutherland [35] recommended a set of descriptive gait terminologies similar to Perry [20] and reported the general timing of the gait terminologies in percentages of a gait cycle (%GC) as shown in Table 2.3.

Table 2.3: Gait events, periods and phases in %GC [35]

Event	% Gait Cycle	Period	Phase
Foot Strike	0	Initial double limb support	Stance, 62% of cycle
Opposite Foot-Off	12	Single limb support	
Opposite Foot Strike	50	Second double limb support	
Foot-Off	62	Initial swing	Swing, 38% of cycle
Foot Clearance	75	Mid swing	
Tibia vertical	85	Terminal swing	
Second foot strike	100		

2.2.6 Roll Over Shape

Roll-over shape (ROS) was vaguely implied by Saunders et al. [36], as the fourth and fifth determinants: foot and knee mechanism. Perry [20] described it as three sequential ankle/foot actions, as heel, ankle and foot rockers. ROS attracts the attention of researchers and biomechanical models of human walking related to ROS were proposed, such as Passive Dynamic walking [37], Rocker Based Inverted Pendulum [38, 39] and Step-to-Step Transition with roll-over foot [40].

The working principle of ROS can be illustrated with a wheel rotating on a surface as shown in Figure 2.8. A local coordinate system is defined within the wheel. As the wheel rotates forward, it moves in a straight linear line but the motion is an arc as seen from the local coordinate within the wheel. A combination movements of knee, ankle and foot (KAF) create similar arc, analogy to a wheel but flatter as shown in Figure 2.9. ROS is mostly examined in the sagittal plane. 3D ROS (a surface) is worth examined for studying its contribution to stability and other unknown functions. ROS begins from heel contact (HC) and ends at opposite heel contact (OHC).

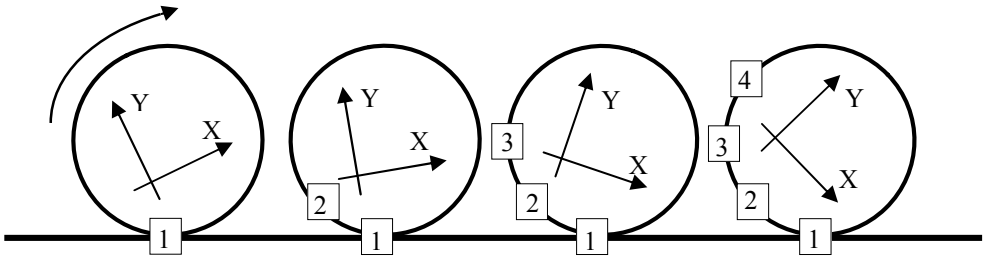

Figure 2.8: Principle of Roll-Over Shape [41]

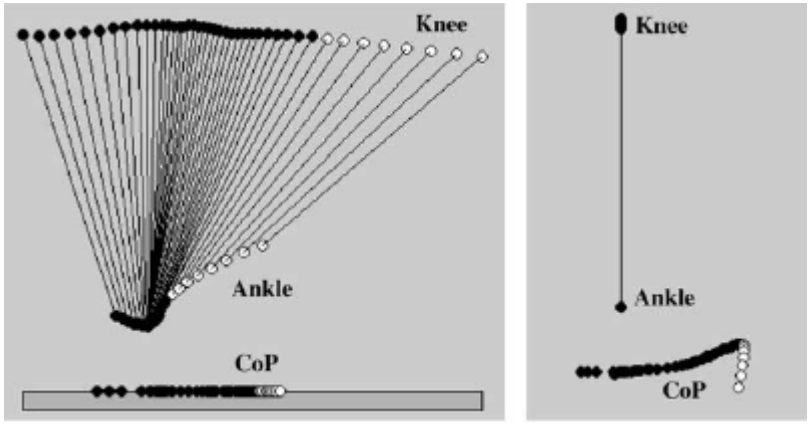

Figure 2.9: Analogy of Roll-Over Shape in a KAF system [41]

Hansen [41] concluded that the radius of ROS is statistically invariant to walking speed and the centre is found best fitted in between the ankle and the knee. Somehow, ROS shape changes in position with walking speed. In a recent study [42], the position of the effective ROS centre were examined in initiation, steady state walking and termination. ROS centre is found to shift posterior during initiation; neutral at the shank during steady state walking and interiorly during termination. Horizontal shift of the centre proportional to the increment of walking speed was reported.

Roll-over shape in KAF system [43] is reported to self-adapt and orient itself for inclined and declined ramp. The ankle is found to be the main adapting joint when walking uphill whereas it is the knee when walking downhill. From the view of energy, Adamczyk et al. [40] reported the optimum ROS radius is 0.3L (anatomical leg length) at the minimum of metabolic cost.

2.3 Gait Measurement Instruments

A collection of literature reviews regarding the instruments for gait analysis is listed in Table 2.4. These instruments measure temporal, kinematic or kinetic properties of the body segments during motions such as quiet stance, walking, running etc. Two major groups could be categorized, i.e. stationary and ambulatory. A gait measurement system is classified stationary if the system is limited in a confined space such as a gait laboratory. On the other hand, the system is classified as ambulatory if the system is portable and could be mounted solely on a subject's body. It is normal to have a combination of instruments as seen in a gait laboratory. Some of the commercial products come as a complete solution that comes together with the sensory measurement units and a series of gait analysis software. For example, motion capture camera of Qualisys.

Table 2.4: Instruments for gait analysis. Compiled from [20-22, 25, 26]

No	Instrument	Description	Category	Example
1	Footswitch	Multiples tiny on/off switches are mounted beneath the shoe. Timings of floor contact of the foot are examined.	Ambulatory	micro switch, thin film sensors such as Force Sensitive Resistor (FSR).
2	Electrogoniometer	An electronic device to measure angular displacements.	Ambulatory	Potentiometer, flexible strain gauges, bend sensor.
3	Foot Pressure	A device to map the pressure distribution of insole.	Ambulatory / Stationary	thin film sensors such as FSR, glass plate examination, pressure map, pedobarograph, Tekscan, Pedar-X.
4	Electromyography	A device to record the muscle activities during action.	Ambulatory	surface electrodes, invasive electrodes.

5	Accelerometer	A motion sensor to measure static tilt angles relative to the gravity and linear acceleration around the sensor axis during action.	Ambulatory	single axis, multi axes.
6	Gyroscope	A motion sensor to measure the angular rate around the sensor axis during rotational action.	Ambulatory	single axis, multi axes.
7	Energy consumption	A device to estimate the body energy expenditure during action	Stationary	Douglas bag for O_2 and CO_2 analysis .
8	Force platform	A platform consists of an array of load cells which measure the vectorial ground reaction force once stepping on it. It is a vital device in gait analysis. Normally installed in a walkway.	Stationary	Commercial solutions such as Kistler, AMTI.
9	Motion capture camera	An imaging measurement technique. Active or passive markers are mounted on anatomical landmarks. Kinematic data can be achieved by calculating the relative distance between the global coordinate with local coordinates.	Stationary	Commercial solutions such as Vicon Motion Camera, Qualisys Track Manager (QTM), OptiTrack.
10	Video tape	Video of gait at certain view during walking. Qualitative observation only.	Stationary	Any video recorder.

The gait measurement instruments are assessed qualitatively depending to their functions, cost, size and precision as listed in Table 2.5. Function is categorized according to the nature of the measurement parameters either temporal, kinematics or kinetics. The cost is judged if the instrument is affordable at the price of hobby electronics. The instruments are likely to be cost highly if they are a commercial solution such as Pedar-X for insole pressure mapping, Kistler force plate for GRF measurements, Vicon motion capture camera for kinematic measurements of body segments etc. If the instrument is light and small to be handled with ease, it is categorized as small otherwise it will be categorized as big. The instruments such as accelerometer and gyroscope are small and light weight. They are most suitable for an ambulatory system. Stationary instruments such as the force plate and the motion capture camera are bulky and heavy. The precision is evaluated qualitatively if the instrument could exhibit reliable and consistent outputs. Most commercial solutions would guarantee the measurement precision in low percentages of error. Details of most commercial solutions are available online. The precision of certain instruments such as electrogoniometer and foot pressure varies and is relative to the quality of the sensors used.

The selection of gait measurement instruments relies on a number of factors such as parameters of interest, cost, size, sensory precision and the nature of the application either indoor or outdoor. Compromising amongst these factors might be necessary during system selection. An ambulatory system could be used indoor or outdoor. It would be self-contained with a number of sensors and a data acquisition system that feature on light-weight and small size but probably compromise in measurement precision, short duration of electric power supply duration, data sampling rate and storage size. Comparatively, a stationary system would be assigned for indoor applications. The indoor applications might not have the issue of electric power supply, instrument size and weight. With sufficient financial supports, a stationary system could possibly be equipped with the gait measurement instruments that feature on synchronous hybrid measurements, high sampling rate, high storage, high sensory resolution and precision. For example, a gait laboratory that integrates a motion capture camera and a multi-axial force platform.

Table 2.5: Reviews of the instruments for gait analysis

No	Instrument	Function	Cost	Size	Precision
1	Footswitch	Temporal. Timing of gait events	Low	Small	High
2	Electrogoniometer	Kinematic. Angular displacement	Low	Small	Relative high dependent to the sensor used.
3	Foot Pressure	Kinetic. Insole pressure	Low. High if a commercial solution.	Depend on the selection	Relative high dependent to the sensor.
4	Electromyography	Bio-signals of muscle activities.	High	Small	largely dependent to the filtering algorithm used.
5	Accelerometer	Kinematic. Linear acceleration	Low. High if a commercial solution	Small	High
6	Gyroscope	Kinematic. Angular rate	Low. High if a commercial solution	Small	High
7	Energy consumption	Metabolic rate.	High	Big	High % of CO_2 and O_2
8	Force platform	Kinetic. GRF	High	Big	High
9	Motion capture camera	Kinematic data of body segments.	High	Big	High
10	Video tape	Qualitative observation only.	Low	Small	Observation only

2.4 Human Walking Models

Up to date, a number of human walking models are introduced. The models suggest key parameters or determinants that should be investigated during the study of human walking. These models are listed below.

2.4.1 The Six Determinants

In 1953, Saunders, Inman and et al. [36] published an influential paper on the six determinants of human walking where pelvic rotation as the first determinant, pelvic tilt as the second, stance-phase knee flexion as the third, foot and knee mechanism as the fourth and the fifth, lateral pelvic displacement as the six. They hypothesized that "In translating the centre of gravity through a smooth undulating pathway of low amplitude, the human body conserves energy…". Their theory was pervasive in clinical, research and educational fields as found in literatures [19] and textbooks [20-22, 25, 26]. Later determinants one to three (pelvic rotation, pelvic tilt and knee flexion in stance phase) were questioned, challenged and proven inappropriate as the key determinants by Gard et al. [38, 39, 44-51]. Pelvic rotation was found to increase step length especially at faster walking speed, but it has little effect on the vertical displacement of BCOM. Similarly, pelvic tilt and knee flexion in stance phase show no significant influence on the vertical excursion of BCOM during able-bodied walking. However the six determinants still provides a comprehensive description regarding the human gait.

2.4.2 Inverted Pendulum

Two human walking models are constructed based on the principle of the inverted pendulum. They are Dynamic Walking and Rocker Based Inverted Pendulum.

2.4.2.1 Dynamic Walking

Efficient bipedal gait expends less energy as showed by McGeer [37] and he named it as passive dynamic walking. Kuo and et al. [47, 48, 52] further enhanced McGeer's theory on passive dynamic walking and proposed a human walking model as a step-to-step transition. Leg is modelled as a pendulum in swing phase and the BCOM vaults over on a single leg like an inverted pendulum during single limb stance. Ideally they should obey the law of conservation, requiring zero muscular work. During double stance, the leading leg collides on the ground and

negative work (W^-) is induced. The trailing leg at push off produces an equal amount of positive work (W^+) to counteract on the negative work simultaneously. The resultant of the positive and negative work redirects BCOM velocity. Ideally at double limb stance, if push-off is equal to collision, $W^+ = W^-$, no additional work is needed during single limb stance. If $W^+ > W^-$, additional negative work is needed during single limb stance to slow BCOM. This could happen during walking uphill. If $W^+ < W^-$, additional positive work is needed during single limb stance to speed up BCOM. This could happen during walking downhill. Based on this principle, Kuo et al. outlined four new periods from the stance phase, as Collision, Rebound, Pre-load and Push-off.

2.4.2.2 Rocker Based Inverted Pendulum

Evolving from the concepts of inverted pendulum, Gard and Childress [8, 25] proposed a simple model based on the roll-over shape. For the sake of simplicity and ease of calculation, the roll-over shape is assumed to be a solid arc with a fix radius and a common centre at the shank, and the vertical movement of the BCOM and the trunk are assumed identical. As shown in Figure 2.10, the roll-over shape projects real human legs to virtual human legs which are longer and walking on a virtual walking surface. Inman [1] was the first man to coin the term, "virtual leg length" which he approximated at 2.2 times of actual leg length for normal walking. However, Gard and Childress [38, 39] corrected it and claimed that the ratio was approximately 1.5 to 1.8 for normal walking. This model associated the relationship of variables like vertical excursion of the body (h), step length (S_l), anatomical leg length (L), foot rocker radius (r) and virtual leg length (L_v). Equations (2.6) and (2.7) are proposed to relate these parameters. From equation (2.6), the foot rocker radius (r) cannot be equal to anatomical leg length (L). The radius [40] is reported optimal at 0.3L, where the metabolic cost of walking is at its minimum.

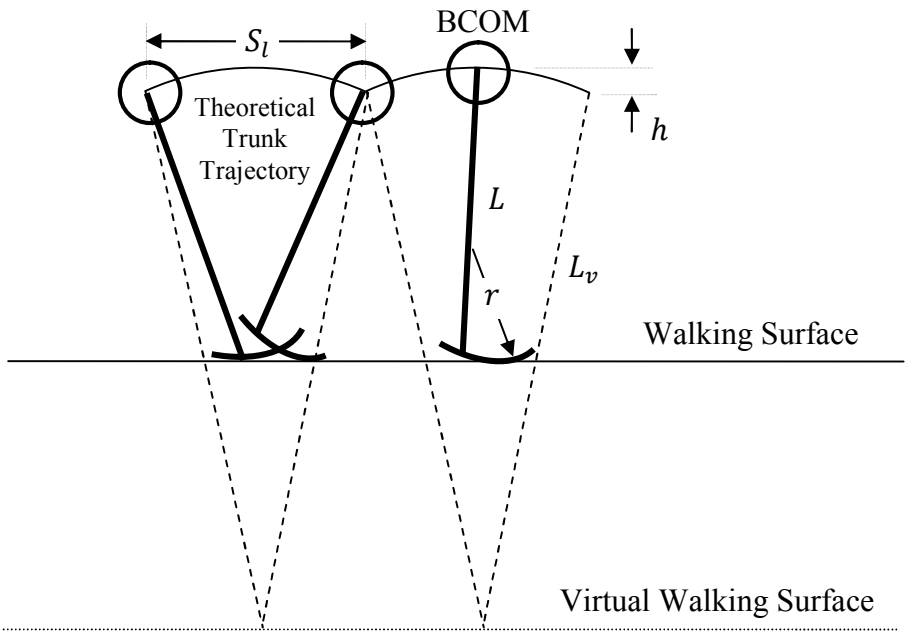

Figure 2.10: Rocker Based Inverted Pendulum [38]

$$L_v = \frac{L^2}{L - r} = L\left(\frac{1}{1 - r/L}\right) = L\rho \qquad \text{[39]} \qquad (2.6)$$

$$h = \frac{S_l^2}{8L\rho} = \frac{S_l^2}{8L_v} \qquad \text{[39]} \qquad (2.7)$$

2.5 Lower Limb Prosthetic Alignments

2.5.1 The Need for Proper Alignments

Contemporary lower limb prosthesis consists of multiple modules and segments, such as sockets, knee joint, ankle, foot and interlink accessories. Proper prosthetic alignments are specific to its user, guaranteeing its function and comfort. It is reported [1-3, 53, 54] that the prosthesis needs to provide comfort, function and cosmetic purposes. Alignment of a prosthesis [1] is an iterative process in order to optimize the socket geometrical relationships with relative to other modular prosthetic components. The prosthetic limbs will go through a series of alignments [55] and at most cases, likely to be repetitive. Firstly, the bench alignment [56-58] will inspect the proper assembly of the modular prosthesis viewed at the frontal plane and the sagittal plane according to the manufacturer's guide. After benched

aligned, the amputee needs to go through another alignment procedure called static alignment [12, 13, 59] with the prosthesis put on. At quiet stance, the body load line and its distances between several body landmarks such as shoulder, waist, trochanter, knee and ankle are inspected. The modular prosthesis is adjusted to meet certain advices determined by the manufacturer and the prosthetists. The alignments are further fine-tuned during the process of dynamic alignment [5, 11, 17, 57, 60] where the amputee will walk with the prosthesis. It takes multiple sessions of gait trials. The assessments will include the prosthetist judgements based on experiences and the verbal feedbacks from the amputee.

Researchers [1, 60] believe that there is a unique set of optimum alignments that offers maximum gait quality. However, there is no common agreement on the methods and measurement techniques to define the optimum alignments. To date, lower limb alignments still rely heavily on the verbal feedbacks from a patient and the experiences of a prosthetist. Moreover, the alignment judgements could be possibly inconsistent from one prosthetist to another prosthetist.

Prosthetic misalignment [1-8, 61] could cause great discomfort in the stump/socket interface and disturbance to gait function which might be visually observed. To a great extent, a misaligned prosthesis could cause dermatological damages such as tissue breakdown, bruise, irritation, stump pain and skin problems due to consistent mechanical abrasion and undesirable pressure distribution. Greater gait deviation could be observed as the amputees adapt and attempt to compensate the misalignment. The body might suffer from non-uniform body load bearing and in the long run, deteriorate the musculoskeletal system. Example of misaligned prosthesis includes lumbar lordosis in bilateral amputees as shown in Figure 2.11. During quiet stance, the upper body is leaning forward and the amputee will exert excessive muscle power to compensate the posture.

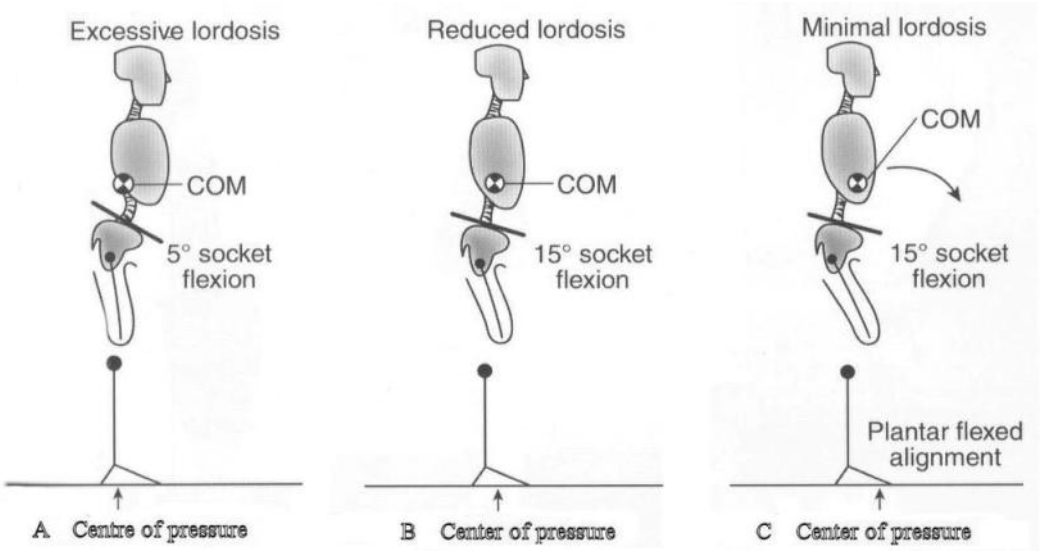

Figure 2.11: Minimizing lumbar lordosis in bilateral amputees [61]

2.5.2 Methods of Alignments

The principle of the body load line [59] is used during bench and static alignment. By simply hanging a plump line from a critical body landmark, the load line can be approximately visualized. Three conventions are mostly recommended, i.e. German type, TKA and MKA. German type uses a plump line laterally and starts from the centre of the socket brim or trochanter to a point in the middle of the foot. TKA also applies a plump line laterally as a visual aid and starts from trochanter. The ankle joint is directly under the line. Knee joint could be located on or behind the line. MKA, later named as UC Berkeley Bench Alignment System [62], uses a plump line medially and starts from the bisector of medial brim (BMB). Ankle joint and knee joint are directly under the line medially. Clearance under the heel is called "safety factor". Higher clearance would cause shorter heel contact time and rapidly transfer of body weight to the ball of the foot, thus increasing knee stability at heel contact. Recommended alignments [59] are reported as:

1. Allocate knee axis 6mm posterior to TKA line
2. Initial knee flexion – 5^0 external rotation
3. Medial end of the knee axis is forward of the lateral end by approximately 6 mm
4. Spacer under heel – 6 to 10mm thick. (To increase knee security)

Berme et al. [56] proposed a three dimensional reference coordinate and a socket axis locator system. This system implements a trial-and-error strategy to allocate the socket axis and the process is very time-consuming. Later, Evans and Evans [63] improved and automated the system by using a magnetic tracking device (3SPACE ISOTRAK Polhemus, Vermont, USA). The system is time saving but the accuracy of measurement could be easily affected by metal or magnetic components within the prosthesis. Sin [57] designed a fully mechanical and manual operated socket axis locator for a BK prosthesis and simplified the process. The system is claimed to exhibit high repeatability and all readings could be determined less than six minutes by a familiar operator.

Other devices include the Berkeley Adjustable Leg [64], the Winnipeg wedge disc alignment units [65], Wilson-Riblett wedge [64], the Proteor Alignment Device [66], In-built One-point Alignment [67], angular protractor, laser angular protractor, electrogoniometer, mechanical aids and fitting stools [58]. In a recent work, Blumentritt [12, 13] introduced a static alignment method called, Laser Assisted Static Alignment Reference (L.A.S.A.R.). The body load line is determined by a force platform and is projected to the body using a laser beam.

2.5.3 Arguments of Alignments

Zahedi et al. [1] had proposed two sets of segment-joint parameters for the lower limb prosthesis alignments as listed in Table 2.6. The alignments include relative tilt angles or shift distance between two prosthetic limb segments where a local Cartesian coordinate system is defined within the limb. Zahedi et al. [1] found that the amputees could adapt to a broad range of acceptable alignments. The human capability of adaptation of misaligned prosthesis was also reported by Fridman et al. [17]. Later Zahedi [10, 18] suggested gait observations via a method called a step-to-step variation. Significant variations of AP and ML ankle moments were noticed as changes in the foot plantar/dorsi flexion angle were made. This process was time-consuming. The concepts of variation stated that different normal subjects exhibit different degree of variation in joint moments [68]. The variation increases in the amputee and deteriorates in higher level of amputation.

Table 2.6: Key parameters for lower limb alignments [1]

No	Below-knee (BK) prosthesis	Above-knee (AK) Prosthesis
1	Toe out/in angle	Toe out/in angle
2	Socket AP shift	Knee AP shift
3	Socket ML shift	Knee ML shift
4	Socket AP tilt	Knee ML tilt
5	Socket ML tilt	Knee height
6	Socket height	Socket AP shift
7		Socket ML shift
8		Socket AP tilt
9		Socket ML tilt
10		Socket rotation
11		Socket Height

Yang [2] conducted another intensive research regarding the effect of the alignments in the socket and the foot onto unilateral above-knee (AK) amputees. He had adopted the alignment definitions and the reference coordinate system proposed by Zahedi [1]. He concluded that the angular displacement of the prosthetic thigh is a key parameter during the assessment. He further concluded that both the socket and the foot are crucial in the alignments. GRF and joint moments at the prosthetic side are emphasized to be the key gait measurement for assessment purposes.

Hannah et al. [9] conducted an experiment collecting lower limbs kinematic data and stated that the optimum alignments were to minimize the asymmetry especially at the hips and knees. He proposed an index of symmetry in time and frequency domain as the measurement of symmetry. He also concluded that the most important change was the foot dorsiflexion while the hip flexion/extension was most sensitive to changes. Somehow, Winter [68] stated that it is insufficient to look at only kinematic variables because there are a potential number of joint moments of force that could produce the same kinematic patterns. The joint moments of force are the compensating attempt to maintain the gait pattern. Instead, Winter proposed three sets of variables in order to match the average pattern over the stride, i.e. Joint angles – ankle, knee and hip; Ground reaction forces - horizontal and vertical; Joint moments of force and support moment.

Saleh [69] disagreed with Hannah's symmetry principle based on angular kinematic information only but suggested multi sets of variables as similar to Winter. He suggested these gait parameters are crucial, i.e. Time-distance measurement, especially the stance phase duration; Joint angle over time; GRF – weight transfer, stability during stance phase and push-off force; External joint moments. Fridman [17] also conducted a similar research on transtibial (TT) prosthesis based on the principle of symmetry. He investigated temporal, step length and foot angle.

Sin et al. [16] had investigated the range of acceptable alignments of transtibial prostheses by including non-level terrains such as walking on ramp and steps. They found that the broad acceptable alignments by the amputees on level walking could be constrained into a much smaller range by non-level walking trials. Figure 2.12 shows that the zone of acceptable alignments of level walking is much broader than at non-level walking. Furthermore the range could be estimated at a smaller range called critical alignment zone. Later, together with Chow et al. [5], they looked for the optimum alignments using the principle of symmetry over a range of AP translational and tilt alignment in TT prosthetics. Fifteen kinematic and kinetic parameters were measured. Different with Hannah, they proposed absolute asymmetry index (AAI) instead of indices of symmetry, as the reference to symmetry. They found that six parameters showed consistent symmetric values and claimed that asymmetry in these values might be an indicator for unacceptable alignments. Eventually, they doubted if there is a unique optimum alignment.

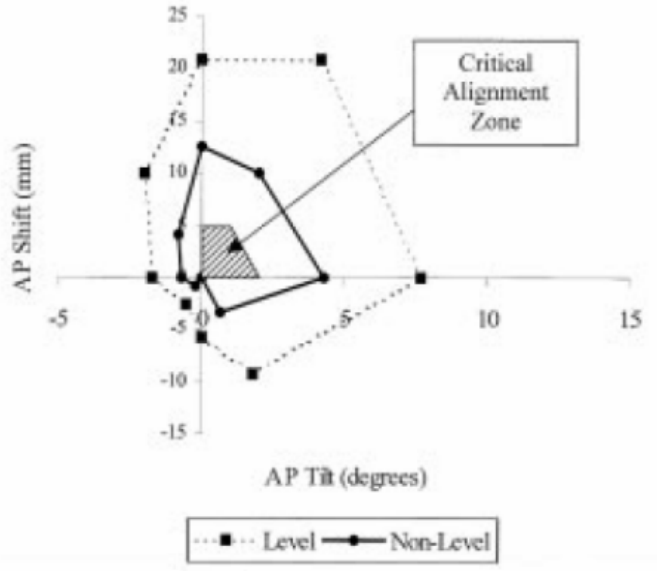

Figure 2.12: Constraint of acceptable alignments [16]

Isokov et al. [3] conducted an experiment to check the effect of varus and valgus tilt of TT prosthesis in quiet stance and proposed three indices to assess the alignments. These indices are Total Sway Activity (TSA) as the resultant of the added forces in AP and ML, Asymmetry (ASYM) of the resultant of subtracted forces in AP and ML and finally Weight-bearing imbalance (WBI).

Geil [70] conducted an experiment by aligning socket tilt angle in AP and ML, and suggested the patterns of insole centre of pressure over a stride as an indicator for the optimum alignment. He noticed the subjects were quickly to adapt to a new alignment.

Hansen et al. [14, 15] published a new idea on the optimum alignment of TT prosthesis by matching the amputee Roll-Over Shape (ROS) to an "ideal" ROS in the sagittal plane (Figure 2.13). He explained that during dynamic alignment, the prosthetists are actually trying to match the optimum alignments with the natural ROS of the amputee. Based on this belief, an automated ROS alignment jig would shorten the process of dynamic alignment in field by finding the optimum alignments in the jig rather than trial-and-error. The optimum position and orientation are computed and later transferred to the jig. This concept may be a future reference guide to complete the aligned prosthesis without going through the process of dynamic alignment. It is questionable at present that an "ideal" ROS achieving from able-bodied could represent the natural ROS of the amputee. Cross relationship of the three-dimensional spatial position and angular alignment parameters towards the "ideal" ROS are still unclear.

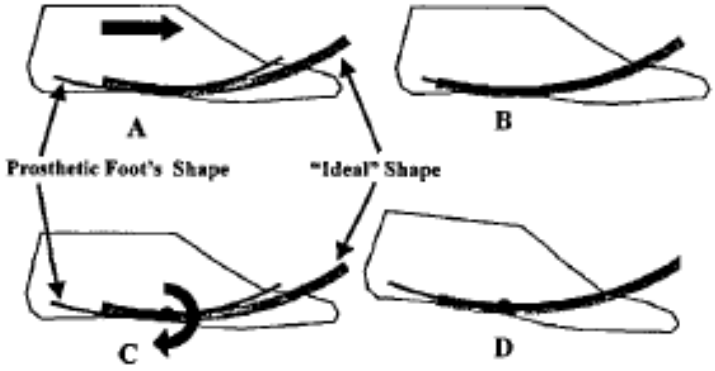

Figure 2.13: Alignments by matching to an "ideal" ROS [15]

Researchers [1, 2, 5, 14, 16, 17, 69] have commented and questioned that a subjective assessment of the dynamic alignment is inefficient, unreliable and insensitive. Geil [60] reported that variability between the prosthetists is small, meaning that consistency exists among the prosthetists. He suggested that an automated alignment system might not be necessary. Nevertheless, his conclusion is not significant since few prosthetists were participated in the study and only one amputee involved.

2.5.4 Common Alignment Values

Radcliffe suggested some alignment parameters and their values but later Zahedi et al. had refined them. They are listed in Table 2.1.

Table 2.1: Common alignments parameters and values [1]

	Zahedi [1]	Radcliffe, [71]
Socket shifts, AP (mm)	20.8	38.1
Socket shift, ML (mm)	-1.9	12.5
Socket tilt, AP (Degree)	4.89	5
Socket tilt, ML (Degree)	3.53	5
Toe Out/In, (Degree)	5.5	-

By means of a new system called Laser Assisted Static Alignment Reference (L.A.S.A.R), Blumetritte et al. [12, 13] concluded that the knee centre should be located 10 to 30 mm posterior to the load line and the optimal is at 15mm. They also stated that the posterior position of the ankle should depend to the foot type and the plantar/dorsi flexion angle should depend on the demand of the amputee.

2.6 Summary

A general review of human biomechanics is reported. Critical definitions in human walking and gait analysis provide a background knowledge for the subsequent works. Many gait analysis instruments are investigated, providing an understanding regarding the technologies available. Disagreements regarding the human biomechanics could also be observed from different human walking models proposed. Specific reviews on the issues of lower limb prosthetic alignments focus

on the problem background, previous research works and arguments. Lastly, the main contributions of this research to the body of knowledge are listed.

CHAPTER 3
AN AMBULATORY SYSTEM

3.1 Introduction

This chapter presents the development of an ambulatory system used for this research. The system includes a miniature battery-powered datalogger, five Inertial Measurement Units (IMUs), IMU fixtures, a vest as the system carrier and other connecting cables to measure kinematic properties at the BCOM, the thighs and the shanks. At present, for simplicity reasons, the foot is excluded from the investigation since it comprises of multi-linked bones and joints, exhibiting complex motions in many degree-of-freedom. Calibration of the datalogger is demonstrated. IMU calibration requires a lengthy explanation and will be introduced in Chapter 4. Five critical body landmarks to mount the IMUs are specified. A new notation to replace the original IMU axes at these body landmarks is recommended. The new notation will provide a uniform reference for the subsequent works. Preliminary trials on level walking were performed to check the function of the ambulatory system. The results of these trials are reported in this chapter.

3.2 Background

In the prescription point of view, it could be impractical and costly in clinical practices to spend excessive time on a patient. Gait observation during a schedule gait trial could be insufficient to provide sufficient gait data for analysis. Moreover, the amputee would adapt to a new gait pattern over the long run upon any alignment updates. An ambulatory gait measurement system which could continuously collect sufficient amount of gait data out of the clinic could achieve this objective to a certain extent.

Table 3.1: Literature reviews of accelemetric and gyroscopic devices

No	Author	Sensor Type	Sensor Brand	Input	Location	Sampling Freq. (Hz)	Datalogger
1	Moe-Nilsen [72]	*acc*	Logger Technologi HB	3	BCOM	128	Portable PMCIA datalogger, Logger Tech., Sweden
2	Tong [33]	*gyro* *FSR*	Murata, ENC-05EA *nm*	2 4	Shank, Thigh Insole	50	Portable. Verified with a motion capture system, Vicon
3	Aminian [32]	*gyro* *FSR*	Murata, ENC-03J Interlink, LU	3 2	Shanks, right thigh Insole	200	Portable. Physilog, BioAGM, CH
4	Moe-Nilsen [73]	*acc*	Logger Technologi HB	3	Trunk (L3)	128	Portable PMCIA datalogger, Logger Tech., Sweden
5	Auvinet [74]	*acc*	Locometrix™	2	Trunk (L3-L4)	50	Portable. Locometrix™
6	Mansfield [30]	*acc* *FSR*	Analog D., ADXL202 *nm*	2 1	Trunk Heel	200/500	Portable. BM42, Biomedical Monitoring Ltd.

Table 3.1 (continued): Literature reviews of ambulatory devices

No	Author	Sensor Type	Sensor Brand	Input	Location	Sampling Freq. (Hz)	Datalogger
7	Pappas [34]	*gyro* *FSR*	Murata, ENC-03JA Interlink, 152NS	1 3	Foot Insole	100	Portable. BX-24 board with microcontroller (ATMEL) from NetMedia, Inc.
8	Luinge [75]	*IMU*	Murata, ENC-05 *Analog D., ADXL05*	6 x 2	Pelvis Trunk (T4-T5)	100	Portable. Verified with a motion capture system, Vicon.
9	Henriksen [76]	*acc*	Mega Electronics	3	Trunk (L3	250	Portable.
10	Luinge [77]	*IMU*	Murata, ENC-05 Analog D., ADXL05	6 x 3	Pelvis Trunk (T10) Forearm	100	Portable. Verified with a motion capture system, Vicon.
11	Jasiewicz [78]	*IMU* *FSR*	Murata, ENC-03JA Analog D., ADXL202 MIE, Leeds	3 x 2 2 x 2	Foot Insole	200 25	Microprocessor (AT-Mega103L, ATMEL) PDA
12	Torrealba [79]	*acc* *pot*	*nm*	2 x 2 1	Thigh, shank (Knee angle)	50	Portable. Customized microcontroller.

Table 3.1 (continued): Literature reviews of ambulatory devices

No	Author	Sensor Type	Sensor Brand	Input	Location	Sampling Freq. (Hz)	Datalogger
13	Lau [31]	*IMU* *FSR*	Murata, ENC-03J Analog D., ADXL202E *nm*	3 x 3 4	Thigh, shank, foot Insole	240	Vicon 370
14	Takeda [80]	*IMU*	Murata, ENC-03M Hitachi Metals, H34C	6 x 7	Abdomen, thighs, shanks, foots	100	Portable. Verified with a motion capture system.
15	Torrealba [79]	*acc*	*nm*	2 x 2	Thigh, shank	60	Stationary station
16	González [81]	*acc*	Xsens, MTx	2	Trunk (L3)	100	Stationary station. Verified with a motion capture camera system and s force platform.
17	Gouwanda [82]	*IMU*	Microstrain, Inertia-Link (wireless)	6 x 4	Thighs, shanks	200	Stationary station. Labview 8.5

nm *not mentioned*
acc *accelerometer*
gyro *gyroscope*
IMU *Inertial Measurement Unit (accelerometer + gyroscope)*
FSR *Force Sensitive Resistor*
pot *potentiometer*

Many ambulatory systems utilize miniature motion sensors that are light-weight, compact size and battery-powered such as accelerometer and gyroscope, working along with a portable datalogger. Many of these devices were tested by the researchers as listed in Table 3.1. A rather recent review regarding the ambulatory system was published by Rueterbories et al. [83]. MEMS type accelerometers and gyroscopes such as ADXL202 (Analog Device) and ENC-03J (Murata) are applied as motion feedback sensors in many applications including gait monitoring. These type of sensors are light weight and are reasonably precise. They are rather low-cost in the form of integrated circuit (IC) but could become expensive if incorporated in a commercial solution such as Inertia Link (Microstrain) and MTx (Xsens). The motion feedbacks from the sensor are available in single, dual or triaxial, dependant to the need of the application. It is vital to measure motions in anterior-posterior (AP), medial-lateral (ML) and vertical directions during human walking. A number of body landmarks are chosen as the position to mount the devices, ranging from the body trunk, thighs, shanks and foots. The sensors localized in the above body landmarks could reveal critical kinematic information regarding the gait.

The data logger for an ambulatory system must be light weight, compact size and battery-powered. A commercial portable datalogger is usually expensive and its price could escalate with the additional selection of input/output (IO) channels, storage size and features such as wireless, communication using Bluetooth or USB port. Detail information of commercial dataloggers could be assessed online or via a sale representative. Another option for the researchers is to build the datalogger using a programmable controller or a personal digital assistant (PDA). Electronic and programming literacy are necessary in order to build a customized system. Building a customized data logger could offer a few advantages such as low cost, flexibility in IO expansion according to requirements, storage option and communication option. Human gait data collection does not need a high sampling rate since a normal human walking is slow. Sampling frequency as low as 25Hz is sufficient for most applications regarding the study of human walking. Setting a higher sampling frequency is possible if the datalogger could support it and the storage size is big enough to accommodate the data during data collection.

Some researchers justified the reliability of the system using another instrumental reference such as the knee angular reference from a potentiometer, the gait tempo feedback from insole FSRs [30-34, 78], the kinematic reference from a

motion capture camera system [33, 75, 77, 80] and the kinetic reference from a force platform [81]. Another way to justify the reliability of the system over a duration is to use a statistical analysis [31, 72, 76] such as a test-retest reliability.

3.3 Aims and Objectives

The aim of this project is to design and develop a low-cost ambulatory system for the purpose of assessing objective gait quality for the lower limb prosthetic alignment. The ambulatory system consists of motion sensors and a portable datalogger. Multi axial sensory kinematic information at the lower limbs and the pelvis are to be collected using the motion sensors.

It is decided to monitor multi-axial kinematic information at the BCOM, the thighs and the shanks. At the time of this investigation, an off-the-shelf IMU with five degree-of-freedom (dof) is available in a single PCB breakout (SparkFun Inc., http://www.sparkfun.com/) offered at the lowest price as compared to others. Practically, it is possible to apply more IMU with more than 5 dof. It is intended to measure accelerations in the unit of g collected from above body landmarks in AP, ML and vertical directions. Angular velocities are measured at the thighs and the shanks in lateral and frontal planes. Meanwhile body twisting at the transverse plane and the lateral plane during walking are also measured. In total, the research needs a datalogger that accommodates 25 analog inputs (5 IMU-DOF x 5 body landmarks). However, commercial dataloggers with high number of analog inputs ports are expensive and it is out of the research budget. A customized datalogger is proposed.

The system should meet these requirements:

The datalogger:

1. Light-weight and portable
2. Battery powered
3. Sampling rate at least twice the walking frequency but not too high since sufficient data storage is needed for the duration of trials.
4. Able to accommodate at least 25 analog input channels
5. Sufficient data storage (at least for the duration of trials)

IMU:

1. Light-weight and portable
2. Multi axial accelerometer and gyroscope

3. Powered at 3.3VDC

Other fixtures to accommodate the datalogger and the IMUs onto the body must be easily detachable and light-weight.

3.4 Datalogger

The datalogger consists of a microcontroller, analog inputs, data storage, LCD display, a battery, power regulator and connecting cables and ports. Technical information regarding the Mbed microcontroller, Serial Peripheral Interface (SPI), Analog-to-Digital converters and the secure digital (SD) card are available in Appendix A.

3.4.1 Circuitry, PCB and others

The circuitry and the PCB boards are designed using a computer aided design (CAD) software called Eagle V5.5.0. To make the datalogger compact size, two PCB (3" x 4") boards, i.e. the main board and the sub-board are stacked. The main board (Figure 3.1) consists of a Mbed microcontroller, a circuitry for 5VDC power regulator using LM7805 and other connecting pins. A 9VDC battery is used as the DC power source. The sub-board (Figure 3.2) consists mainly the IO expansion chips (MCP3008) and connecting pins. The peripheral ports are connected to the sub-board. Both PCB board drawings are shown in Figure 3.3.

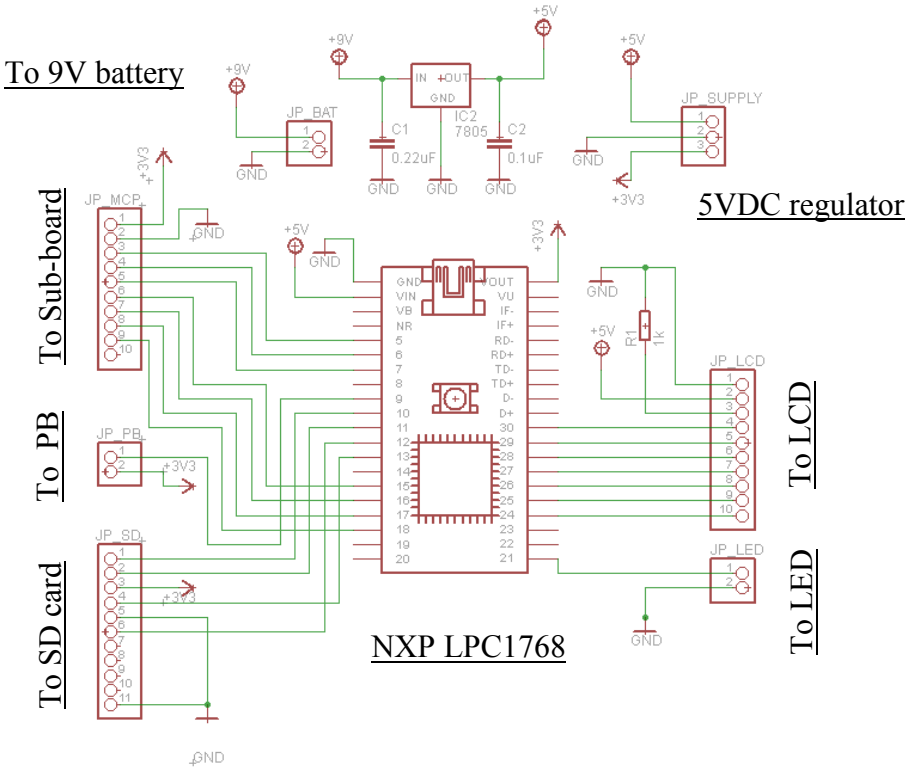

Figure 3.1: Main board circuitry

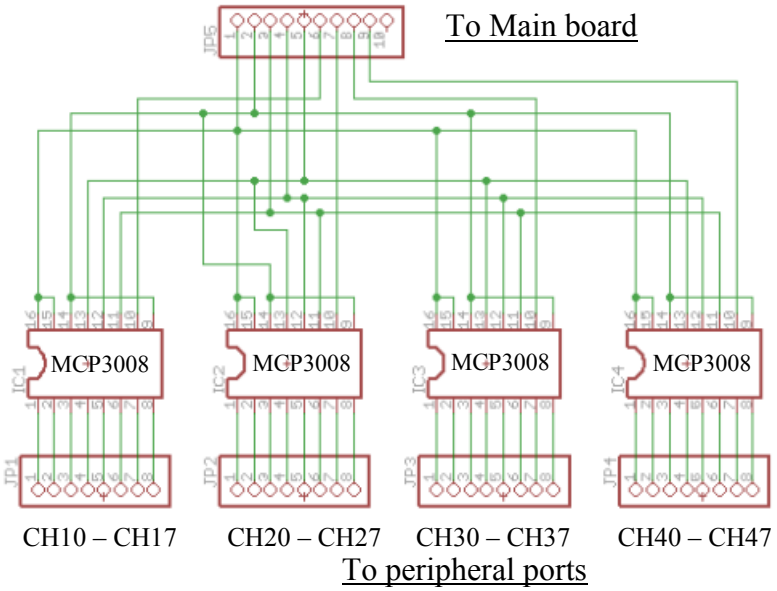

Figure 3.2: Sub-board circuitry

(a)

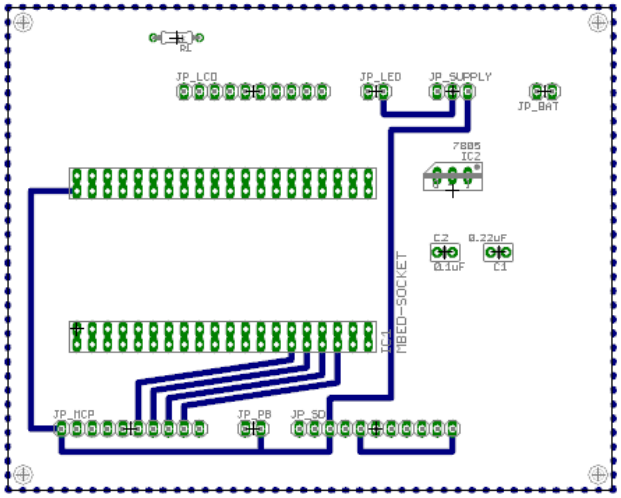

(b)

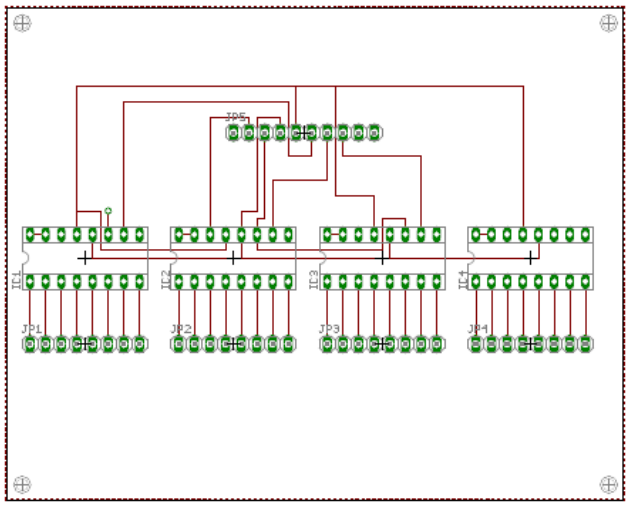

Figure 3.3: PCB board drawing of (a) main board (b) sub-board

3.4.2 Assembly of the Datalogger

The datalogger is assembled as shown in Figure 3.4. It has 32 analog input channels, 200Hz sampling rate, a 2x16 LCD display, 1GB storage using a Secure Digital (SD) card, a LED to indicate the data logging event and a push button (PB) to trigger the data logging events. Six peripheral ports made from 10 ways IDC sockets are labelled as shown in Figure 3.5. The IO assignment between the analog input channels and the IMUs via the peripheral ports are shown in Table 3.2.

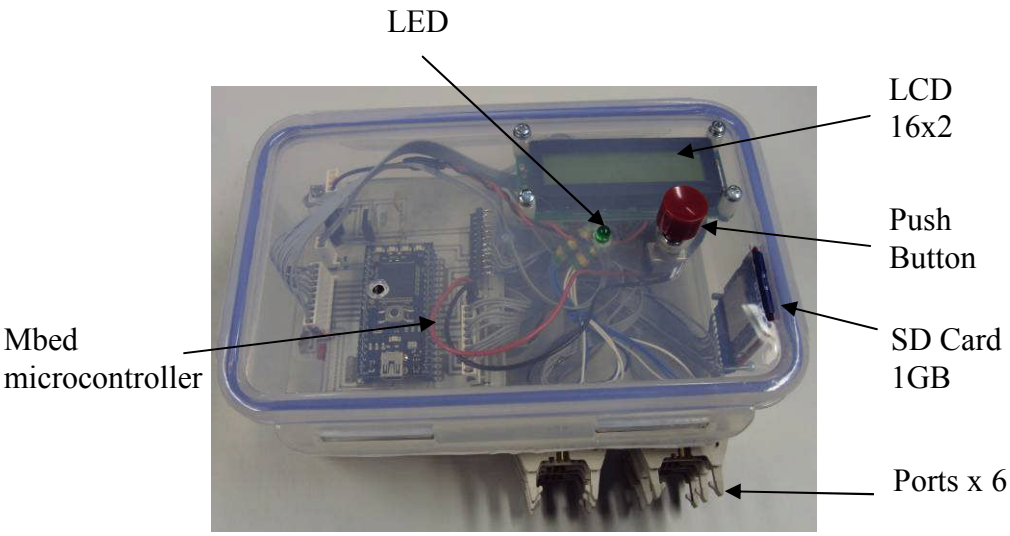

Figure 3.4: The datalogger

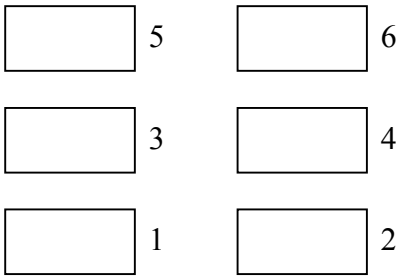

Figure 3.5: The peripheral ports and socket numbers (as shown in Figure 3.4, Ports x 6)

Table 3.2: IO assignments for the datalogger and IMUs

Header/ socket pins	IMU pins	Socket 1	Socket 2	Socket 3	Socket 4	Socket 5	Socket 6
1	3.3VDC	3.3VDC	3.3VDC	3.3VDC	3.3VDC	3.3VDC	Spare
2	GND	GND	GND	GND	GND	GND	Spare
3	XR	CH13	CH20	CH25	CH32	CH37	Spare
4	YR	CH14	CH21	CH26	CH33	CH40	Spare
7	Z	CH12	CH17	CH24	CH31	CH36	Spare
8	Y	CH11	CH16	CH23	CH30	CH35	Spare
9	X	CH10	CH15	CH22	CH27	CH34	Spare

3.4.3 The Program

Mbed (http://mbed.org/) provides an online C editor and compiler. Program could be written in the editor provided. The program must be compiled into a binary file before transferring the compile file into the microcontroller via a USB cable. Many tested libraries such as SPI protocol, SD file system FAT16, standard IO addressing protocols etc. are provided online. The program is planned as shown in Figure 3.6. Upon being powered, the system is initialized (if the pushbutton is switched off) to these states:

1. the LED off
2. the LCD displays: zero count, zero elapsed time, 'temp1.csv'
3. Set SPI clock frequency for MCP3008 equals to 1MHz.
4. No data is collected. Stay idle.

Once the pushbutton is on and locked, a timer is triggered on to keep a record of the elapsed time. Meanwhile a counter is adding itself in every loop. The loop calls a SPI subroutine for each MCP3008 consecutively and writes sampled integer data from each input into a file of comma-separated values (CSV) format. The integer ranges from 0 to 1023 (10 bits) which corresponds to 0 to 3.3VDC. A delay is added at the end of loop for sampling frequency adjustment. Once the pushbutton is off, total elapsed time and total counter number are written to the last line of the CSV file. The LCD display as shown in Figure 3.7 shows the total count number and total elapsed time on first line and next CSV file number in the second line. The sampling frequency in the unit of Hertz (Hz) could be calculated as total count divided by total elapsed time. The program is included in Appendix B.

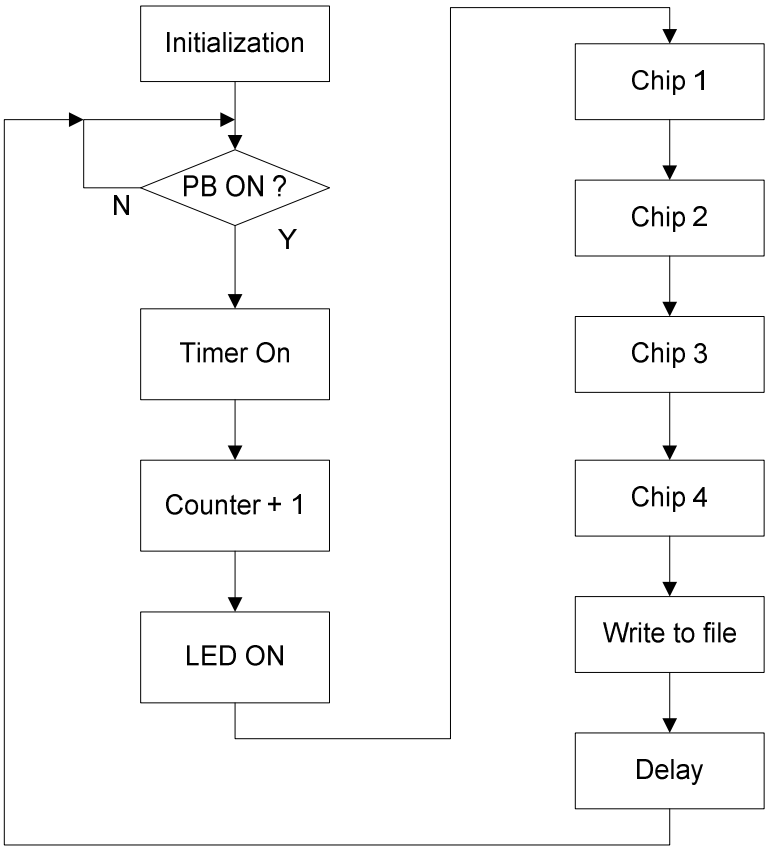

Figure 3.6: Mbed microcontroller programming logic flow

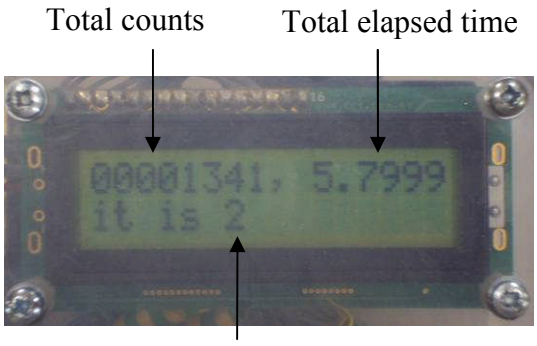

Figure 3.7: LCD display message

3.4.4 Calibration of the A/D Input Channels

The calibration is needed for two purposes. Firstly, a linear model could be formulated based on the data collected. Secondly, the error margin of the datalogger could be identified. All analog input channels are connected together and calibrated by varying an input voltage from 0V to 3.3V and from 3.3V to 0V, stepping at 0.1V

interval for approximately 10 seconds per sample. The result of voltages versus discrete numbers (2^{10} = 1024) per collected samples is shown in Figure 3.8. Equation (3.1) represents the digital-to-analog (D/C) relationship between the measured voltage (V) and corresponding digital number (N). The voltage error margin as represented in equation (3.2) is defined as the maximum standard error of the collected samples within 95% confidence interval. The voltage margin error (e_{max}) is found fluctuating around 6.7mV.

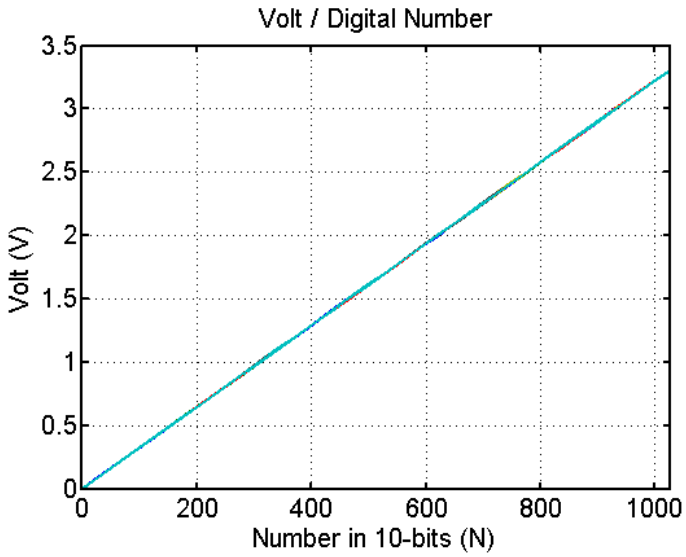

Figure 3.8: Calibration of 32 analog input channels

$$\boldsymbol{V = \frac{N \times 3.3}{1024}\ (V)} \tag{3.1}$$

$$\boldsymbol{e_{max} = \mp 1.96\ \mathrm{SE}_{\max}\ (V)} \tag{3.2}$$

3.5 Inertial Measurement Unit

Two types of IMU (SparkFun Inc., http://www.sparkfun.com/) are used in this application. They have five degree of freedom (dof). IMU type 1 consists of a triaxial accelerometer (ADXL330) and a gyroscope (IDG300). IMU type 2 consists of a triaxial accelerometer (ADXL335) and a gyroscope (IDG500). Both types (shown in Figure 3.9) are in the form of a PCB breakout of size 20x23mm and are light-weight (2g). Five units of IMUs are assigned to be mounted at five body segments located at the shanks, the thighs and the sacrum (BCOM). Meanwhile five

simple fixtures of size 70x22x35 (mm) such as shown in Figure 3.10 were designed and fabricated from acrylic. Mounted with the IMUs, these fixtures were stitched into flexible straps and Velcro patches. The triaxial accelemetric axes are labelled as (X, Y, Z) while the dual-axial gyroscope axes are labelled as (XR, YR). The axes are defined using Right-hand rule (RHR). It is worth noting that the gyroscope, IDG500's outputs are negative in counter clockwise direction (CCW), which do not agree with the RHR as shown as in Figure 3.9b.

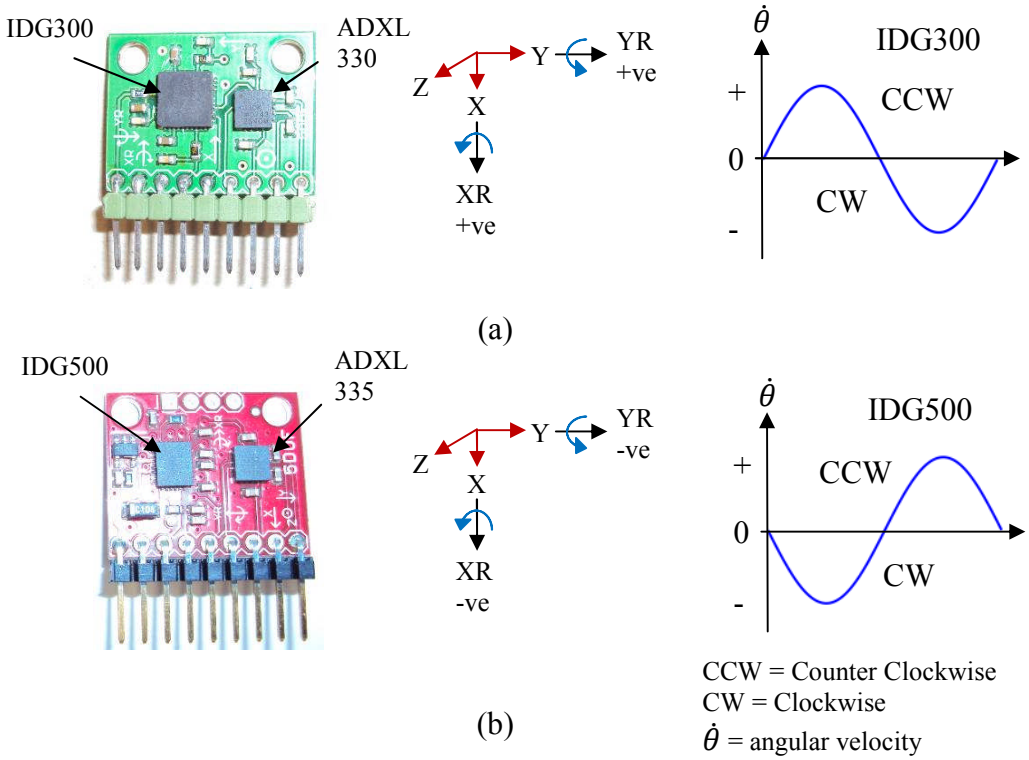

Figure 3.9: IMU. (a) Type 1 - ADXL330/IDG300 (b) Type 2 - ADXL335/IDG500

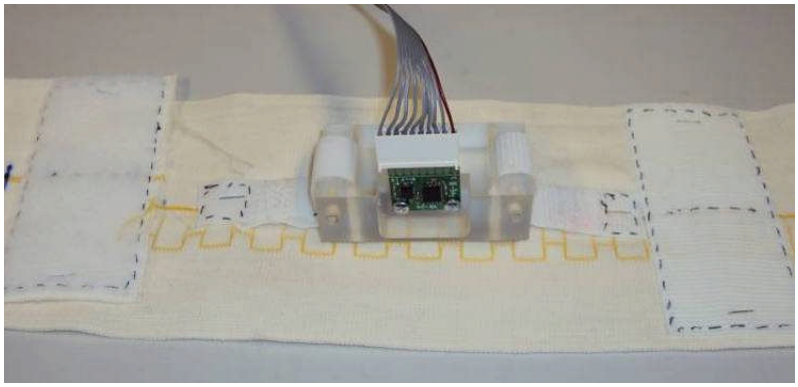

Figure 3.10: The fixture and strap of an IMU

3.6 The Ambulatory System

The assembled ambulatory system is shown in Figure 3.11. The IMUs are strapped at the lateral shanks, the lateral thighs and the sacrum (BCOM). At the time of this investigation, an off-the-shelf IMU with five degree-of-freedom (dof) is available in a single PCB breakout (SparkFun Inc., http://www.sparkfun.com/) offered at the lowest price. Practically, it is possible to apply more IMU with more than 5 dof. It is intended to measure accelerations in the unit of g collected from above body landmarks in AP, ML and vertical directions. Angular velocities are measured at the thighs and the shanks in lateral and frontal planes. Meanwhile body twisting at the transverse plane and the lateral plane during walking are also measured. All IMUs are connected to the datalogger using IDC sockets and flat cables. Table 3.3 lists the IMU allocation at the predefined body landmarks and their connection to the datalogger. The IMUs are located at the predefined body landmarks by visual judgement and palpation. The repeatability of the instruments and its sensory installation are statistically checked using test-retest reliability (see Chapter 5). The cables are tidied neatly to minimize tripping during walking. A vest is put on and the datalogger is stuck onto it as shown using Velcro patches.

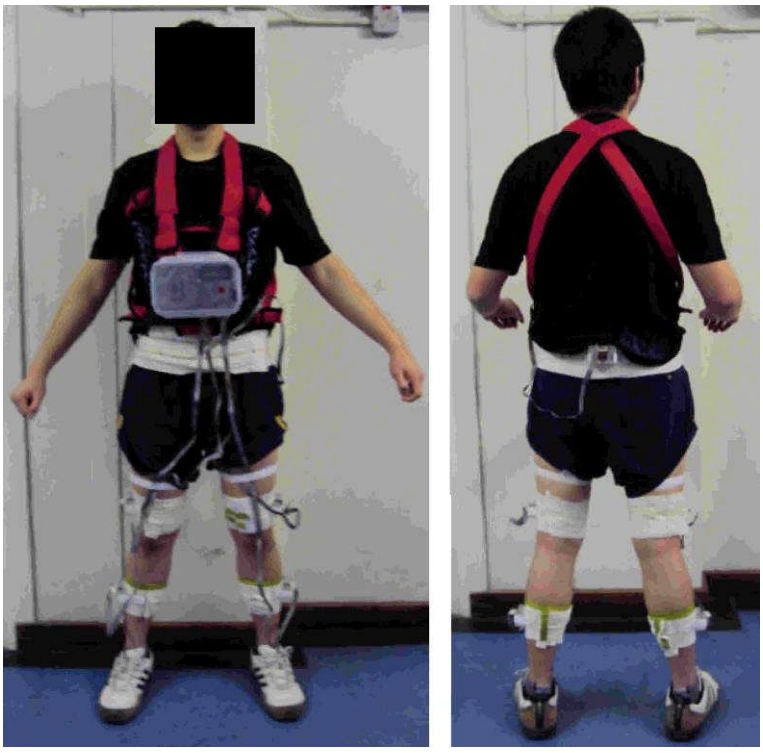

Figure 3.11: The ambulatory system

Table 3.3: IMU allocation at the predefined body landmarks

IMU No	Components (Accelerometer plus Gyroscope)	Body Landmarks	Datalogger Socket No.
1	ADXL330, IDG330	Lateral Right Shank	1
2	ADXL330, IDG330	Lateral Left Shank	2
3	ADXL330, IDG330	Lateral Right Thigh	3
4	ADXL335, IDG500	Lateral Left Thigh	4
5	ADXL335, IDG500	BCOM	5

3.6.1 The Body Landmarks and Their Axes Assignments

A set of original IMU axes at the predefined body landmarks is defined in Figure 3.12(a). The original IMU axes impose several issues during the interpretation of the body movements.

1. Y-axes of the left leg and the right leg are in the opposite direction
2. XR-axes of the left leg and the right leg are in the opposite direction

A new notation is proposed in replacement of the original IMU axes. The new notation converts the IMU axes into the body axes. All gyroscope axes in CCW are positive. Table 3.4 lists the rules for the conversion. Figure 3.12b shows the IMU axes assignments after the conversion.

Table 3.4: Rules for the conversion from the IMU axes to the body axes

No	Both legs	BCOM
1	X points laterally.	X points vertically
2	Y points anteriorly.	Y points laterally
3	Z points vertically.	Z points anteriorly
4	XR is +ve when the shank swings anteriorly.	XR is +ve when the body turns right to left.
5	YR is +ve when the shank swings medially.	YR is +ve when the body leans forward.
+ve = positive		

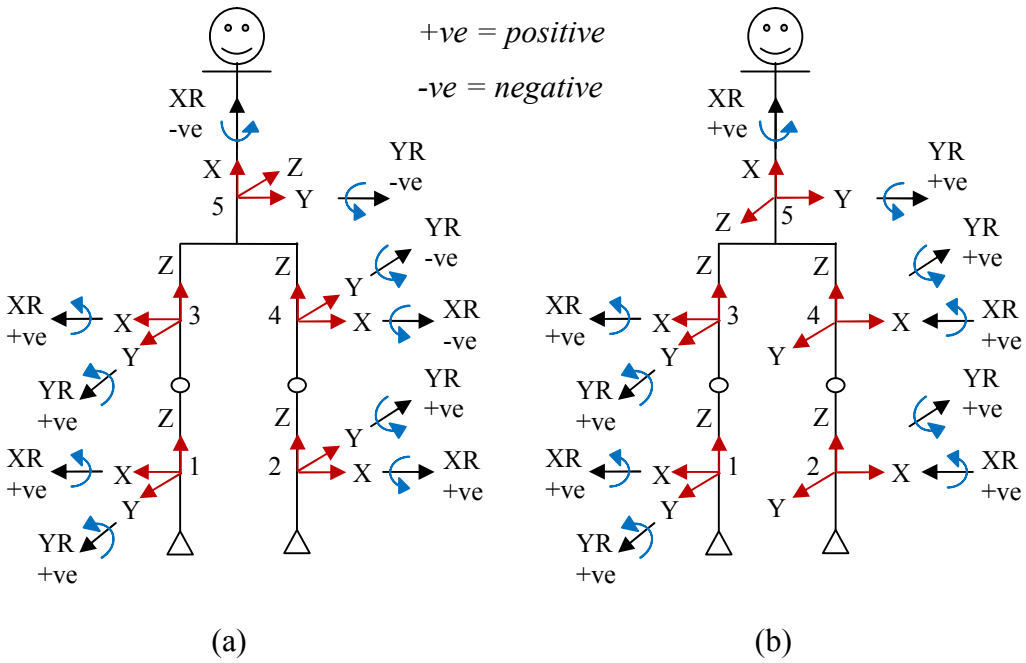

Figure 3.12: IMU. (a) Original Axes (b) Body Axes

3.6.2 Preliminary Trials

For preliminary trials, a healthy subject was recruited. The subject put on the system and walked on a flat gangway for a few trials. The trials showed promising results before converting the measurements into relevant kinematic data. Preliminary results in the original IMU axes at BCOM, left/right thighs and left/right shanks are shown in Figure 3.13, Figure 3.14 and Figure 3.15 respectively. The plotted signals are not filtered nor transformed into the body axes as proposed above. These results are in term of volt (V) versus time (s). It is noted that (Y, XR) of the right shank are opposite to the left shank. This is the main reason for a new notation in the body axes.

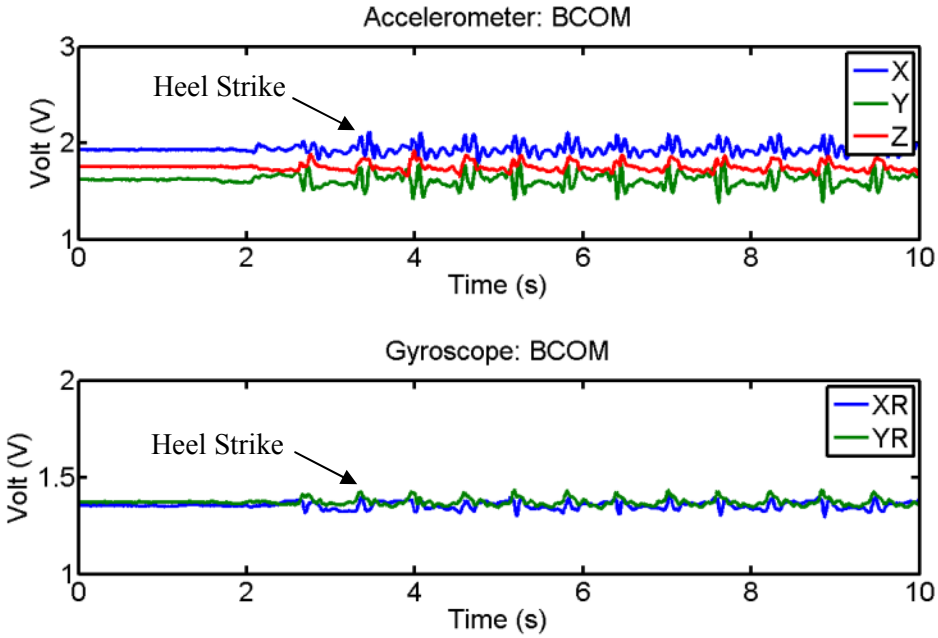

Figure 3.13: Preliminary results of BCOM

(a)

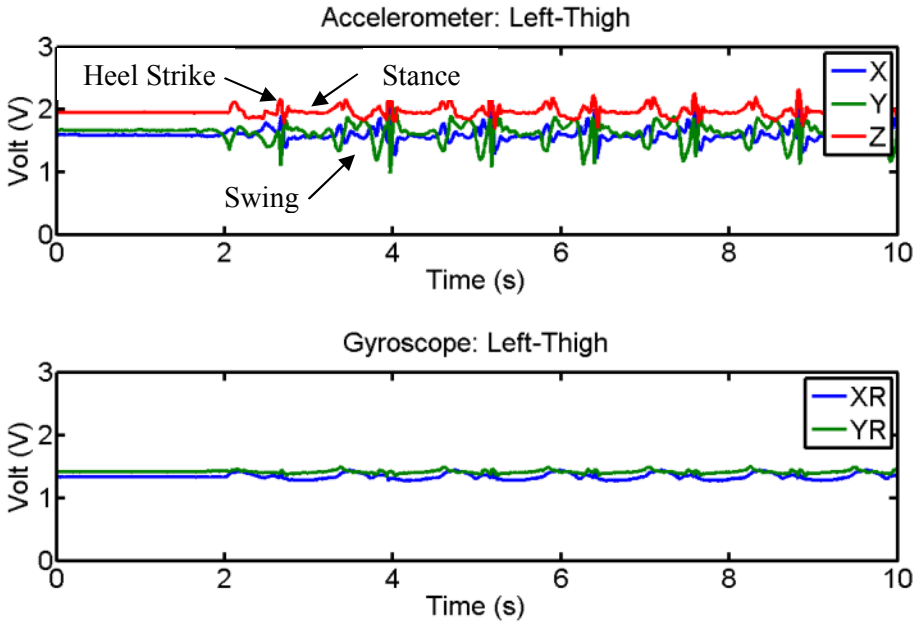

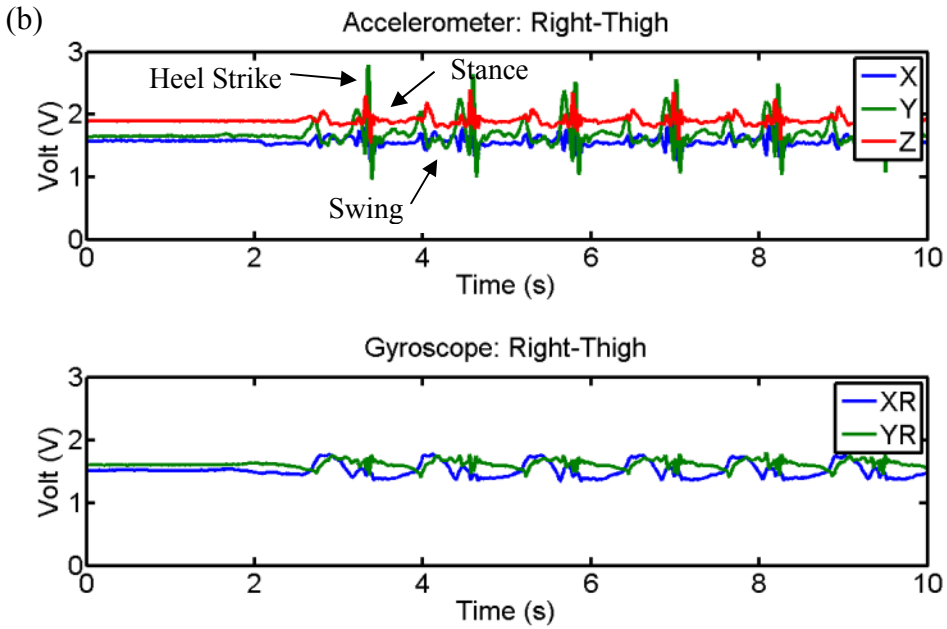

Figure 3.14: Preliminary results of (a) left thigh (b) right thigh

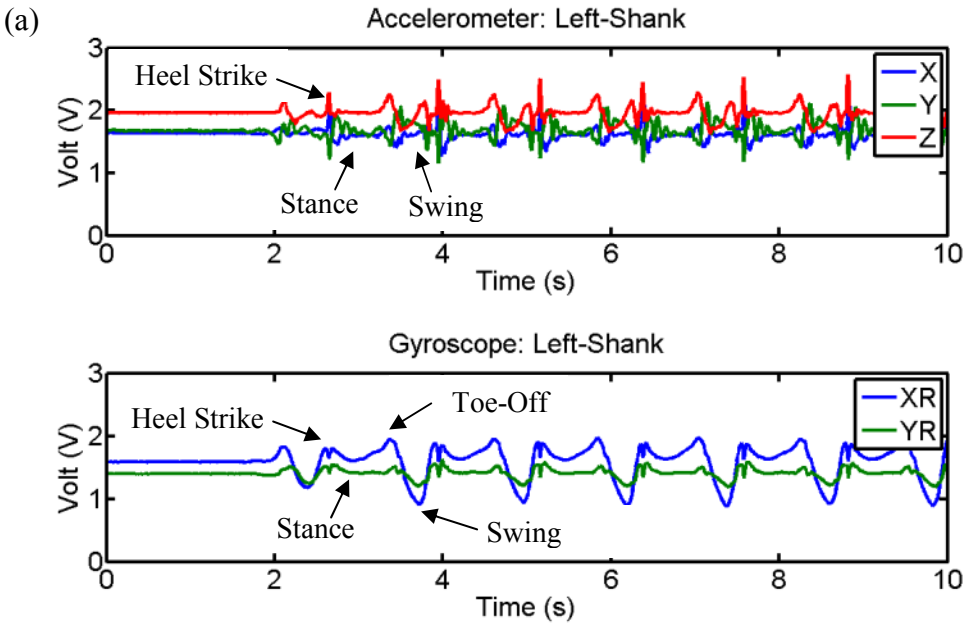

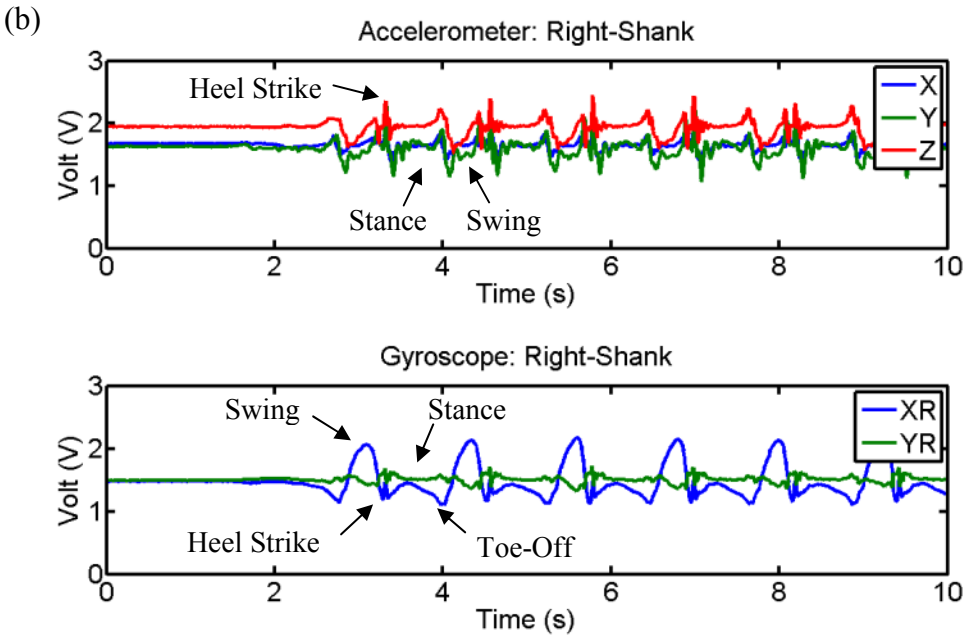

Figure 3.15: Preliminary results of (a) left shank (b) right shank

The IMUs outputs in their pre-assigned axes could describe the gait as interpreted according to the gait definitions. The IMUs were able to display the motion of the body and the lower limb segments. These rhythmic cycles reveal crucial kinematic information from each body landmark as the subject was walking naturally on a flat gangway. The gait information could be interpreted qualitatively from the above figures in the direction of the IMU assigned.

IMU outputs reveal accelerations and angular velocities in the assigned axes and planes. These outputs viewed from different body aspects show that walking performance could be observed as a highly synchronization of body sway and body bobbing up and down. As the subject walked, cyclic body sways in AP and ML directions could be interpreted from relevant IMU outputs. During the progression of walking, cyclic body bobbing up and down were also observed in both the AP and vertical directions. IMU at the BCOM revealed the body motion as the body fell forward and was supported by the limbs cyclically. In addition, due to the gyroscopic axis (XR) assigned in the direction of the spine, body twists to the left and the right during walking were observed. Other IMUs located at the thighs and the shanks were able to reveal kinematic information of the lower limbs as the body fell and was supported by the lower limbs.

At the stance phase, the leg is in contact with the floor. At the beginning of the stance phase, significant accelemetric spikes (X, Y, Z) were observed cyclically.

An accelemetric spike (Heel Strike) was the result of a sudden impact at the moment that the heel was in contact with the floor. At the beginning of the stance, the heel contact on the floor also caused a sudden angular velocity drop, which could be observed easily from the shank lateral gyroscopic outputs (XR). By comparing on the same time axis, the number of spikes at the BCOM were twice the number of other leg segments, indicating steps information from each legs. The timing of the accelemetric spikes of the left leg and the right leg were offset at a step cycle repetitively. At mid stance, the subject was in single stance and the body swung forward like an inverted pendulum, supported on a leg. There were small excursions of accelemetric and gyroscopic changes being observed during single stance.

At the swing phase, the leg is swinging forward like a pendulum. The swings at the left leg and the right leg were offset at a step cycle repetitively. Of all body landmarks, the shanks revealed the most significant feature of the swing. At terminal stance, the ankle is raised on the ball of the foot before toeing off (Toe-Off) the floor. A sudden change in the shank lateral gyroscopic output explained this gait definition. At the shanks, near sinusoidal excursions were observed during the swing phase. Lateral gyroscopic outputs (XR) were the most significant. The leg swings effortlessly from posterior to anterior. The swing does influence the leg accelerations especially the shanks. Accelerations dropped, beginning from the onset of the swing until heel contact. The magnitudes of outputs at the shanks were the highest, followed by the thighs and the BCOM. Thighs excursions were earlier than the shanks, suggesting that the thighs could be the voluntary control of the leg. The stance and the swing phases repeat.

3.7 Summary

An ambulatory system to measure the kinematic properties of the lower limb body segments and BCOM is introduced. The development procedures are presented to meet the system requirements. A rapid prototyping microcontroller from Mbed with strong online supports is used to design the datalogger. All devices are checked and tested for their functions. Five critical body landmarks to be mounted with an IMU at the shanks, the thighs and BCOM are introduced. A new notation based on the body axes is recommended to replace the original IMU output axes. Preliminary results show promising repetitive IMU outputs during normal level walking.

CHAPTER 4
STATIC AND DYNAMIC CALIBRATION OF AN IMU

4.1 Introduction

Inertia Measurement Units (IMUs) of microelectromechanical (MEMS) type are becoming popular in many applications related to the studies of motions such as gaming, navigation, gait analysis etc. Some researchers have attempted to fuse a magnetometer into an IMU but in this chapter, an IMU as an integrated system of a triaxial accelerometer and a dual-axial gyroscope is demonstrated. An accelerometer would measure the linear accelerations in the directions of its axes while a gyroscope would measure the angular velocities about its rotating axes. Before use, the accelerometer and the gyroscope are required to be calibrated under certain procedures. This chapter will demonstrate the calibration techniques of IMUs. The calibrated procedures are suitable to most IMUs.

Calibrations are essential to determine: firstly, scale factors and zero biases in every IMU axis; secondly, repetitive performances of the sensory unit. There are two major categories of calibrations, i.e. static calibration and dynamic calibration. Static calibration measures repetitive performance of an IMU when it is oriented in a set of known stationary positions related to the gravity. This method is particularly crucial to the calibration of an accelerometer where its axial outputs are relative to the gravity. Three static calibration techniques are demonstrated. They are the rotary table method, the six/twelve-known positions method, and the in-use calibration. Conventionally, a rotary table rotating in a vertical plane is used to statically calibrate an accelerometer. Using this method, every plane (XY, YZ and ZX) of an IMU can be calibrated separately. On the other hand, according to the working principle of an accelerometer, two simplified methods of calibrations, i.e. six-known

positions and twelve-known positions are proposed. These methods calibrate a triaxial accelerometer using known permutations of a cube. Lastly, an in-use calibration method as proposed by Lotters [84] is attempted. This method identifies and extracts quasi-static positions from dynamic motion data. At quasi-static positions, the norms of a triaxial accelemetric outputs are assumed to be equal to 1g. Using this principle, a triaxial accelerometer is modelled as a cost function which is a function of voltages and the setup parameters. Given the corresponding voltages during quasi-static moments, the setup parameters (scale factors, zero biases and inter-axis misalignment errors) are computed by optimizing the cost function. Statistical analysis is applied at all the methods above. Mean results are eventually calculated and used. Standard error is used as an indicator to show the variation of a result. The static calibration techniques mentioned are then compared and discussed regarding some practical considerations such as cost, time, computational time, accuracy etc.

Dynamic calibration measures repetitive performance of an IMU during specific motions, particularly in a known rotating motion. This calibration serves two purposes. Firstly, it is specifically crucial for the calibration of a gyroscope since it measures rotation. Secondly, this method is also used to validate an IMU outputs under a predefined motion using the principle of circular motion. A pendulous test rig is designed to be used for the required experiments.

For the purpose of this research, the calibration ensure that the IMUs are performing in the expected kinematic ranges with known marginal errors.

4.2 Inertial Measurement Unit

The sensory units [85] is small in size, light-weight, inexpensive, reliable, consuming low power and easily available from the market. An IMU consists of an accelerometer which measures the linear acceleration of a motion in the unit of the gravity and a gyroscope which measures the angular velocity about a rotating axis. Their working principles are briefly explained below.

4.2.1 Accelerometer

An accelerometer is a device to measure the linear acceleration of the device itself. The measurement unit is often reported in the unit of the gravity or g-force. The

working principle is based on Newton's Laws and could be illustrated using a system of a proof mass and a spring as shown in Figure 4.1. The force (f) is an inertial force when the accelerometer is accelerated. According to Hooke's Law, the spring displacement while the spring is working within the elastic limit is proportional to the force applied onto it.

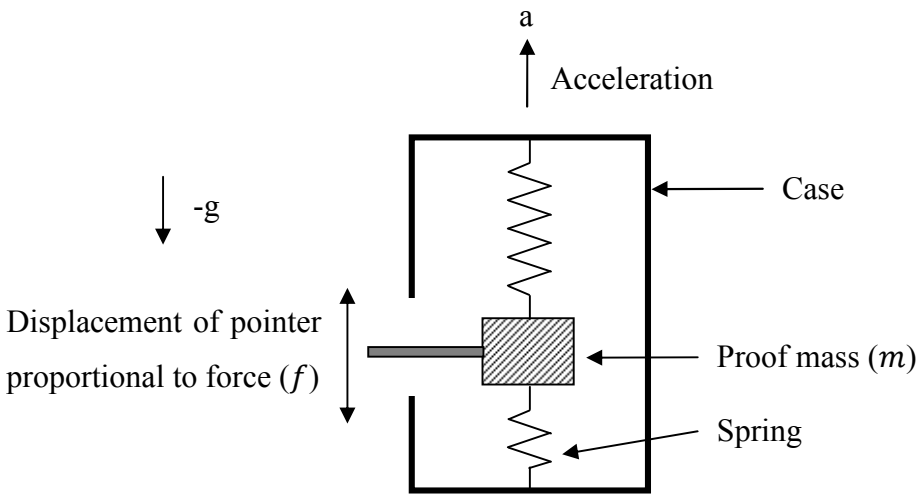

Figure 4.1: A simple accelerometer. Redrawn from [85]

The total force ($F = ma$) acting onto the mass as shown in equation (4.1) is the sum of the inertial force (mf) and the weight of the mass (mg) under the effect of the gravity. During static or moving in a constant linear speed, the inertial force (f) will be zero leaving only the gravitational term in the equation. The formula represents the acceleration per unit mass.

$$\boldsymbol{F = ma = mf + mg} \qquad \textbf{(4.1)}$$

The accelerometers are available in single axial, dual axial or tri-axial models. There are a number of constructions for the accelerometer but are working under the same principle. Piezoelectric, piezoresistive or capacitive components are used to construct an accelerometer. These products are often applied in commercial or industrial applications. More recently, microelectromechanical (MEMS) accelerometers in the form of an integrated circuit appear in many applications such as automobile, gaming, medical studies etc.

Practically, the acceleration is often modelled linearly in proportional to an electrical output. In the simplest form, the accelerometer could be modelled as

equation (4.2). The accelerometer is ratiometric, meaning that the outputs are in proportional to the supply voltage. Hence, it is essential to regulate a constant and stable voltage supply to the accelerometer. A static calibration will identify the scale factor and the zero bias of each operational axis.

$$\boldsymbol{V = k.s + b} \tag{4.2}$$

where,

$\boldsymbol{V}$	*accelerometer output in the unit of volt (V)*
$\boldsymbol{s}$	*acceleration in the unit of gravity (g)*
$\boldsymbol{k}$	*scale factor in the unit of volt/g*
$\boldsymbol{b}$	*zero bias in the unit of volt*

4.2.2 Gyroscope

A gyroscope is a device to measure the angular velocity of a rotation about an axis. The measurement unit is reported in degree per second $(°/s)$ or radian per second (rad/s). The working principle of a gyroscope is based on the Coriolis effect as illustrated in Figure 4.2. In dynamics, a proof mass experiences Coriolis acceleration [85] that is perpendicular to the plane of rotating axis (ω) and moving direction (v). The Coriolis force is the cross product of the linear motion and rotation. Generally, the construction of a gyroscope would implement a vibratory proof mass as a reference of the linear motion. On the occurrence of a rotation, the Coriolis force would tend to vibrate the vibrating mass accordingly in orthogonal directions. The vibration is electrically measured and processed before modelled linearly proportional to the rotation.

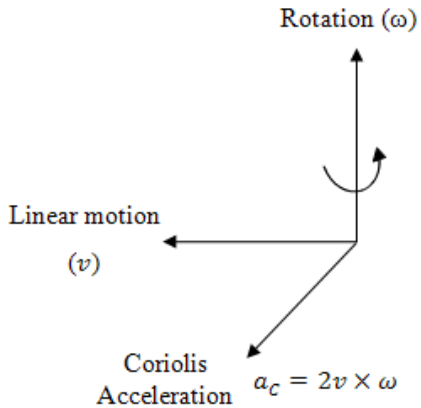

Figure 4.2: The principle of Coriolis Acceleration. Redrawn from [85]

Most MEMS gyroscopes fall in the design called Rotational Vibratory Coriolis Gyroscope (RVCG) [86]. The gyroscope's proof-masses are electro-statically oscillated at resonance. An internal automatic gain control circuit precisely sets the oscillation of the proof masses. When the sensor is rotated about an axis, the Coriolis effect causes a vibration that can be detected by a capacitive pickoff. The resulting signal is processed to produce an analog voltage that is proportional to the angular velocity.

In the simplest form, a gyroscope could be modelled linearly as equation (4.3).

$$\boldsymbol{V = k_g \omega + b_g} \tag{4.3}$$

where,

$\boldsymbol{V}$ *gyroscope output in the unit of volt (V)*

$\boldsymbol{k_g}$ *scale factor in the unit of* $V/°/s$

$\boldsymbol{\omega}$ *angular velocity in the unit of* $°/s$

$\boldsymbol{b_g}$ *zero bias in the unit of volt (V)*

Most MEMS gyroscopes are not ratiometric, meaning that their outputs are not changing with respect to the supply voltage. When powered, the zero bias could be determined when the gyroscope is in static. In most cases, the scale factors and zero biases of a MEMS gyroscope are provided by its manufacturer. A dynamic calibration is needed to validate them and the IMU dynamic performances.

4.2.3 The IMU Used in the Research

Two types of IMUs and their physical properties are listed in Table 4.1. Both types of IMUs (Figure 4.3a and Figure 4.3b) are in the form of a PCB breakout (SparkFun, Inc) and their output axes are as shown. The IMU consists of a triaxial accelerometer (X Y Z) and a dual axial gyroscope (XR YR), forming five degree-of-freedom (dof). It is named as IMU-5DOF. The orientations and the axial directions of the triaxial accelerometer in both types of IMU are the same. However, it should be highlighted that the gyroscope outputs of Type-1 and Type-2 are inverse. It is worth noting that the gyroscope, IDG500's outputs are negative in counter clockwise direction (CCW) as shown in the figure. Table 4.2 lists the key information provided by their manufacturers. This information is item, scale factor, zero bias and the output condition. Detail specifications of the devices could be

downloaded on line. Three units of Type-1 IMU-5DOF and three units of Type-2 IMU-5DOF as shown in Table 4.3 are used in this study. Their tag names are used throughout the texts.

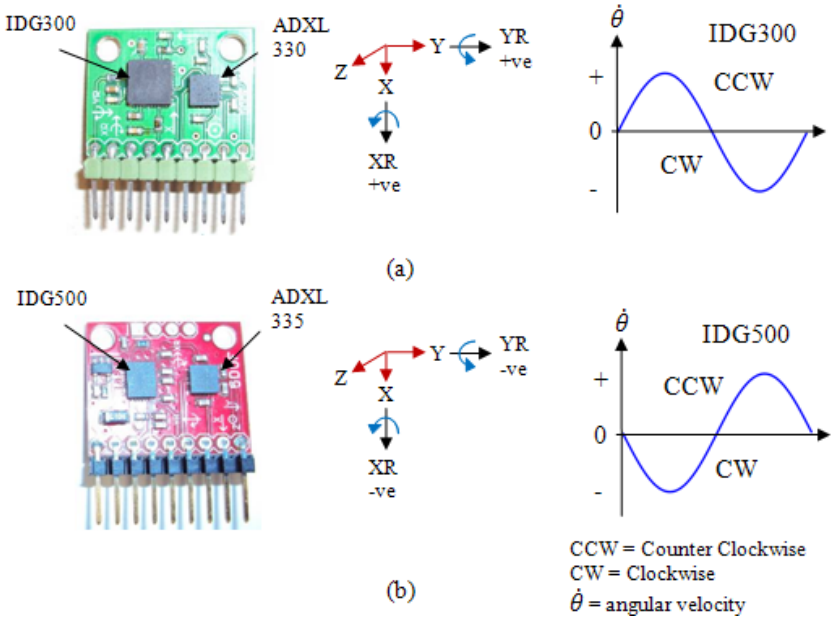

Figure 4.3: IMU-5DOF (a) Type-1 (b) Type-2

Table 4.1: Types of IMU-5DOF used in this application

IMU Type	Accelerometer	Gyroscope	Weight	Size
Type-1	ADXL330	IDG300	2g	20x23mm
Type-2	ADXL335	IDG500	2g	20x23mm

Table 4.2: Key specifications of the IMUs from the manufacturers

Devices	Items	Scale Factor	Zero Bias	Condition
Triaxial Accelerometer	ADXL330* [87]	270 ~ 330 (mV/g)	1.2 ~ 1.8 V	Ratiometric
	ADXL335* [88]	270 ~ 330 (mV/g)	1.2 ~ 1.8 V	Ratiometric
Dual-axial Gyroscope	IDG300** [89]	2.0 $(mV/°/s)$	1.5 V	Non-ratiometric
	IDG500** [90]	2.0 $(mV/°/s)$	1.5 V	Non-ratiometric

* *Ratiometric. Specification given based on V_s = 3.0VDC*

** *Specification based on full scale range at* $\mp 500°/s$

Table 4.3: Quantity of IMUs and their tag names

IMU	Item	Quantity	Name
Type-1	ADXL330 IDG300	3	IMU1 ~ IMU3
Type-2	ADXL335 IDG335	3	IMU4 ~ IMU6

4.3 Static Calibration

Static calibration is mainly focusing on the investigation of an accelerometer in searching for its setup parameters. Three different methods are demonstrated. They are the rotary table method, the 6/12 known positions method and the in-use calibration. Although the gyroscope cannot be completely calibrated during static calibration, its outputs (XR, YR) are recorded to determine their zero biases. Scale factors of the gyroscope will be determined during dynamic calibration.

4.3.1 Method 1: Conventional Rotary Table

A triaxial accelerometer could be defined in three different planes, i.e. the XY plane, the YZ plane and the ZX plane. Since all planes will abide the same working principle, a XY plane is explained in the following texts. In a vertical plane that is parallel to the gravity, an accelerometer is orientated statically as shown in Figure 4.4.

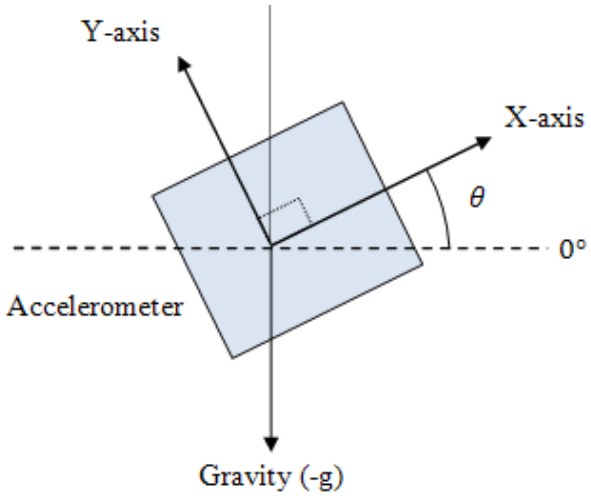

Figure 4.4: Static calibration in a vertical plane.
Redrawn from [91]

The gravity components of the horizontal axis and the vertical axis should match the sinusoidal excursions which fluctuate between ±1g as shown in equation (4.4) and equation (4.5), for $0° \leq \theta \leq 360°$.

$$\boldsymbol{Horizontal\ axis,} \qquad \boldsymbol{X = 1g.\sin(\theta)} \tag{4.4}$$

$$\boldsymbol{Vertical\ axis,} \qquad \boldsymbol{Y = 1g.\cos(\theta)} \tag{4.5}$$

From equation (4.2), the accelerometer model can be rewritten as equation (4.6).

$$\boldsymbol{V_i = K.s_i + b} \tag{4.6}$$

where,

$\boldsymbol{V_i}$ *output vector* $[v_X \quad v_Y]^T$ *in the unit of volt at i-sample*

$\boldsymbol{s_i}$ *gravity components* $[g_x \quad g_y]^T$ *at i-sample*

$\boldsymbol{K}$ *diagonal matrix,* $Diag[k_X \quad k_Y]$ *of scale factors in the unit of volt/g.*

$\boldsymbol{b}$ *zero bias vector* $[b_X \quad b_y]^T$ *of each axis in the unit of volt*

There are four unknowns i.e. two scale factors (k_x, k_y) and two zero biases (b_x, b_y) to be determined. Mathematically, equation (4.6) needs at least four different samples to solve the linear algebra if there is a solution. Although it is possible to be any arbitrary samples, however it is simpler to apply the g-components in unity values. Critical angles that results in ±1g are located at $\theta(0^0, 90^0, 180^0, 270^0, 360^0)$. At 90° and 270°, the g-component of the horizontal axis is in +1g and -1g respectively and their corresponding voltage outputs are simplified as shown in equation (4.7) and (4.8). Similarly, at 0° and 180°, the g-components of the vertical axis is in +1g and -1g respectively. Their corresponding voltage outputs are shown in equation (4.9) and (4.10).

$$\boldsymbol{\theta = 90°} \qquad \boldsymbol{v_{x1g} = k_x \cdot (+1g) + b_x} \tag{4.7}$$

$$\boldsymbol{\theta = 270°} \qquad \boldsymbol{v_{-x1g} = k_x \cdot (-1g) + b_x} \tag{4.8}$$

$$\boldsymbol{\theta = 0°} \qquad \boldsymbol{v_{y1g} = k_y \cdot (+1g) + b_y} \tag{4.9}$$

$$\boldsymbol{\theta = 180°} \qquad \boldsymbol{v_{-y1g} = k_y \cdot (-1g) + b_y} \tag{4.10}$$

By summing and subtracting equation (4.7) and (4.8), zero bias and scale factor of the horizontal axis could be formulated as equation (4.11) and (4.12) respectively.

$$\textbf{Zero bias} \quad b_x = \frac{v_{x1g} + v_{-x1g}}{2} \tag{4.11}$$

$$\textbf{Scale factor} \quad k_x = \frac{v_{x1g} - v_{-x1g}}{2} \tag{4.12}$$

Similarly zero bias and factor scale of the vertical axis could be formulated as equation (4.13) and (4.14) respectively.

$$\textbf{Zero bias} \quad b_y = \frac{v_{y1g} + v_{-y1g}}{2} \tag{4.13}$$

$$\textbf{Scale factor} \quad k_y = \frac{v_{y1g} - v_{-y1g}}{2} \tag{4.14}$$

Alternatively, when an accelemetric axis is in static and 0g, the zero bias could be computed as the mean voltage output. The calibration method is valid for other planes such as the YZ plane and the ZX plane.

4.3.1.1 Experiments

An IMU-5DOF is calibrated using an experiment setup as shown in Figure 4.5. The calibrating system includes a rotary table [92], an adjustable platform, an electronic spirit level, a customized datalogger and a machined bar. An adjustable platform with four M6 screws at its four corners is aligned orthogonal to the gravity with the aid of an electronic spirit level (resolution 0.1^0). In Figure 4.5, the IMU is positioned in the XY plane. At the starting position, the X-axis is aligned horizontally and the Y-axis is aligned vertically.

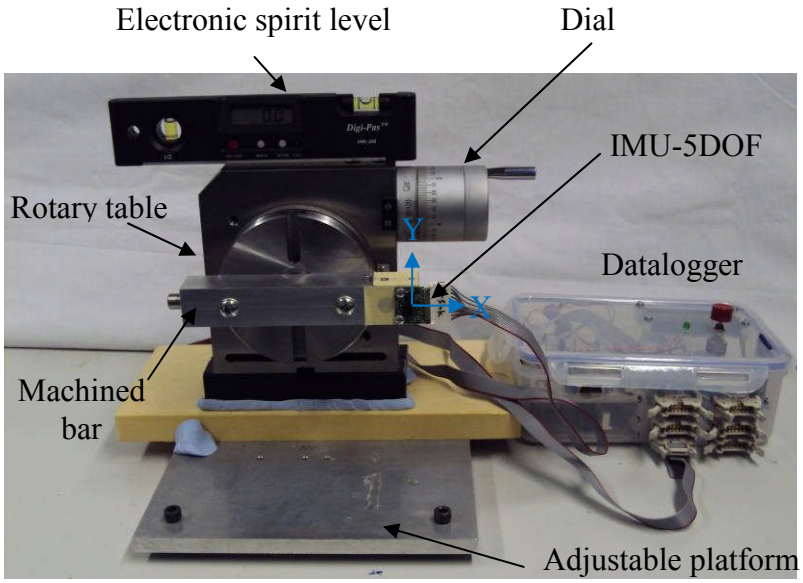

Figure 4.5: Setup of the rotary table method

The IMU is mounted on a machined bar that provides three orthogonal planes (XY, YZ, ZX) as illustrated in Figure 4.6. For all planes, a starting position is defined when the horizontal axis is at 0g (0°) and the vertical axis points toward +1g (90°). The third axis is assumed to be orthogonal to the vertical plane and is always at horizontal level, i.e. 0g (0°) for all positions. For example, in the XY plane, Z-axis will always rest horizontally (0g) for all positions.

The accelerometer will be calibrated through these procedures. The rotary table is turned manually in counter clockwise (CCW) direction. From 0° to 360°, stepping at 1° interval, IMU outputs (X, Y, Z, XR, YR) are recorded. The data are saved in a secure digital (SD) card for post-processing. Multiple experiments are repeated in every plane. All IMUs (IMU1 ~ IMU6) are calibrated using the same procedures.

A Matlab m-file is written and could be found in the CD attached.

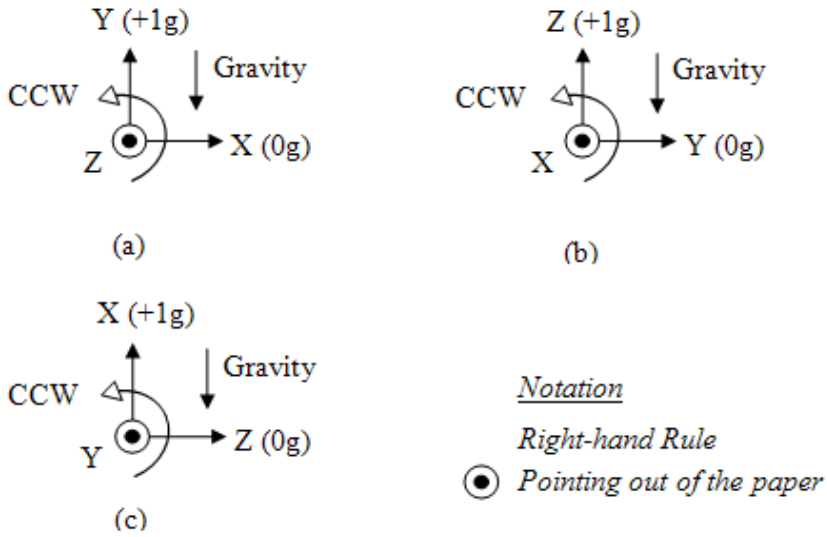

Figure 4.6: The starting position in (a) XY plane (b) YZ plane (c) ZX plane

4.3.1.2 Results

The procedure of calibration are similar for IMU1 to IMU6. For ease of explanation, the procedure results are presented based on IMU6. All calibrated IMUs' results (zero biases and scale factors) will be listed at the end of this sub section.

Three sets of experiments were conducted in XY, YZ and ZX planes respectively. The results showed that there were statistically little variations (*Standard Error, SE* ≤ 0.09014 *V*) in each set of data (X, Y, Z, XR, YR) collected in 1~2 seconds, suggesting highly repetitive and consistent system performance. The number of sampled data is around 200 to 400 per position. Mean value per

outputs are used in the following analysis. By using equations (4.11) to (4.14), the zero biases and the scale factors at critical angles $\theta(0^0, 90^0, 180^0, 270^0, 360^0)$ are calculated and listed in Table 4.4. An example of unnormalized static outputs (volt) in all three planes is plotted in Figure 4.7 and their critical angles are marked.

Table 4.4: IMU6. Calibrated results in three planes

XY plane			
Angle (°)	X	Y	Z
0	1.6208	1.9203	1.6626
90	1.9419	1.6015	1.6582
180	1.6177	1.2708	1.6593
270	1.2967	1.5899	1.6630
360	1.6208	1.9203	1.6627
Mean zero bias (*b)*	1.6193	1.5956	1.6612
Mean scale factor (*k)*	0.3226	0.3248	na
YZ plane			
Angle (°)	X	Y	Z
0	1.6216	1.5950	1.9891
90	1.6240	1.9200	1.6628
180	1.6159	1.5978	1.3362
270	1.6124	1.2699	1.6592
360	1.6210	1.5943	1.9882
Mean zero bias (*b)*	1.6190	1.5950	1.6627
Mean scale factor (*k)*	na	0.3251	0.3265
ZX plane			
Angle (°)	X	Y	Z
0	1.9420	1.5991	1.6538
90	1.6236	1.5951	1.9876
180	1.2968	1.5932	1.6628
270	1.6166	1.5982	1.3340
360	1.9421	1.5989	1.6560
Mean zero bias (*b)*	1.6194	1.5969	1.6608
Mean scale factor (*k)*	0.3226	na	0.3268

na *not available*

(X, Y, Z) in the unit of volt (V)
Zero bias in the unit of volt (V)
Scale factor in the unit of volt/g

(a)

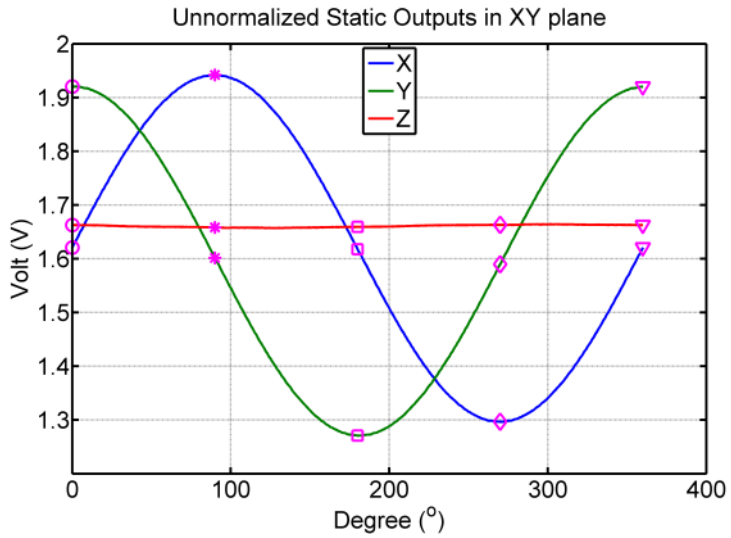

(b)

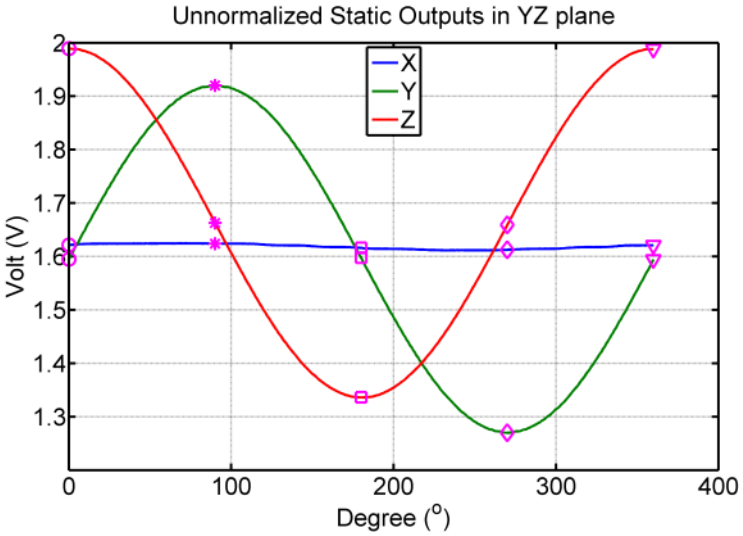

(c)

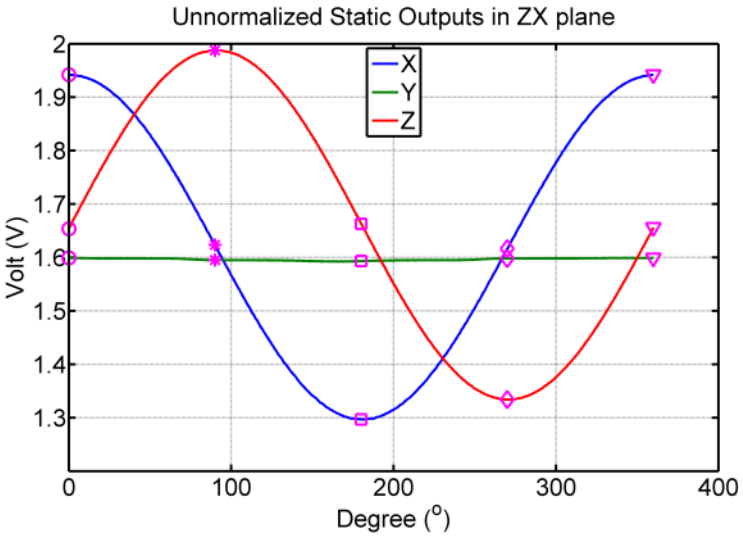

Figure 4.7: IMU6. Unnormalized outputs of a triaxial accelerometer in (a) XY plane, (b) YZ plane, (c) ZX plane
(○ 0°, * 90°, □ 180°, ◊ 270°, ▽ 360°)

Listing in Table 4.4, the zero bias and the scale factor in each axis of IMU6 vary slightly. Their mean results in different planes of IMU6 are listed in Table 4.5. Low variations (standard error, $SE_{RT} \leq 0.0006$) suggest high repeatability in outputs. By inserting the mean ($\bar{x}_{RT}$) of the mean results into equation (4.6), normalized static outputs for each plane are plotted. An example of normalized static outputs (g-forces) of IMU6 in all planes is plotted in Figure 4.8. They are compared to their theoretical outputs according to equation (4.4) and (4.5). Root mean square (RMS) error between the normalized static outputs and the mathematical models are calculated and listed in Table 4.6, together with their maximum values in unit of g. Low RMS (≤0.0127) shows great matches between the actual outputs and the models, suggesting that the mean results fit the equations.

Table 4.5: IMU6. Statistical results of the zero biases and the scale factors

	Zero Bias			*Scale Factor*		
Plane	b_X	b_Y	b_Z	k_X	k_Y	k_Z
XY	1.6193	1.5956	1.6612	0.3226	0.3248	na
YZ	1.6190	1.5950	1.6627	na	0.3251	0.3265
ZX	1.6194	1.5969	1.6608	0.3226	na	0.3268
$\bar{x}_{RT}$*	1.6192	1.5958	1.6616	0.3226	0.3250	0.3267
SE_{RT}**	0.0001	0.0006	0.0006	0.0000	0.0002	0.0001

* *mean* *Zero bias in the unit of volt (V)*
** *Standard Error* *Scale factor in the unit of volt/g*
na *not available*

Initially it is assumed that the third axis is always orthogonal to the vertical plane for all positions. However in reality it is not perfectly orthogonal to the plane. This phenomena is called inter-axis misalignment error. Figure 4.9 displays the accelerometer inter-axis misalignment errors of IMU6 during 0g for the XY plane, the YZ plane and the XZ plane respectively. Their corresponding axial outputs fluctuate slightly as the rotary table is turned. It is of interest to justify the errors in term of angle. Maximum and minimum of the inter-axis misalignment errors are compared to the mean error and their absolute differences are divided by the pre-calibrated scale factors respectively. Possible ranges of errors in angle (°) due to the inter-axis misalignments are displayed in Table 4.7. These inter-axis alignment errors are reported in the specification.

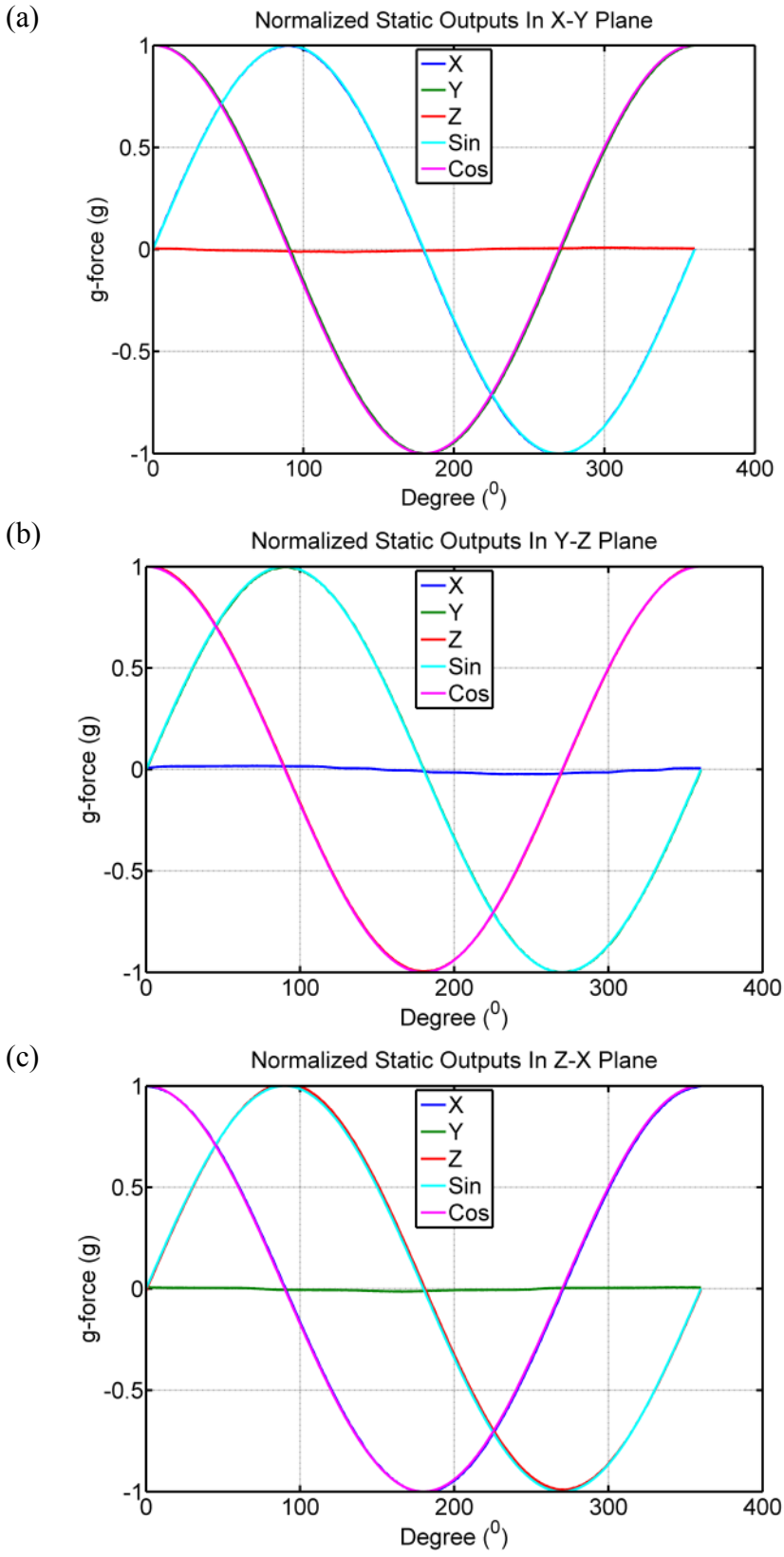

Figure 4.8: IMU6. Normalized static outputs in (a) XY plane (b) YZ plane (c) ZX plane

Table 4.6: IMU6. RMS errors between the normalized static outputs and the models

	X	Y	Z
XY	0.0038	0.0127	0.0000
YZ	0.0000	0.0040	0.0052
ZX	0.0079	0.0000	0.0115
Max.	0.0079	0.0127	0.0115

RMS of (X, Y, Z) in the unit of volt (V)

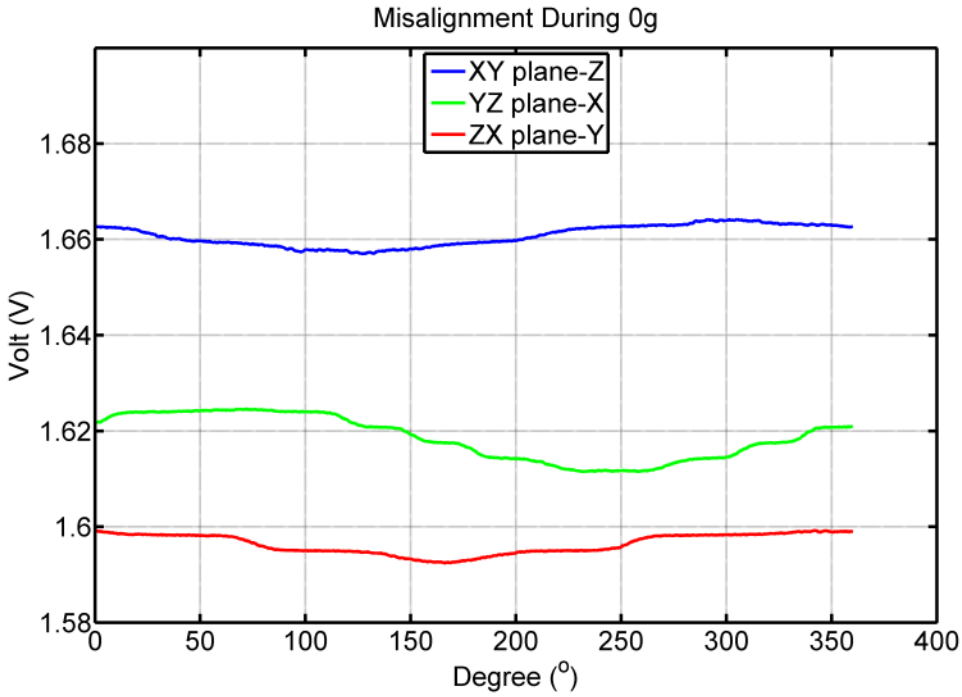

Figure 4.9: IMU6. Inter-axis misalignments during 0g

Table 4.7: IMU6. Inter-axis misalignment errors during 0g

	Max (V)	Mean (V)	Min (V)	Error (°) $asin\left(\frac{\lvert \max - mean \rvert}{\bar{x}_{RT}{}^{*}}\right)$	Error (°) $asin\left(\frac{\lvert \min - mean \rvert}{\bar{x}_{RT}{}^{*}}\right)$
X	1.6246	1.6186	1.6115	1.0580	1.2562
Y	1.5992	1.5964	1.5924	0.4978	0.4978
Z	1.6642	1.6608	1.6570	0.6003	0.6604

* *mean pre-calibrated scale factor*

The gyroscope outputs during static mode are not a constant but rather fluctuating slightly at different static angles. Similar observations were noticed in

IMU1 to IMU6. An example of IMU6 – gyro-outputs in all planes is shown in Figure 4.10. These fluctuations could cause a reading error when the gyroscope is not moved. There are a number of spikes displayed in the figure but the locations of these spikes are not always fixed but randomly located as another set of experiment data was checked. The causes of the error are unknown. The error is reported in its manufacturer's datasheet [90] as initial calibration tolerance (IDG300 = ±100mV, IDG500 = ±20mV). All IMUs in the study are working within the range of the specification. The voltage outputs of the gyroscope vary at different planes. Mean voltage outputs at each plane are listed in Table 4.8. Mean of the mean results are calculated. These gyroscope zero biases show low variations ($SE \leq 0.0009V$) from all the planes, suggesting high repetitive outputs.

(a)

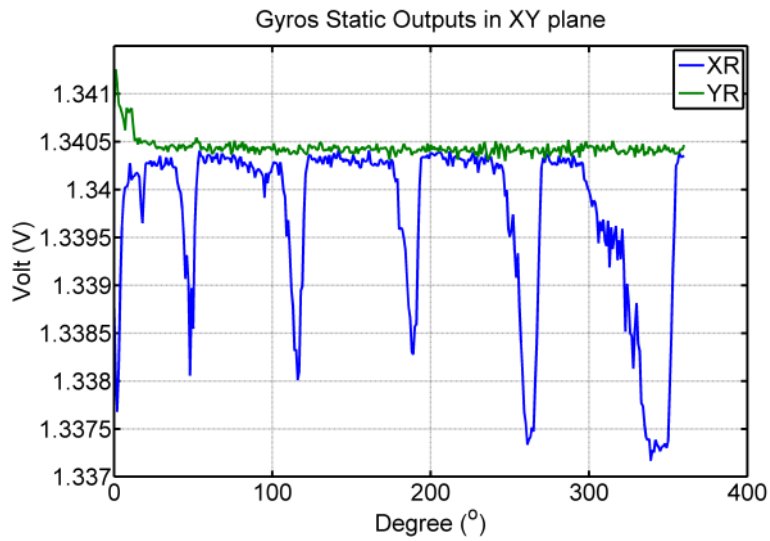

(b)

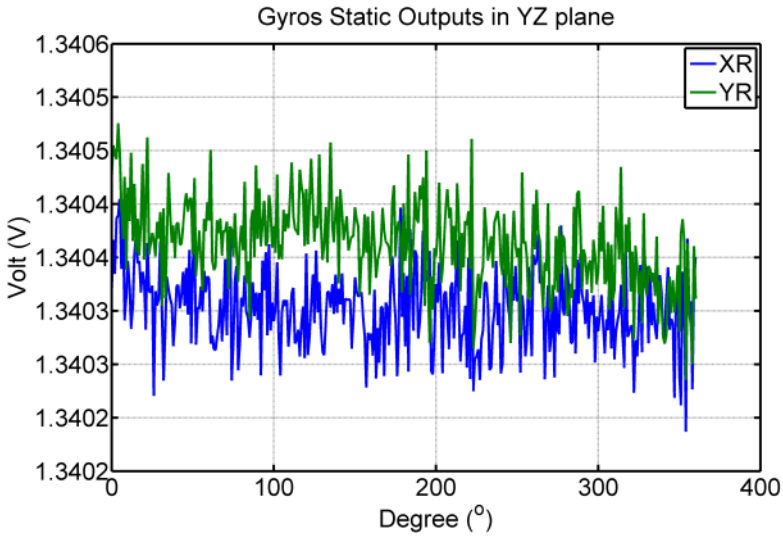

(c)

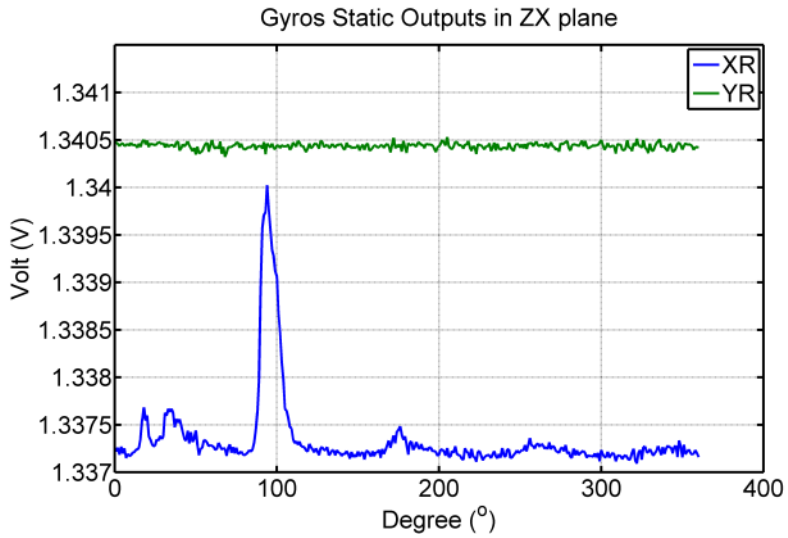

Figure 4.10: IMU6. Gyroscope static outputs at (a) XY plane, (b) YZ plane, (c) ZX plane

Table 4.8: IMU6. Zero biases for the gyroscope

	Zero Bias# of XR (b_{XR})	Zero Bias# of YR (b_{YR})
XY	1.3398	1.3404
YZ	1.3404	1.3404
ZX	1.3373	1.3404
Mean	1.3392	1.3404
*SE**	0.0009	0.0000

* *Standard Error*

\# *Zero Bias in the unit of volt (V)*

IMU1 to IMU6 are statically calibrated using the rotary table method. Their calibrated results for the axial accelerometers are listed in Table 4.9. Meanwhile, the mean results of the zero biases of the gyroscopes are listed in Table 4.10. These results are ready to be used in practical applications.

Table 4.9: Calibrated results of the accelerometers (IMU1 ~ IMU6)

		Zero Bias[#]			*Scale Factor*[##]		
		b_X	b_Y	b_Z	k_X	k_Y	k_Z
IMU1	*mean*	1.6357	1.6658	1.6118	0.3216	0.3312	0.3333
	*SE**	0.0008	0.0013	0.0015	0.0006	0.0000	0.0001
IMU2	*mean*	1.6464	1.6530	1.6297	0.3213	0.3276	0.3288
	*SE**	0.0007	0.0001	0.0006	0.0002	0.0002	0.0000
IMU3	*mean*	1.6136	1.6544	1.5685	0.3329	0.3382	0.3226
	*SE**	0.0003	0.0005	0.0006	0.0000	0.0025	0.0013
IMU4	*mean*	1.6158	1.6282	1.6262	0.3277	0.3351	0.3262
	*SE**	0.0003	0.0001	0.0001	0.0002	0.0001	0.0001
IMU5	*mean*	1.6229	1.6283	1.6346	0.3274	0.3302	0.3198
	*SE**	0.0001	0.0003	0.0008	0.0002	0.0002	0.0052
IMU6	*mean*	1.6192	1.5958	1.6616	0.3226	0.3250	0.3267
	*SE**	0.0001	0.0006	0.0006	0.0000	0.0002	0.0001

* *Standard Error* # *Zero Bias in the unit of volt (V)*
Scale Factor in the unit of volt/g

Table 4.10: Calibrated zero biases of the gyroscopes (IMU1 ~ IMU6)

		Zero Bias[#]	
		b_{XR}	b_{YR}
IMU1	*mean*	1.4159	1.4888
	*SE**	0.0031	0.0026
IMU2	*mean*	1.5175	1.4098
	*SE**	0.0053	0.0018
IMU3	*mean*	1.5150	1.6492
	*SE**	0.0151	0.0168
IMU4	*mean*	1.3152	1.3943
	*SE**	0.0004	0.0010
IMU5	*mean*	1.3372	1.3550
	*SE**	0.0000	0.0008
IMU6	*mean*	1.3392	1.3404
	*SE**	0.0009	0.0000

* *Standard Error* # *Zero Bias in the unit of volt (V)*

4.3.2 Method 2: 6/12 Known Positions

The output precision of an accelerometer suffers from small angle inter-axis misalignments (α_{xy} α_{xz} α_{yx} α_{yz} α_{zx} α_{zy}) as indicated in Figure 4.11 between the sensor coordinate $[x^a \quad y^a \quad z^a]$ and the platform coordinate $[x^p \quad y^p \quad z^p]$. Using the principle of direction cosine and small angle approximation, an error model could be formulated as equation (4.15).

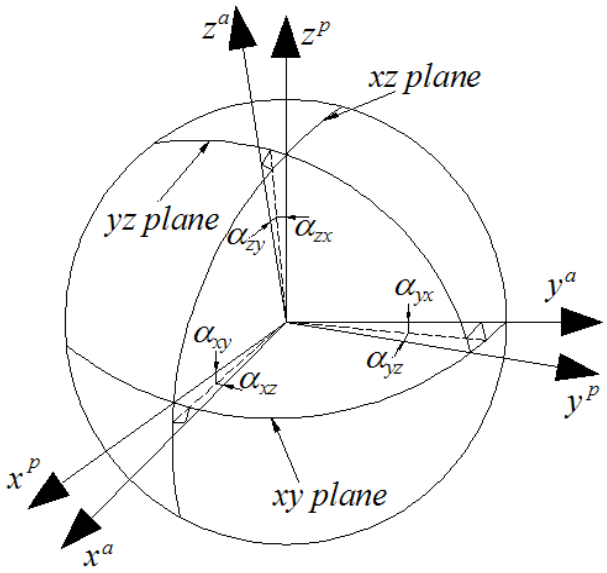

Figure 4.11: Inter-axis misalignments. Redrawn from [93, 94]

$$\boldsymbol{C^p = T_a^p C^a}, \quad \boldsymbol{T_a^p} = \begin{bmatrix} \mathbf{1} & -\boldsymbol{\alpha_{yz}} & \boldsymbol{\alpha_{zy}} \\ \boldsymbol{\alpha_{xz}} & \mathbf{1} & -\boldsymbol{\alpha_{zx}} \\ -\boldsymbol{\alpha_{xy}} & \boldsymbol{\alpha_{yx}} & \mathbf{1} \end{bmatrix} \tag{4.15}$$

where C^p and C^a are g-vectors in the platform coordinate and the sensor coordinate respectively whereas T_a^p is a transformation matrix named as inter-axis misalignment correction matrix that maps C^a to C^p. Skog [93] showed that the error model can be simplified by assuming that x^p coincides with x^a. Thus, its lower triangular matrix could be eliminated as shown in equation (4.16).

$$\boldsymbol{C^p = T_a^p C^a}, \quad \boldsymbol{T_a^p} = \begin{bmatrix} \mathbf{1} & -\boldsymbol{\alpha_{yz}} & \boldsymbol{\alpha_{zy}} \\ \mathbf{0} & \mathbf{1} & -\boldsymbol{\alpha_{zx}} \\ \mathbf{0} & \mathbf{0} & \mathbf{1} \end{bmatrix} \tag{4.16}$$

The sensor can be linearly modelled as equation (4.17).

$$\boldsymbol{V_i = K\left[T_a^p\right]^{-1} C_i^p + b} \tag{4.17}$$

where,

$\boldsymbol{V_i}$ *output vector,* $[v_x \quad v_y \quad v_z]^T$ *in the unit of volt at i-sample*

$\boldsymbol{K}$ *diagonal matrix,* $Diag[k_x \quad k_y \quad k_z]^T$ *of scale factors in the unit of volt/g.*

$\boldsymbol{T_a^p}$ *inter-axis misalignment correction matrix in the unit of radian*

$\boldsymbol{C_i^p}$ *g-force vector,* $\left[g_x^p \quad g_y^p \quad g_z^p\right]^T$ *in the platform coordinate at i-sample*

$\boldsymbol{b}$ *zero bias vector,* $[b_x \quad b_y \quad b_z]^T$ *of each axis in the unit of volt*

From equation (4.17), there are nine setup parameters i.e. $\left(k_x \; k_y \; k_z \; \alpha_{yz} \; \alpha_{zy} \; \alpha_{zx} \; b_x \; b_y \; b_z\right)$ to be determined. It is worth noting that if there is no inter-axis misalignment, T_a^p will be a unity matrix and only the scale factors and the zero biases are of concern. Mathematically, equation (4.17) needs at least nine different samples to be solved if there is a solution. Equation (4.17) is expanded into equation (4.18).

$$\begin{bmatrix} \boldsymbol{v_x} \\ \boldsymbol{v_y} \\ \boldsymbol{v_z} \end{bmatrix}_i = \begin{bmatrix} \boldsymbol{k_x} & \boldsymbol{0} & \boldsymbol{0} \\ \boldsymbol{0} & \boldsymbol{k_y} & \boldsymbol{0} \\ \boldsymbol{0} & \boldsymbol{0} & \boldsymbol{k_z} \end{bmatrix} \begin{bmatrix} \boldsymbol{1} & \boldsymbol{-\alpha_{yz}} & \boldsymbol{\alpha_{zy}} \\ \boldsymbol{0} & \boldsymbol{1} & \boldsymbol{-\alpha_{zx}} \\ \boldsymbol{0} & \boldsymbol{0} & \boldsymbol{1} \end{bmatrix}^{-1} \begin{bmatrix} \boldsymbol{g_x^p} \\ \boldsymbol{g_y^p} \\ \boldsymbol{g_z^p} \end{bmatrix}_i + \begin{bmatrix} \boldsymbol{b_x} \\ \boldsymbol{b_y} \\ \boldsymbol{b_z} \end{bmatrix}$$

$$\begin{bmatrix} \boldsymbol{v_{xi}} \\ \boldsymbol{v_{yi}} \\ \boldsymbol{v_{zi}} \end{bmatrix} = \begin{bmatrix} \boldsymbol{b_x + k_x g_{xi}^p + \alpha_{yz} k_x g_{yi}^p - k_x g_{zi}^p (\alpha_{zy} - \alpha_{yz}\alpha_{zx})} \\ \boldsymbol{b_y + k_y g_{yi}^p + \alpha_{zx} k_y g_{zi}^p} \\ \boldsymbol{b_z + k_z g_{zi}^p} \end{bmatrix} \tag{4.18}$$

It is obvious that Z-axis is the simplest and has only two unknowns ($b_z \; k_z$) followed by Y-axis with three unknowns ($b_y \; k_y \; \alpha_{zx}$) and lastly X-axis with four unknowns ($b_x \; k_x \; \alpha_{yz} \; \alpha_{zy}$). Using *i* number of samples corresponding to the number of unknowns in each axis, equation (4.18) can be broken into three linear equations separately in the sequence of Z, Y and X axis as listed in equation (4.19), (4.20) and (4.21) respectively.

$$\begin{bmatrix} \boldsymbol{v_{z1}} \\ \boldsymbol{v_{z2}} \end{bmatrix} = \begin{bmatrix} 1 & \boldsymbol{g_{z1}^p} \\ 1 & \boldsymbol{g_{z2}^p} \end{bmatrix} \begin{bmatrix} \boldsymbol{b_z} \\ \boldsymbol{k_z} \end{bmatrix} \tag{4.19}$$

$$\begin{bmatrix} \boldsymbol{v_{y1}} \\ \boldsymbol{v_{y2}} \\ \boldsymbol{v_{y3}} \end{bmatrix} = \begin{bmatrix} 1 & \boldsymbol{g_{y1}^{p}} & \boldsymbol{g_{z1}^{p}} \\ 1 & \boldsymbol{g_{y2}^{p}} & \boldsymbol{g_{z2}^{p}} \\ 1 & \boldsymbol{g_{y3}^{p}} & \boldsymbol{g_{z3}^{p}} \end{bmatrix} \begin{bmatrix} \boldsymbol{b_y} \\ \boldsymbol{k_y} \\ \boldsymbol{d} \end{bmatrix} \tag{4.20}$$

where,

$$\boldsymbol{\alpha_{zx}} = \frac{\boldsymbol{d}}{\boldsymbol{k_y}}$$

$$\begin{bmatrix} \boldsymbol{v_{x1}} \\ \boldsymbol{v_{x2}} \\ \boldsymbol{v_{x3}} \\ \boldsymbol{v_{x4}} \end{bmatrix} = \begin{bmatrix} 1 & \boldsymbol{g_{x1}^{p}} & \boldsymbol{g_{y1}^{p}} & \boldsymbol{-g_{z1}^{p}} \\ 1 & \boldsymbol{g_{x2}^{p}} & \boldsymbol{g_{y2}^{p}} & \boldsymbol{-g_{z2}^{p}} \\ 1 & \boldsymbol{g_{x3}^{p}} & \boldsymbol{g_{y3}^{p}} & \boldsymbol{-g_{z3}^{p}} \\ 1 & \boldsymbol{g_{x4}^{p}} & \boldsymbol{g_{y4}^{p}} & \boldsymbol{-g_{z4}^{p}} \end{bmatrix} \begin{bmatrix} \boldsymbol{b_x} \\ \boldsymbol{k_x} \\ \boldsymbol{e} \\ \boldsymbol{f} \end{bmatrix} \tag{4.21}$$

where,

$$\boldsymbol{\alpha_{yz}} = \frac{\boldsymbol{e}}{\boldsymbol{k_x}}$$

$$\boldsymbol{\alpha_{zy}} = \frac{\boldsymbol{f}}{\boldsymbol{k_x}} + \boldsymbol{\alpha_{yz}\alpha_{zx}}$$

Equation (4.19), (4.20) and (4.21) could be arranged in the form of a linear algebra, such as $y = Ax$. For known outputs (y) and coefficient matrix (A), solving for x is done by multiplying the inverse of the coefficient matrix with its outputs, $x = A^{-1}y$, if there exits a solution. A solution of a linear equation is non-singular and unique if these conditions are met [95]:

Condition 1: $rank(A) = full\ rank$

Condition 2: $rank(A|y) = at\ least\ as\ large\ as\ rank(A)$

4.3.2.1 Experiments

A test rig was developed as shown in Figure 4.12 consisting of an adjustable platform, a cube mounted with an IMU and a V-block. Before experiments, the platform is adjusted horizontally with the aid of an electronic spirit level (resolution, 0.1^0).

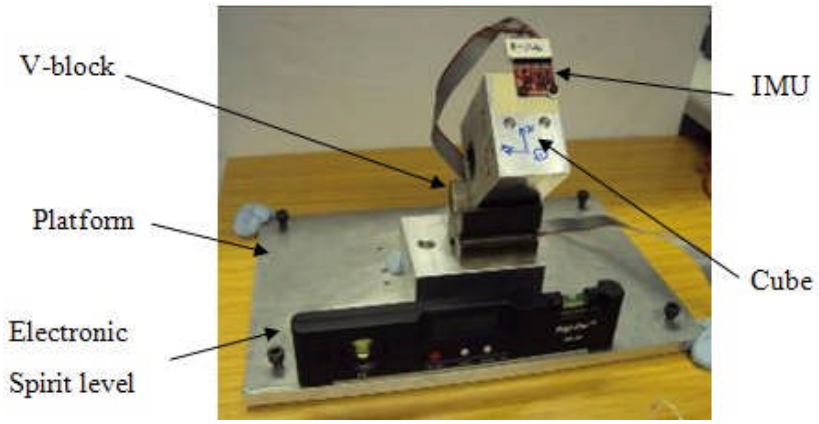

Figure 4.12: Setup of the twelve-known positions method

Theoretically, it can be any arbitrary known positions but for uniformity and ease of operations, twelve-known positions as proposed by Hung [96] are applied. They are illustrated in Figure 4.13. Non-orthogonal positions (1,3,5,9,10,12) are tilted at 45^0 with respect to the platform by placing the cube inside a V-block. Six orthogonal positions (2,4,6,7,8,11) are performed by rotating the cube with respect to the platform. The IMU outputs are sampled for approximately 10 seconds per position, at 200Hz sampling rate.

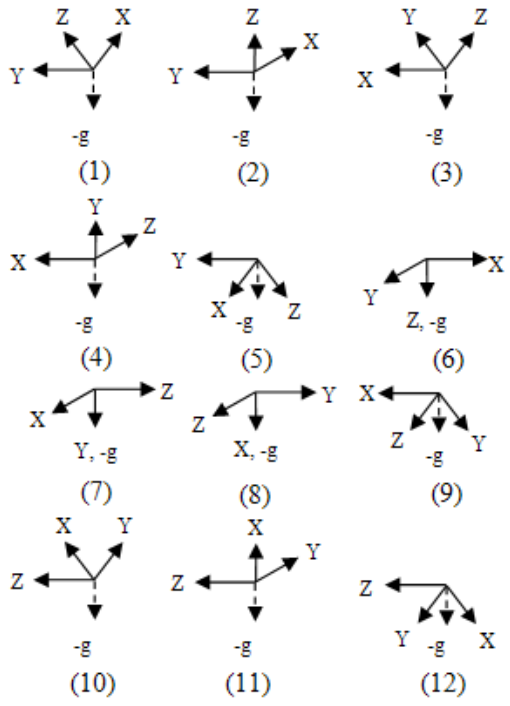

Figure 4.13: Twelve-known positions in the platform coordinate. Redrawn from [96]

Known g-values in the platform coordinate in all known positions are listed in Table 4.11. A positive g-component means that the accelerometer axis is pointing against the gravity and vice versa. For example, at position-1, X and Z axes are tilted at 45° upward, their outputs are $+1g \cdot \sin(45°) = 0.7071g$ while Y-axis is at 0g. These measured outputs displayed very high repeatability as the maximum standard deviation of measured outputs at $4.7 \times 10^{-5}V$ was observed, suggesting negligible noises for all collected data. An example of mean voltage outputs of IMU6 at the twelve-known positions are illustrated in Figure 4.14. IMU1 to IMU6 are calibrated by the same procedure.

A Matlab m-file is written and could be found in the CD attached.

Table 4.11: G-values at the twelve-known positions

Position	X	Y	Z
1	0.7071	0.0000	0.7071
2	0.0000	0.0000	1.0000
3	0.0000	0.7071	0.7071
4	0.0000	1.0000	0.0000
5	-0.7071	0.0000	-0.7071
6	0.0000	0.0000	-1.0000
7	0.0000	-1.0000	0.0000
8	-1.0000	0.0000	0.0000
9	0.0000	-0.7071	-0.7071
10	0.7071	0.7071	0.0000
11	1.0000	0.0000	0.0000
12	-0.7071	-0.7071	0.0000

Note: (X, Y, Z) are in the unit of g

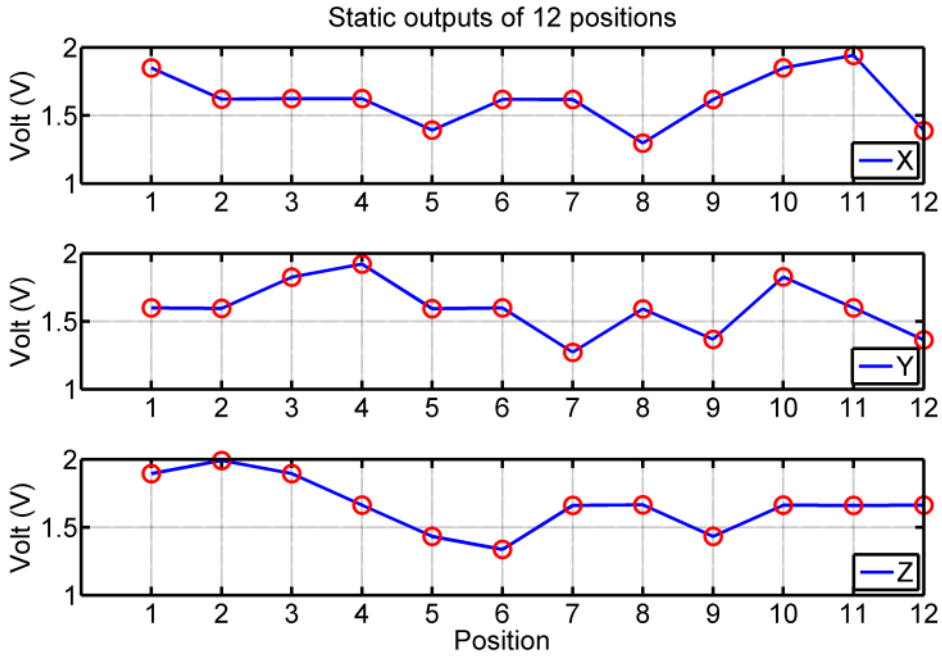

Figure 4.14: IMU6. Static outputs at the twelve-known positions

4.3.2.2 Results

The results presented are based on IMU6. Other IMUs (IMU1~IMU5) are calibrated and analysed in the similar way. Their results will be listed at the end of the sub section.

Two sets of positions were analysed for comparison purposes. Set1 is at twelve-known positions [1 2 3 4 5 6 7 8 9 10 11 12] while Set2 is at six-known orthogonal positions [2 4 6 7 8 11]. By referring to equations (4.19), (4.20) and (4.21), the number of combinations or iterations for potential solutions for *j* unknown, can be calculated using a binomial formula as shown in equation (4.22) and they are listed in Table 4.12. For Set1, the total number of positions is twelve *(n = 12)* while for Set2, the total number of positions is six *(n = 6)*. For instance, in Set1 (twelve-known positions), two known positions are needed to determine two unknowns in Z-axis based on Equation (4.19). The possible solutions are the number of combinations, i.e. two out of twelve positions $\binom{12}{2}$, which is equivalent to 66 combinations. The combination number of Set1 is larger than Set2. Each combination will produce a solution if the linear equation is non-singular and unique.

$$\boldsymbol{C = \binom{n}{j} = \frac{n!}{j!\,(n-j)!}} \tag{4.22}$$

Table 4.12: Combination for all possible solutions in Set1 and Set2

Set1:Twelve-known Positions (n = 12)			
	X	Y	Z
unknowns (*j*)	4	3	2
Combinations (*C*)	495	220	66
Set2: Six-known Positions (n = 6)			
	X	Y	Z
unknowns (*j*)	4	3	2
Combinations (*C*)	15	20	15

Means and standard deviations ($\bar{x}_{12}$, s_{12}) of non-singular solutions using twelve-known positions (Set1) are listed in Table 4.13. Low variations (max. at 0.0069) in both the scale factors and the zero biases suggest that the solutions are highly repetitive and consistent for all non-singular solutions. Although relative standard deviation ($RSD = \left|\frac{s}{\bar{x}}\right| \times 100\,\%$) of the inter-axis misalignment errors appear to be larger than RSD of the scale factor and the zero biases respectively, but the inter-axis misalignment errors are still kept within a small range of angles (-0.0017 ~ 0.0101 radian or $-0.1^0 \sim 0.58^0$). This agrees with the initial assumptions during the formation of the sensor linear model with error correction. Not all combinations will generate a solution. Table 4.14 lists the solution check for all possible combinations in twelve-known positions. Non-singular solutions occupy a larger portion of all possible combinations. Amongst all axes, X-axis which requires four unknowns, has the largest portion (63.38%) of combinations while Z-axis has the smallest portion (8.45%). Out of all possible combinations, 84.12% will produce non-singular solutions.

Table 4.13: IMU6. The results using the twelve-known positions

Scale Factors (V/g)	k_x	k_y	k_z
$\bar{x}_{12}$	0.3223	0.3253	0.3271
s_{12}	0.0014	0.0069	0.0026
RSD (%)	0.43	2.12	0.79
Misalignment (rad)	α_{yz}	α_{zy}	α_{zx}
$\bar{x}_{12}$	0.0101	-0.0037	-0.0017
s_{12}	0.0049	0.0047	0.0205
RSD (%)	48.51	127.03	1205.88
Zero Bias (V)	b_x	b_y	b_z
$\bar{x}_{12}$	1.6199	1.5951	1.6627
s_{12}	0.0011	0.0049	0.0017
RSD (%)	0.07	0.31	0.10

$\bar{x}_{12}$ = *mean,* s_{12} = *standard deviation*

Table 4.14: Solution checks for the twelve-known positions

	Singular	Non Singular	Total (%)
X	63	432	495 (63.38)
Y	44	176	220 (28.17)
Z	17	49	66 (8.45)
Total (%)	124 (15.88)	657 (84.12)	781 (100)

On the other hand, the results ($\bar{x}_6$, s_6) of non-singular solutions using six-known orthogonal positions (Set2) are listed in Table 4.15. Low variations (max. at 0.0028) in the scale factors and the zero biases suggest that the solutions are highly repetitive and consistent for all non-singular solution. RSD of the inter-axis misalignment errors are much larger than RSD of the scale factors and the zero biases. However, the inter-axis misalignment errors are still kept within small angle range (-0.0053 ~ 0.0095 radian or -0.30^0 ~ 0.54^0). In Table 4.16, non-singular solutions occupy a larger portion (66%) of the combinations. Y-axis has the largest portions (40%) in the total combination while X and Z-axis share equally the rest of the portion.

Table 4.15: IMU6. The results using the six-known positions

Scale Factors (V/g)	k_x	k_y	k_z
$\bar{x}_6$	0.3222	0.3246	0.3274
s_6	0.0006	0.0028	0.0027
RSD (%)	0.19	0.86	0.82
Misalignment (rad)	α_{yz}	α_{zy}	α_{zx}
$\bar{x}_6$	0.0095	-0.0046	-0.0053
s_6	0.0032	0.0026	0.0091
RSD (%)	33.68	56.52	171.70
Zero Bias (V)	b_x	b_y	b_z
$\bar{x}_6$	1.6198	1.5954	1.6626
s_6	0.0006	0.0028	0.0023
RSD (%)	0.04	0.18	0.14

$\bar{x}_6$ = *mean,* s_6 = *standard deviation*

Table 4.16: Solution checks for the six-known positions

	Singular	Non-Singular	Total (%)
X	3	12	15 (30)
Y	8	12	20 (40)
Z	6	9	15 (30)
Total (%)	17 (34)	33 (66)	50 (100)

Computation time in the six-known positions is shorter as the total number of combinations is greatly reduced. Careful observations into combinations which produce singularity during computation indicate no solution if identical axis within a combination is in the same plane. For example, no solution for Y-axis in position (2,6,8) can be found since Y-axis in each position is in the horizontal plane. The percentage (D) of the absolute difference between the mean of the twelve positions and six positions as defined in equation (4.23) are computed. In Table 4.17, low difference percentages in the scale factors and the zero biases suggest that the six-known positions are adequate to calculate the key setup parameters. Although one of the inter-axis misalignment errors displays more than 200% discrepancy but in

general the errors are kept within a small range of angles. In practice, the inter-axis misalignment errors could possibly be ignored since they are very small.

$$\boldsymbol{D} = \left|\frac{\boldsymbol{x_{12}} - \boldsymbol{x_6}}{\boldsymbol{x_{12}}}\right| \times \mathbf{100}\ \% \tag{4.23}$$

Table 4.17: Comparison of twelve-known and six-known positions

Scale Factors (V/g)	k_x	k_y	k_z
$\bar{x}_{12}$	0.3223	0.3253	0.3271
$\bar{x}_6$	0.3222	0.3246	0.3274
D (%)	0.03	0.21	0.09
Misalignment (rad)	α_{yz}	α_{zy}	α_{zx}
$\bar{x}_{12}$	0.0101	-0.0037	-0.0017
$\bar{x}_6$	0.0095	-0.0046	-0.0053
D (%)	5.94	23.32	211.76
Zero Bias (V)	b_x	b_y	b_z
$\bar{x}_{12}$	1.6199	1.5951	1.6627
$\bar{x}_6$	1.6198	1.5954	1.6626
D (%)	0.00	0.00	0.00

This is a novel method since a fast calibration of an triaxial accelerometer could be performed in six or twelve permutations using simple referential tools and simple mathematical operations. The comparison between twelve-known and six-known positions also suggests that the number of permutations could simplified into six orthogonal directions and still produce acceptable results.

4.3.3 Method 3: In-Use Calibration

In any static positions, the vector norm of the g-components of a triaxial accelerometer is equivalent to 1g. It is assumed that quasi-static positions would meet the same criterion. Using a quasi-static detection algorithm proposed by Lotter [84], numerous quasi-static positions can be isolated and extracted from the motion data. A cost function which computes the absolute difference between 1g and the norm of a triaxial accelerometer's estimation outputs could be formulated. It is a function of voltages during quasi-static and the setup parameters. Varying the setup

parameters would virtually create a multi-dimension hyperspace which virtually exhibits ‘mountains’ and ‘valleys’. It is the interest in the optimization computation to identify the ‘valleys’ which represent the minimum error around their circumferences. A local minimum is any ‘valley’ and there could be many local minima in a vector space. However there is only one global minimum which is the lowest ‘valley’ amongst all.

A quasi-static detection algorithm is a five-stage sequential signal processing on the accelerometer’s motion data. Firstly, the norms of the accelerometer voltage outputs, $V_r = norm(V)$ are computed. Secondly, a high pass filter (HPF, cut-off frequency, f_c = 0.5Hz) is performed to shift the DC baseline to 0VDC. Thirdly, the voltage norms are regulated to absolute values. This step is essential when the procedure reaches the last step. Fourthly, a low pass filter (LPF, cut-off frequency, f_c = 0.5Hz) is used to remove any high frequency data (non quasi-static motions) out of the voltage norm. Lastly, a set of quasi-static positions, V_{qs} is identified where the voltage norms are less than or equal to a positive threshold, $T_v = 0.4$. Using the position indexes of the quasi-static position, a set of accelerometer voltage outputs $(v_x\ v_y\ v_z)$ are extracted and will be used during an optimization process to compute the optimal accelerometer’s setup parameters. A quasi-static detection algorithm could be written as equation (4.24).

$$\boldsymbol{V_{qs} = LPF\left(REC\left(HPF(V_r)\right)\right) \leq T_v} \tag{4.24}$$

Referring to equation (4.16) and (4.17), the model is rewritten as equations (4.25) and (4.26).

$$\boldsymbol{C^p = T_a^p C^a}, \quad \boldsymbol{T_a^p} = \begin{bmatrix} \mathbf{1} & -\boldsymbol{\alpha_{yz}} & \boldsymbol{\alpha_{zy}} \\ \mathbf{0} & \mathbf{1} & -\boldsymbol{\alpha_{zx}} \\ \mathbf{0} & \mathbf{0} & \mathbf{1} \end{bmatrix} \tag{4.25}$$

$$\boldsymbol{V_i = K\left[T_a^p\right]^{-1} C_i^p + b} \tag{4.26}$$

where,

$\boldsymbol{V_i}$ *output vector,* $[v_x \quad v_y \quad v_z]^T$ *in the unit of volts at i-sample*

$\boldsymbol{K}$ *diagonal matrix,* $Diag[k_x \quad k_y \quad k_z]^T$ *of scale factors in the unit of volts/g.*

$\boldsymbol{T_a^p}$ *inter-axis misalignment correction matrix*

$\boldsymbol{C_i^p}$ *g-force vector,* $[g_x^p \quad g_y^p \quad g_z^p]^T$ *in the platform coordinate at i-sample*

$\boldsymbol{b}$ *zero bias vector,* $[b_x \quad b_y \quad b_z]^T$ *of each axis in volts*

Nine setup parameters, $\theta[k_x\ k_y\ k_z\ \alpha_{yz}\ \alpha_{zy}\ \alpha_{zx}\ b_x\ b_y\ b_z]$ are to be determined. Mathematically, the g-vector could be written as equation (4.27).

$$\boldsymbol{C_i^p = T_a^p\, K^{-1}(V_i - b)} \tag{4.27}$$

The expected norm of the g-components of a triaxial accelerometer at any static positions is formulated as equation (4.28) where the resultant is equal to 1g.

$$\boldsymbol{norm(C_i^p) = \sqrt{(g_x^p)^2 + (g_y^p)^2 + (g_z^p)^2} = 1} \tag{4.28}$$

On the other hand, it is possible to estimate the norm provided that the output voltages and the accelerometer setup parameter, (V, θ) are given as shown in equation (4.29).

$$\boldsymbol{\hat{h}_i(V_i, \theta) = norm(C_i^p)} \tag{4.29}$$

A cost function as shown in equation (4.30) is the absolute error between the expected g-norm (1g) and the estimated g-norm $\hat{h}(V, \theta)$ at quasi-static positions. Ideally, the error should be zero.

$$\boldsymbol{e(V, \theta) = abs\left(1 - \hat{h}(V, \theta)\right)} \tag{4.30}$$

Voltages $(\boldsymbol{v_x\ v_y\ v_z})$ during quasi-static positions are applied into the cost function and an iterative optimization computation is performed to find an optimum solution. The computation stops when the cost function is at its minimum or lower than a specific value. The result is the best-fit calibrated setup parameters for a particular

triaxial accelerometer. The solution is the scale factors, the inter-axis misalignment errors and the zero biases of a triaxial accelerometer.

There are many optimization solvers [97] such as linear programming, nonlinear programming, simulated annealing, genetic algorithm etc. A nonlinear programming algorithm as shown in equation (4.31) is chosen for the optimization process.

$$\begin{aligned} \textbf{Minimize} \quad & \boldsymbol{f(X)}, [\boldsymbol{X}]_{\boldsymbol{n}} \\ \textbf{Subject to:} \quad & [\boldsymbol{h(X)}]_{\boldsymbol{l}} = \mathbf{0} \\ & [\boldsymbol{g(X)}]_{\boldsymbol{m}} \leq \mathbf{0} \\ & \boldsymbol{X^{low}} \leq \boldsymbol{X} \leq \boldsymbol{X^{up}} \end{aligned} \tag{4.31}$$

$f(X)$ is the cost function to be minimized given the variable X as a vector of size n. The cost function is subjected to two types of constraints, i.e. equality constraints, $[h(X)]_l = 0$ and inequality constraints, $[g(X)]_m \leq 0$. The variable, X is searched through the range of interest confined by $X^{low} \leq X \leq X^{up}$. It is a normal practice to implement a starting vector, *x0*, at the beginning of the optimization search. The starting vector and the constraints for this optimization process are listed in Table 4.18.

Table 4.18: The starting vector and the constraints

	k_x	k_y	k_z
lower bound, X^{low}	0.2835	0.2835	0.2835
starting, x0	0.3150	.3150	0.3150
upper bound, X^{up}	0.3465	0.3465	0.3465
	α_{yz}	α_{zy}	α_{zx}
lower bound, X^{low}	-0.0400	-0.0400	-0.0400
starting, x0	0.0100	0.0100	0.0100
upper bound, X^{up}	0.0400	0.0400	0.0400
	b_x	b_y	b_z
lower bound, X^{low}	1.4175	1.4175	1.4175
starting, x0	1.5750	1.5750	1.5750
upper bound, X^{up}	1.7325	1.7325	1.7325

4.3.3.1 Experiments

The experimental setup for an in-use calibration is shown in Figure 4.15. The test rig consists of an IMU mounted in a cube and a customized datalogger (see Chapter 3). The cube is swung randomly and rotated freely in air for a few seconds. The motion is random but slow. All IMU-axes outputs are recorded. IMU1 to IMU6 are experimented in the same method.

Optimization command '*fmincon*' in Matlab [98] is used to find the minimum of a constrained nonlinear multivariable function. This command checks iteratively all the hyperspace of a cost function given a starting vector. A Matlab m-file is written and could be found in the CD attached.

Alternatively, the cost function could be optimized by using the Optimization Toolbox provided by Matlab, which offers a wide selection of solver. Optimization run time differs greatly depending on the selection of solver. The results might vary if different solvers are used. Other solvers include nonlinear equation solving (*fsolve*), unconstrained nonlinear minimization (*fminunc*), unconstrained nonlinear minimization using derivative-free method (*fminsearch*), etc.

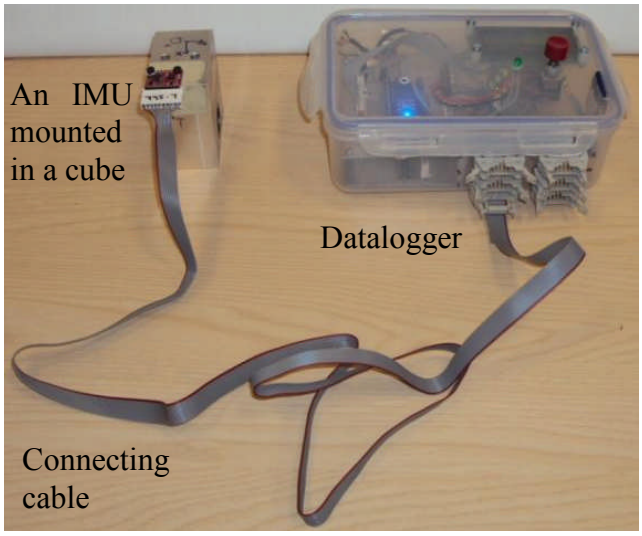

Figure 4.15: Setup of the in-use calibration

4.3.3.2 Results

The results presented are based on IMU6. Other IMUs (IMU1~IMU5) are calibrated and analyzed in the similar way. All results will be listed at the end of the sub section. The results are based on the solver '*fmincon*'. Alternatively, choosing other

types of solvers as offered in Optimization Toolbox could probably save some computation time as their stopping criterion is different. The results could be varying amongst different solvers. Unlike other solvers, this command will investigate and iterate a specific number of data points before the operation stops.

Approximately 54 seconds of motion data were collected. And, 12099 data of quasi-static positions were identified. Figure 4.16 shows five stages of quasi-static positions detection. A quasi-static position array is created and their position indexes are used to index the output voltages at quasi-static moments. Number of quasi-static positions to be fed into the optimization algorithm is flexible. In the example, 1000 out of 12099 quasi-static positions were chosen for the optimization process. The run time increases dramatically as the number of quasi-static positions applied increases. Every quasi-static position will generate a set of optimized results with its corresponding cost function's value. The run time was 613 seconds. There were 1000 sets of results but the result at its lowest cost function's value is retrieved as the best fit results. The best-fit results as listed in Table 4.19 are determined by the lowest cost function's value, 3.73E-12.

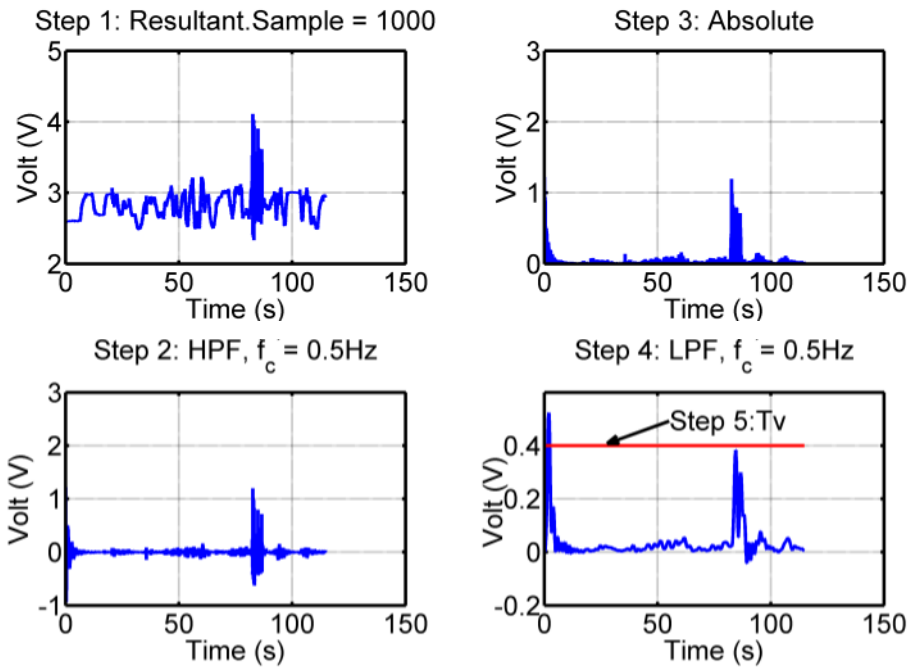

Figure 4.16: IMU6. Quasi-static positions detection

Table 4.19: IMU6. The results using optimization command *(fmincon)*

k_x	k_y	k_z
0.3148	0.3149	0.3144
α_{yz}	α_{zy}	α_{zx}
8.93E-05	-1.80E-04	-1.49E-04
b_x	b_y	b_z
1.5862	1.5658	1.5564

Results at the lowest CF, 3.73E-12.
Quasi-static number = 1000

Using the same method, the results of IMU1 to IMU6 are optimized separately using their own motion data. All solutions will investigate iteratively over 1000 quasi-static positions. Their lowest cost function values are listed in Table 4.20. Calibrated results of all IMUs are listed in Table 4.21. The magnitudes of the scale factors and the zero biases fluctuate at two decimal points. All inter-axis misalignment errors are extremely small, nearly zero.

Table 4.20: Lowest cost function's value for IMU1 to IMU6

	Lowest CF's value
IMU1	1.28E-12
IMU2	9.92E-13
IMU3	1.17E-12
IMU4	8.73E-14
IMU5	1.09E-12
IMU6	3.73E-12
Size =1000 chosen quasi-static positions.	

Table 4.21: The results using the in-use calibration

	Scale Factor (V/g)		
	k_x	k_y	k_z
IMU1	0.3149	0.3147	0.3148
IMU2	0.3150	0.3150	0.3150
IMU3	0.3160	0.3159	0.3165
IMU4	0.3151	0.3162	0.3152
IMU5	0.3152	0.3154	0.3158
IMU6	0.3148	0.3149	0.3144
	Inter-axis misalignment (radian)		
	α_{yz}	α_{zy}	α_{zx}
IMU1	6.38E-05	4.85E-05	1.14E-04
IMU2	-8.57E-06	-6.28E-06	-9.51E-06
IMU3	4.69E-04	6.24E-04	-5.83E-04
IMU4	1.38E-04	-5.81E-05	2.65E-04
IMU5	-1.62E-04	-2.17E-04	-3.00E-04
IMU6	8.93E-05	-1.80E-04	-1.49E-04
	Zero Bias (V)		
	b_x	b_y	b_z
IMU1	1.5791	1.5652	1.5824
IMU2	1.5756	1.5741	1.5757
IMU3	1.5328	1.5352	1.6256
IMU4	1.5675	1.5424	1.5607
IMU5	1.5893	1.5553	1.6010
IMU6	1.5862	1.5658	1.5564

4.3.4 Comparison of Methods

Three static calibration techniques of a triaxial accelerometer are demonstrated. These techniques are compared in terms of: if complex and costly test rigs are needed, time consumed from data collected until the results are computed, assumptions applied during calibration, computational complexity and the result accuracy. Table 4.22 lists the comparison of these three techniques. Cost is the

primary factor in most researches and practical applications. The rotary table method requires an index table that could precisely index at an angle less than 1^0. It is available commercially and expensive. The rotary table method and the 6/12 known positions method require a zero gravity reference in the form of an adjustable platform with the aid of an electronic spirit level. However, the 6/12 known positions method does not need an expensive tool to perform the permutations. A machined cube and a standard V-block are adequate to provide precise permutations relative to the gravity. The in-use method does not require any test rig and hence no additional cost is needed. In comparison with the time spent, the rotary table method inspects the accelerometer's outputs vigorously in small indexing angles for many repeated trials. However, the other two methods do not require very detail and small angles. Time spent on the rotary table method aggregates as all planes of a triaxial accelerometer need to be inspected in detail separately. Instead, for the other methods, all planes are inspected in a single trial.

Table 4.22: Comparison of static calibration techniques

	Rotary Table	6/12 Known Pos.	In-use
Test rig	Yes	Yes	No
Cost	High	Moderate	No cost
Time Consumed	High	Moderate	High
Assumption	Static	Static	Quasi-static
Computation	Low	Moderate	High
Accuracy	High	High	Varying

Both the rotary table method and the 6/12 known positions method take into account static positions for all permutations. However the in-use method identifies quasi-static positions out of motion data using a quasi-static detector which is a sequential computation algorithm. The in-use method requires relatively heavier computation algorithms for optimization. More time are needed in search for optimum results whereas relatively less time is needed for the other two methods since they apply simple linear algebra to solve simultaneous equations. It is unknown if the results computed using the in-use method is the optimum since no global minimum is identified. On the other hand, the rotary table method and the

6/12 known positions method utilize statistical mean as the result and their standard deviations to explain the variation and consistency of the results.

The result accuracy are high in both the rotary table and 6/12 known positions method. Both methods show highly statistical repetitive performance with an accurate gravitational reference (the platform). It must be noticed that the in-use method utilizes the assumption of quasi-static position in the search of the setup parameters. This assumption might pose variations in results if the quasi-static detector is altered especially the positive threshold (T_v). Furthermore the results using the in-use method are dependant to these factors, i.e. the optimization algorithm applied, the computation constraints and the starting values. The results would vary if the above factors vary as well. Comparing the results computed from each method, the in-use method reveals nearly zero or negligible inter-axis misalignment errors while the other two methods reveal small angle inter-axis misalignment errors. This might suggest that the in-use calibration method is not efficient in identifying small angle differences.

The question, “which method is better?”, might be possibly dependant on the applications. If accuracy is the core business, it is vital to investigate in fine and detail angles to reveal the performance and to identify the errors thoroughly. Otherwise, if coarse magnitudes of dynamic motions are of interest, a relatively less accurate calibration would possibly serve the purpose. The nature of the application might pose an influential factor in choosing the right method. For example, idiot proof or friendly applications might not want the end-user to involve in a stringent calibration procedure and hence an in-use method might be applied. However a relatively simple experiment procedure with common and cheap testing tools such as the 6/12 known positions method might provide accurate results for all general purposes.

4.4 Dynamic Calibration

The dynamic calibration serves two purposes, i.e. calibrating the gyroscope and validating the IMU dynamic performances. The first objective is achieved by comparing the angular velocities between the gyroscope output and the pendulous reference. The second objective is achieved by comparing the known pendulous

dynamic performance with the IMU outputs in the working plane, applying the principle of circular motion.

In normal practice, the scale factors provided by the manufacturers are used without further scrutinizing the accuracy of the specification. From equation (4.3), the equation of a gyroscope is rewritten as equation (4.32) for the purpose of the dynamic calibration. A pendulous angular velocity is used as the velocity reference. The zero bias is the average voltage of the gyroscope axial output during static condition.

$$\boldsymbol{V = K_c\dot{\theta}_p + ZB_{av}} \tag{4.32}$$

where,

$\boldsymbol{V}$	gyroscope output in the unit of volt (V)
$\boldsymbol{K_c}$	scale factor to be determined, in the unit of $V/°/s$
$\boldsymbol{\dot{\theta}_p}$	pendulous angular velocity in the unit of $°/s$
$\boldsymbol{ZB_{av}}$	average voltage output during static in the unit of volt (V)

The same experimental procedure is used to validate the dynamic performance of an IMU. Figure 4.17 shows a free body diagram of an IMU's outputs and the theoretical outputs in a pendulous system. The principle of circular motions is applied to formulate the equations. The formulation assumes that initially the IMU outputs ($\hat{a}_H \quad \hat{a}_V$) form an estimated coordinate and its vertical axis is pointing toward the pendulous shaft centre. They are listed as equations (4.33) and (4.34). The estimated horizontal acceleration is the sum of the tangential acceleration and the gravity component while the estimated vertical acceleration is the sum of the radial acceleration and the gravity component. When the pendulum is swinging, the pendulum angle θ_p will change over time. Its 1st and 2nd derivatives are the angular velocity and the angular acceleration respectively. According to the principle of circular motions, the tangential acceleration is the product of the radius multiplied by angular acceleration, $\ddot{\theta}_p$. The radial acceleration is the product of the radius multiplied by square of the angular velocity, $\left[\dot{\theta}_P\right]^2$. During static, only the gravity components are left in the equations.

The IMU is mounted at r radial distance from the pendulous shaft centre to the accelerometer ($A \rightarrow B$) and d horizontal shift. The actual IMU outputs ($a_H \quad a_V$) form an IMU coordinate which is always offset at a fix rotational angle, θ_o with respect to the estimated coordinate as shown in equation (4.35). It is assumed that the estimated coordinate and the IMU coordinate share the same origin. By applying the principle of direction cosine *(if a and b are the unit vector, $cos\ \angle(a,b) = a \cdot b$)*, a rotation matrix is formed as shown in equation (4.36). The actual IMU outputs could be transformed from the estimated IMU outputs using the rotation matrix.

$$\hat{a}_H = r \cdot \ddot{\theta}_p + g \cdot sin(\theta_p + \theta_o) \tag{4.33}$$

$$\hat{a}_V = r \cdot [\dot{\theta}_p]^2 + g \cdot cos(\theta_p + \theta_o) \tag{4.34}$$

$$\theta_o = \sin^{-1}\left(d/r\right) \tag{4.35}$$

$$\begin{bmatrix} a_H \\ a_V \end{bmatrix} = \begin{bmatrix} cos(\theta_o) & -sin(\theta_o) \\ sin(\theta_o) & cos(\theta_o) \end{bmatrix} \cdot \begin{bmatrix} \hat{a}_H \\ \hat{a}_V \end{bmatrix} \tag{4.36}$$

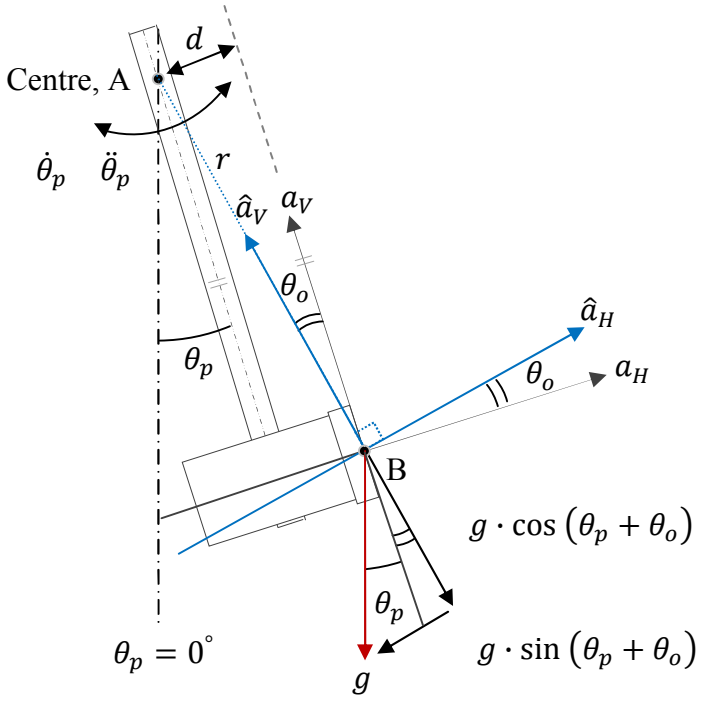

Figure 4.17: Free body diagram of an IMU-5DOF in a pendulous system

4.4.1 Experiments

In this study, two types of dual-axial gyroscopes, i.e. IDG300 and IDG500, were calibrated. The gyroscopes were compared to a reference angular speed measured from a specific plane motion provided by a pendulous test rig. An IMU-5DOF is calibrated using the test rig (Figure 4.18) consisting of a compound pendulum, a potentiometer designed as an electronic protractor as well as a tachometer, an electronic spirit level and a customized datalogger (see Chapter 3) sampling at 200Hz. A plump line hanging freely from the pendulum shaft centre is used a visual reference of the gravity. A stopper is used to mark the starting angle. With the help of an electronic spirit level, the test rig platform is aligned horizontally. A circuitry as shown in Figure 4.19 is designed for the potentiometer (R2) to perform as an electronic protractor that works at the range of $-40°$ to $+40°$. A unity buffer is included in the circuitry to isolate the potentiometer from the differential op-amp circuitry. The resistive trimmer (R1) is used to shift the DC baseline of the output (Vout). The amplification gain ($R12/R10$) is adjusted by trial-and-error to match as close as possible the angle range ($-40°$ to $+40°$) to the voltage range (0VDC to 3.3VDC). When the pendulum is not loaded with any dead weight, the neutral position of a free-loaded pendulum is defined as 0° which is parallel to the gravity.

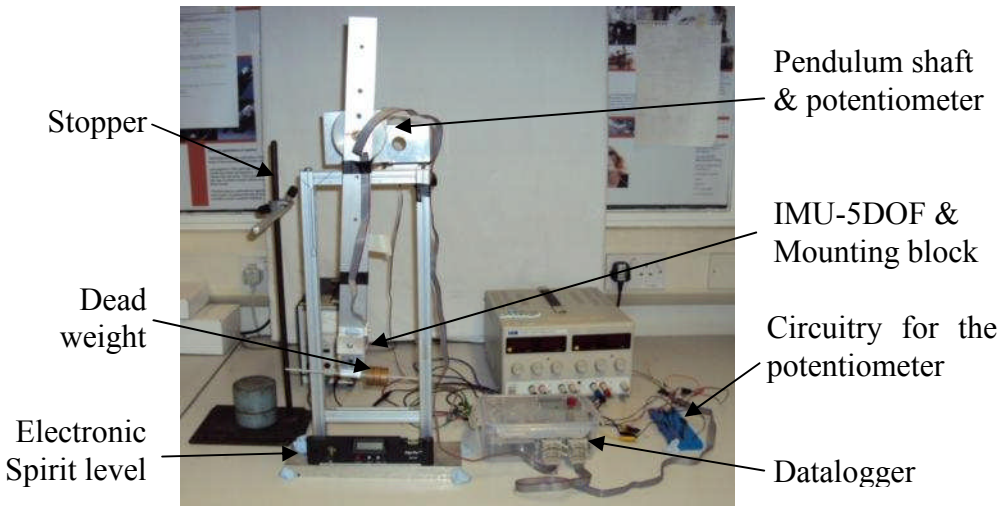

Figure 4.18: Setup of the dynamic calibration

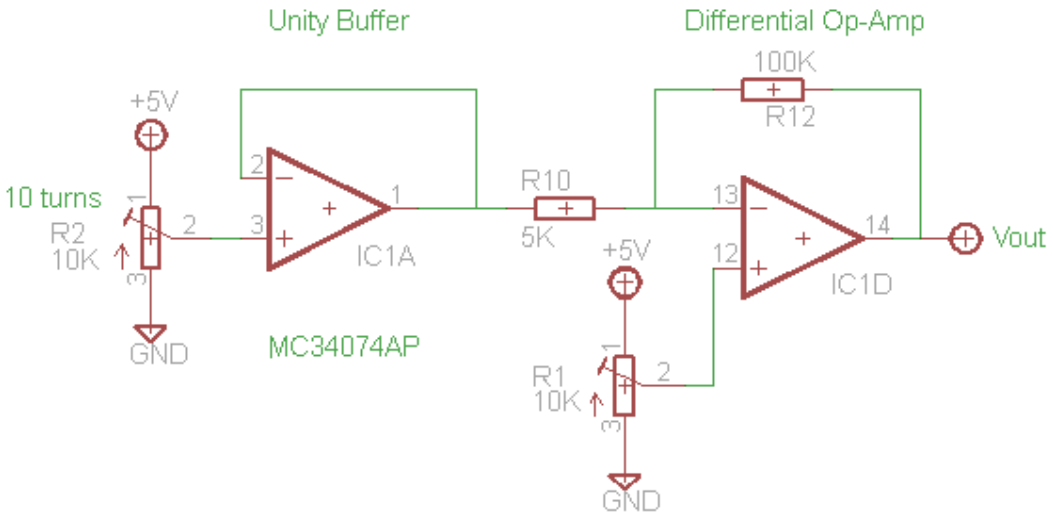

Figure 4.19: Circuitry of an electronic protractor

First of all the potentiometer is statically calibrated as an electronic protractor over the working range, -40^0 to $+40^0$. Using an electronic spirit level mounted horizontal at the pendulum arm, the pendulum arm is indexed at 5^0 interval, starting from -40^0 to $+40^0$ and vice versa. The same procedure is repeated five times. The outputs were recorded by the datalogger. The results were plotted in Figure 4.20. A linear regression equation (equation (4.37)) of mean voltages versus angles is modelled. The maximum standard deviation of the measurements at 0.011178V is observed and thus the standard error is 0.004999V. For 95% confident interval (Student t-value, $\alpha_{0.05,4} = 2.776$), the error could possibly cause a maximum error less than 0.6^0. Once the potentiometer is calibrated, it shall not be disturbed to avoid any misreading in future.

$$y = \mathbf{0.02765} \cdot x + \mathbf{1.437} \qquad \textbf{(4.37)}$$

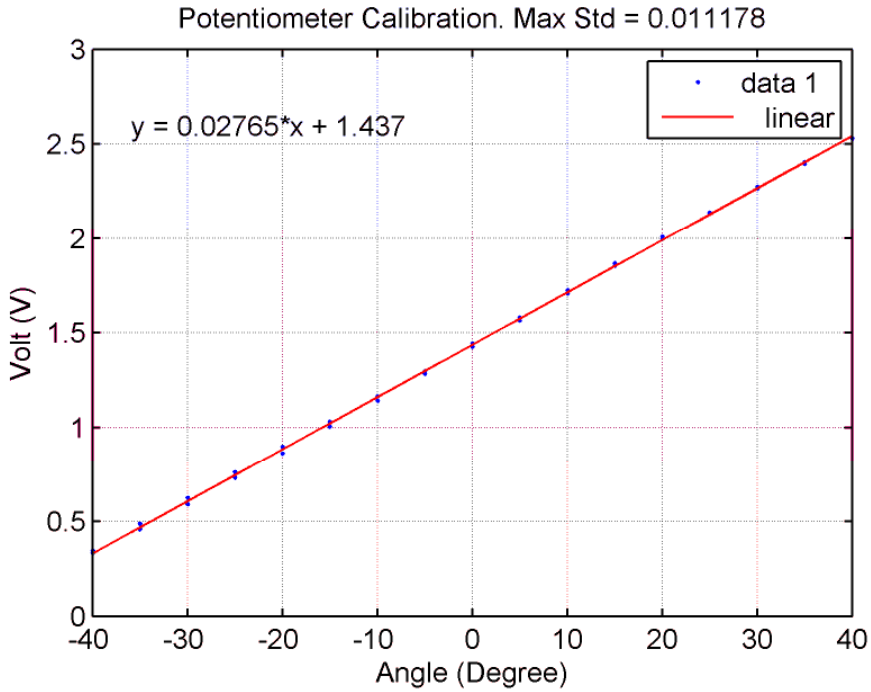

Figure 4.20: Calibration of the potentiometer

After the calibration of the potentiometer, the pendulous test rig is ready for dynamic calibration. For each trial, an IMU-5DOF is aligned in a specific plane such as YZ plane for XR axis or ZX plane for YR axis. The pendulum arm is released at -40^0 specified by the stopper. Data logging starts at the starting angle until the pendulum stops naturally. Repetitive trials were carried out. The same procedures were repeated for both gyroscopes in two planes. IMU1 to IMU6 are calibrated in the same way.

A Matlab m-file is written for the calibration of the potentiometer as a digital electro protractor. Another m-file is written for the dynamic calibration of a gyroscope and the validation of an IMU dynamic performance comparing to the theoretical models. Both m-files could be found in the CD attached.

4.4.2 Results

The procedure to analyze both axes (XR, YR) of a gyroscope is similar. The procedure results presented are based on YR axis in ZX plane. All calibrated results for the gyroscopes of the IMUs in the study are listed at the end of the sub section.

The gyroscope outputs in the ZX plane (YR axis) of IDG300 (IMU1 – IMU3) and IDG500 (IMU4 – IMU6) in volt are shown in Figure 4.21. Both gyroscopes' outputs are flattening during static when the pendulum arm is held still

at the starting angle, $-40°$. The zero biases (ZB) values vary for different IMUs. They are calculated as the average voltages (ZB_{av}) when the pendulum is static. The output (YR) starts to fluctuate sinusoidally as the pendulum is released until it stops naturally. For the same range of swings, both types of the gyroscopes do not share the same peak-to-peak excursions. The output of IDG500 fluctuates inversely as compared to IDG300. Each output is nearly half of IDG300 for the same swings.

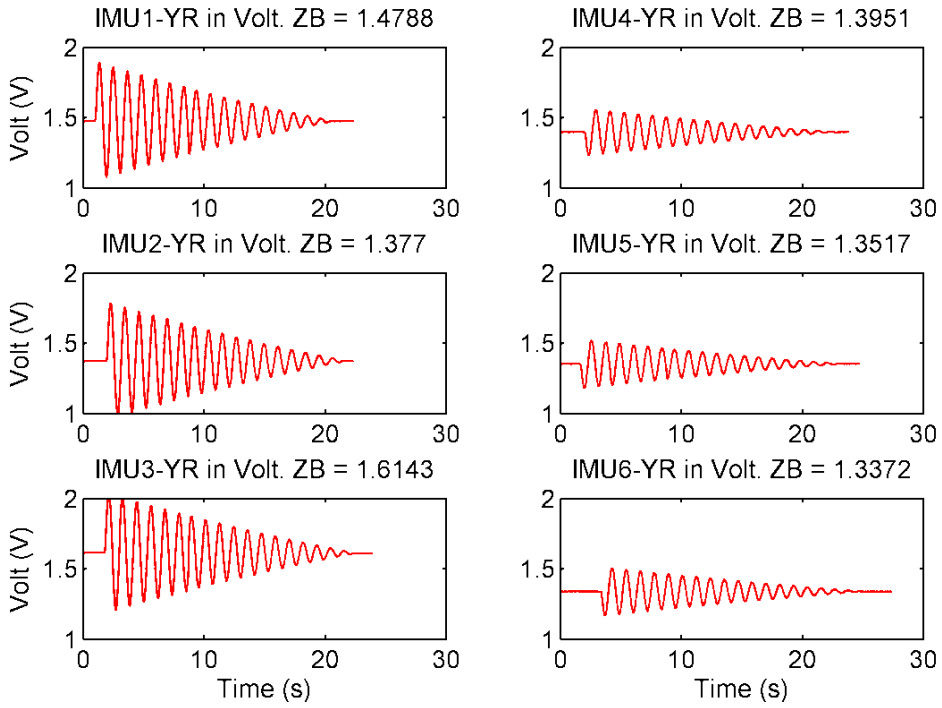

Figure 4.21: Gyroscope output-YR for IMU1 to IMU6

Higher cut-off frequency for a digital filter is possible but human walking is slow (~1s per stride or ~0.5s per step) and a cycle of the pendulous output is approximately 1s. Cut-off frequency at 3Hz should be sufficient for the application. For comparison purposes, a zero phase delay FIR low pass filter (ZPLP) with the cut-off frequency, f_c = 3Hz, is applied in order to filter high frequency noises but still maintains the same phase. The 1st derivative of the pendulous angle (θ_p) is the angular velocity ($\dot{\theta}_p$). Plots of the ZPLP angular velocities (^{0}/s) of the pendulum for each IMU are shown in Figure 4.22. It is worth noting that the pendulous angular velocities appear to be almost identical, suggesting highly repetitive performances.

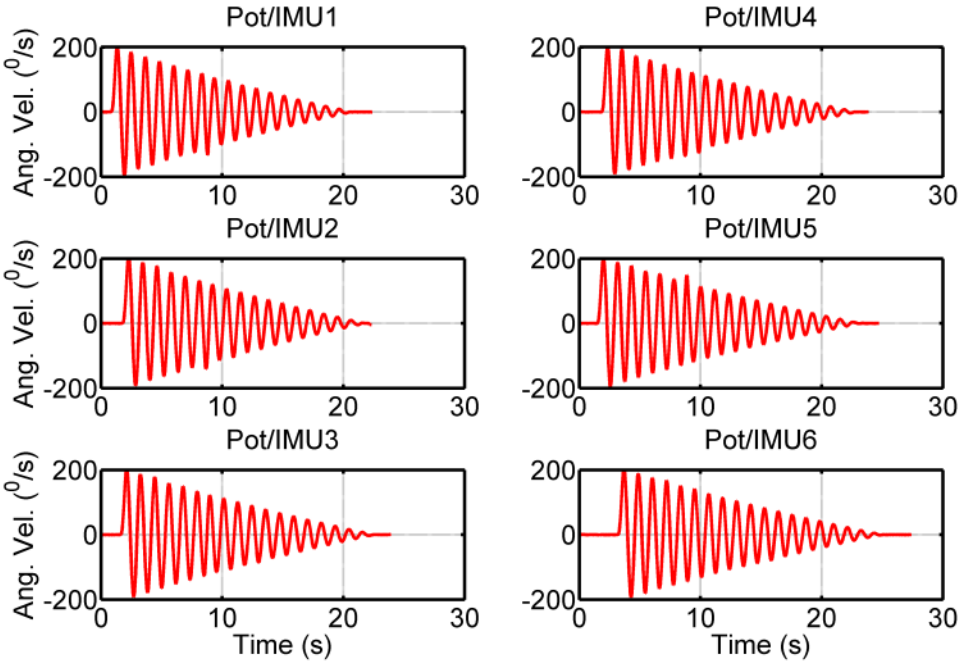

Figure 4.22: ZPLP pendulous angular velocities for IMU1 to IMU6

By applying equation (4.32), the scale factors (K_c) of the gyroscopes in YR-axis are computed and plotted as shown in Figure 4.23. However, K_c is not evenly distributed along the experimental time, probably due to division of steep gradients at a near zero pendulous angle. It is found that an averaging method will tend to overestimate or underestimate the results. To rectify this dilemma, the noisy K_c is filtered with ZPLP and a frequency distribution method is proposed. This method will count the number of computed scale factors that fall within a range of predefined frequency intervals (named as pockets). According to the manufacturer's specification, the scale factor for both types of gyroscopes is $2mV/°/s$. For a precision of 1%, the frequency pocket size is set at $2 \times 1\% = 0.02mV/°/s$. The scale factor will search through 0 to 0.01 $V/°/s$, stepping at $0.02mV/°/s$. The results were plotted in Figure 4.24 where the maximum count (frequency) is the expected scale factor, K_c.

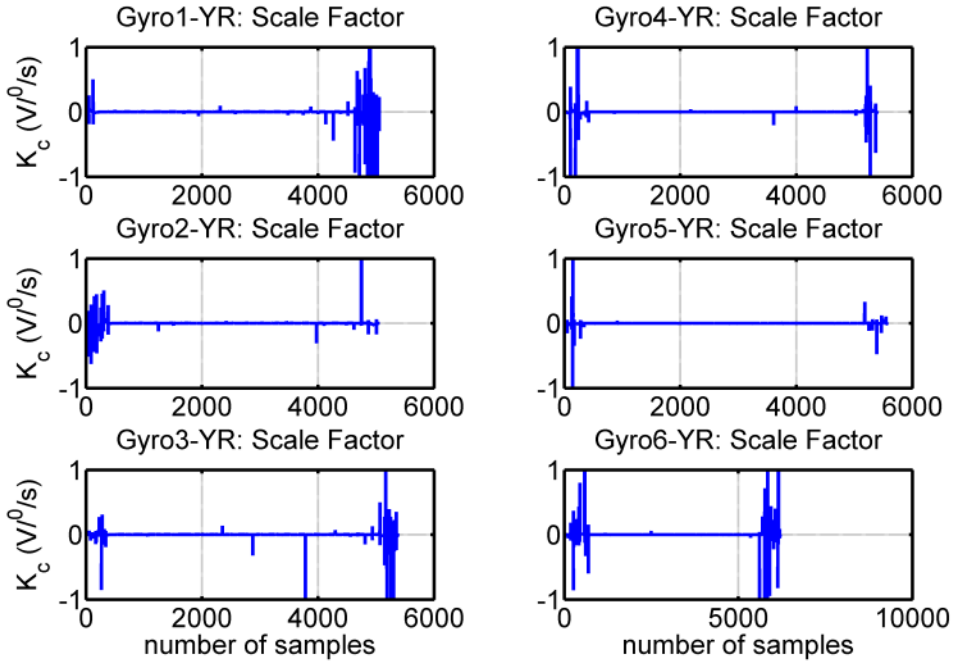

Figure 4.23: Scale factors of gyroscope output-YR for IMU1 to IMU6

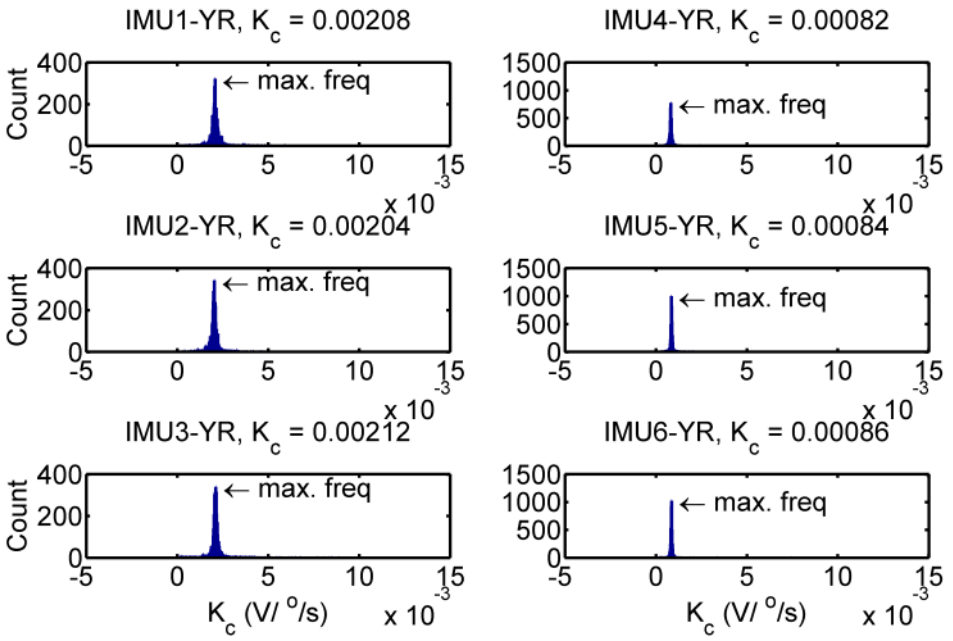

Figure 4.24: Frequency distribution of the scale factors of the gyro-outputs (YR) for IMU1 to IMU6

The same procedure is repeated for both the ZX plane (YR) and the YZ plane (XR). Table 4.23 lists the calibrated gyroscope scale factors in every axis. It is very obvious that the scale factor of IDG300 is close to the value provided by the manufacturer but IDG500 exhibits nearly half of the value. Hence, a new scale

factor of $0.83mV/°/s$ is proposed for IDG500 while IDG300 will keep the same value as provided by the manufacturer. On the other hand, the zero biases of each axis of the gyroscopes vary and are given in Table 4.24.

Table 4.23: Calibrated scale factors of the gyroscopes

Scale factors (V/°/s) of IDG300		
IMU	XR	YR
1	0.00196	0.00208
2	0.00204	0.00204
3	0.00196	0.00212
mean	0.00199	0.00208
Std	0.00005	0.00004
Scale factors (V/°/s) of IDG500		
IMU	XR	YR
4	0.00080	0.00082
5	0.00082	0.00084
6	0.00086	0.00086
Mean	0.00083	0.00084
Std	0.00003	0.00002

Table 4.24: Calibrated average zero biases of the gyroscopes

	Zero Bias (V)	
IMU	XR-ZB	YR-ZB
1	1.4633	1.4788
2	1.5924	1.3770
3	1.4916	1.6143
4	1.3137	1.3951
5	1.3316	1.3517
6	1.3380	1.3372

In an effort to validate the dynamic performances of the gyroscopes, the same pendulous test rig is used. By replacing the calibrated scale factors and the zero biases for the gyroscopes of IMU1 to IMU6, the gyroscope outputs could be

compared with the pendulum angular velocity. An example of the gyroscope outputs (Angular Velocity, ^{0}/s) in the ZX plane (YR) of IMU1 and IMU6 is shown in Figure 4.25. the root mean square (RMS) values of the gyroscopes for IMU1 to IMU6 are checked and listed in Table 4.25. It must be highlighted that IMU1 to IMU3 represent the gyroscope, IDG300 whose scale factor is the same as that recommended by the manufacturer but IMU4 to IMU6 represent the gyroscope, IDG500 whose scale factor is revised and its output sign is inverted to match the sign of the pendulum angular velocity. RMS values between the gyroscope output and the pendulum angular velocity in all cases are low, indicating matched calibrated scale factors and zero biases results. At the same time, high repetitive excursions and low RMS indicate that the sensory units are reliable and consistent.

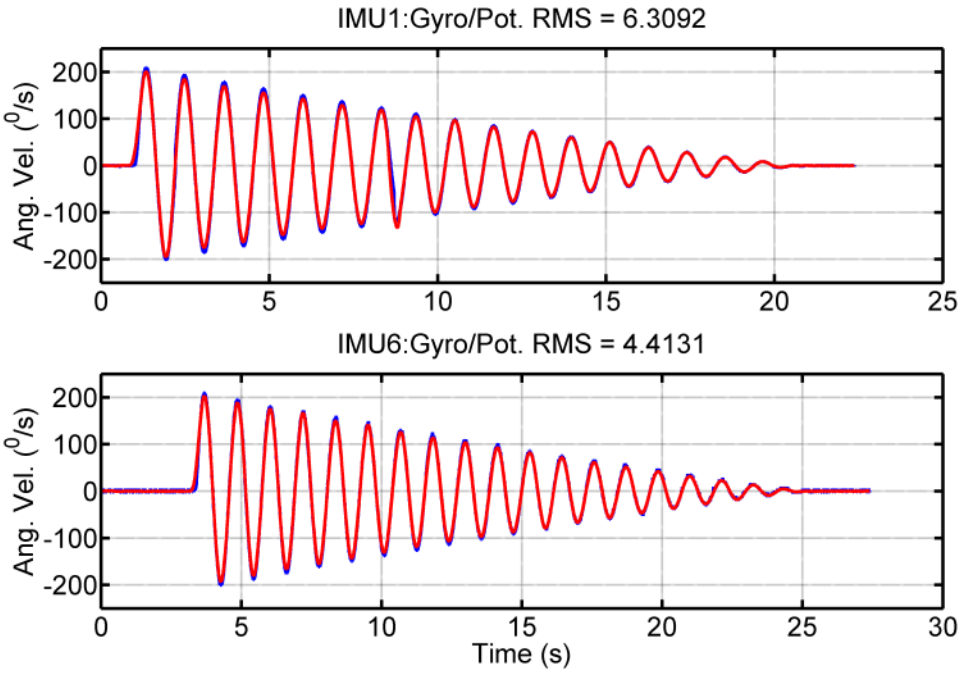

Figure 4.25: The comparison of the calibrated gyro-outputs (YR) with the reference angular velocity
(— Gyroscope — Potentiometer)

Table 4.25: RMS between the gyroscope and the reference (Pot)

IMU	RMS – XR/*Pot*	RMS – YR/*Pot*
1	3.7299	6.3092
2	4.6884	4.6036
3	3.3195	7.3905
4	4.3243	4.1309
5	5.2884	6.6633
6	5.5098	4.4131

Pot *Potentiometer*

To validate the dynamic performance of the triaxial accelerometer in a vertical plane, a number of key parameters are crucial by referring to equation (4.33) to equation (4.36). The pendulous angle (θ_p), angular velocity ($\dot{\theta}_p$) and acceleration ($\ddot{\theta}_p$) are the external references for the purposes of validation. Due to the geometry of an IMU (referring to Figure 4.17) mounted the ZX plane or the YZ plane, the rotational offset (θ_o) could be determined by measuring the radius, *r* and horizontal displacement, *d*. They are listed in Table 4.26.

Table 4.26: Geometry offsets of an IMU in a pendulous system

	ZX Plane	YZ plane
r (mm)	296	285
d (mm)	24	7
θ_o (degree)	4.65°	1.41°

An example of the accelerometer outputs (g-forces in Z-axis and X-axis) of IMU6 in ZX plane is illustrated in Figure 4.26. The dynamic performances of IMU1 to IMU6 are listed in Table 4.27 where consistent and low RMS values suggest great matches between the computational outputs and the actual outputs. Highly repetitive outputs also suggest that the sensory units are reliable and consistent.

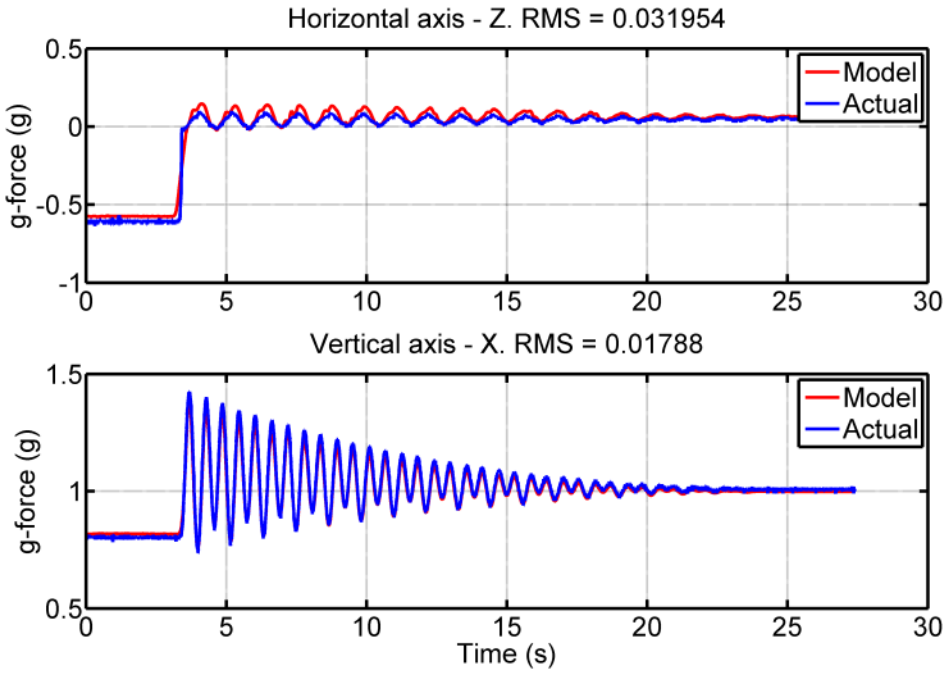

Figure 4.26: IMU6. Comparison between the models and the actual outputs in the ZX plane

Table 4.27: RMS between the models and the actual outputs for IMU1 to IMU6

IMU	Outputs	RMS in ZX plane	RMS in YZ plane
1	a_H	0.029383	0.025461
	a_V	0.014546	0.018140
2	a_H	0.028794	0.032807
	a_V	0.015191	0.018557
3	a_H	0.029648	0.029910
	a_V	0.037377	0.018202
4	a_H	0.037248	0.024468
	a_V	0.014331	0.016318
5	a_H	0.045020	0.030627
	a_V	0.016955	0.015967
6	a_H	0.031954	0.026414
	a_V	0.017880	0.021550
	Mean	0.026527	0.023202
	Std	0.010507	0.005909

4.4.3 Discussion

Dynamic calibration for an IMU is expensive if a gimbal system with a precise and stable control of rotational speed is used. However, the method proposed in this study is relatively simpler and economic. The pendulous test-rig is built using simple parts available in the market. On the other hand, the procedure is simple and fast. However there are still some limitations. Firstly, the operation range is limited because the pendulum is dependant on the gravity only. The range of the pendulum angular speed can be slightly increased by releasing at a bigger angle. Adding dead weights at the end of the pendulum would reduce the damping ratio (inversely proportional to moment of inertia), meaning that the pendulum will swing longer before coming into a halt. Secondly, the pendulum is working entirely on the gravity and it is not easy to acquire higher speed range without major mechanical design changes. It is convenient and cheap for the applications that operate in a low range of angular information such as the gait measurement. The dynamic calibration of the gyroscope shows very promising results. Discriminative scale factors and zero biases for IDG300 and IDG500 are identified via this method. The accuracy of the IDG300 is close the specification given by the manufacturer but this does not apply to IDG500. Moreover the performances of the IMUs are reassured by validating them with the theoretical models.

4.5 Summary

An IMU is an integrated system of an accelerometer and a gyroscope. It needs to be calibrated properly before use. Multiple static calibration techniques are introduced. A rotary table method is a vigorous technique that looks into fine indexing angles and is time-consuming. This technique is preferable if a detail and precise accuracy is needed in an application. A 6/12 known positions method simplifies known positions into multiple permutations of a cube. It is a coarse study of the IMU, revealing rather precise results and is suitable for all general purpose applications. Lastly, an in-use calibration which needs IMU motion data provides a fluctuating accuracy, dependant on the criteria and the solver chosen during an optimization process. It is crucial to inspect an IMU dynamically. A simple and economic method that implements the working principle of a compound pendulum is introduced. The

pendulous system could calibrate a gyroscope and validate the dynamic performance of an IMU at the same time. The results show that the IMUs reveal promising and reliable performances.

CHAPTER 5
HUMAN GAIT TRIALS

5.1 Introduction

This chapter reports the experimental designs, preparation and setup of the human gait trials for the investigation of a novel lower limb prosthetic alignment monitoring system. A series of gait data analysis is introduced. The system is designed to monitor the effect of the lower limb prosthetic alignments by collecting kinematic data from human lower limb segments for post-processing. There are many alignment parameters [1] but two key restrictions, i.e. ankle [2, 17] and walking level [16], are identified as the crucial criteria that affect the gait. At this early stage, only healthy volunteer participants were used to generate gait data under the above restrictions. Parts of the gait data will be used to validate the functionality and the reliability of a customized ambulatory device. In addition, the gait data will be used to present a gait assessment methodology for the lower limb prosthetic alignments.

The experiments received an ethical approval from the Research Support Unit of the University of Leeds. Participant consents were received before performing the human gait trials. Besides, the participant consents for the agreement to photographic and video records were also collected.

5.2 Overview of Human Gait Trials

Human gait trials involve stringent experimental requirements as shown in Figure 5.1. First of all, an experiment protocol is drafted and submitted to the Research Support Unit of the University of Leeds. Repeated amendments are necessary if the committee is not satisfied with the protocol and the explanation. The protocol includes the detail of the experiments such as aims and objectives of the experiment,

number of participants, equipments and procedures, health and safety precautions, data protection, volunteers' recruitment and consents, etc. The information could be found in Appendix C. The recruitment is carried out once an ethical approval is granted. The recruitment involves inviting the targeted population, interviewing the volunteers and briefing the information to them. Participant consents are documented once the volunteers agree to take part in the trials. Besides, the participants are asked to give their consents for the usage of their photos and videos in academia publications or presentations. The data collections of human gaits are scheduled to meet both the time of the investigator and the participants.

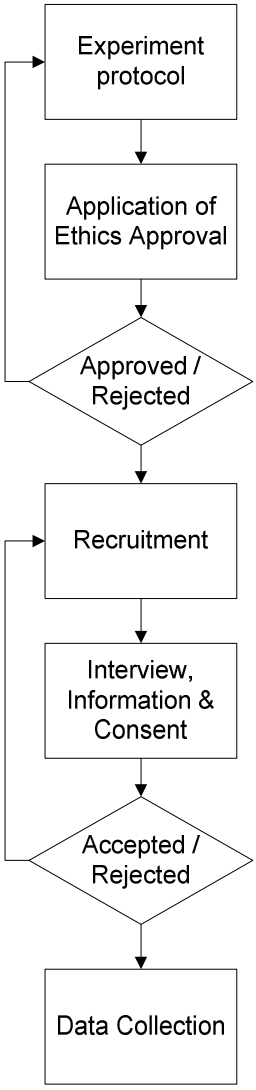

Figure 5.1: Overview of the human gait trials

5.3 Aims and Objectives

The aim of the experiments is to collect different gait data in level and non-level walking under the constraint of normal and misaligned ankles. The collected gait data would serve two purposes. Firstly, the data are used to testify and justify if a customized ambulatory gait data collection system is functional and reliable. Secondly, the data is used to preliminarily justify a novel lower limb prosthetic alignment monitoring system if it is capable of recognizing different gait patterns under different gait constraints.

5.4 Equipment

A customized ambulatory gait data collection system (see Chapter 3) will collect kinematic gait data from the participants. It consists of five units of Inertial Measurement Unit (IMU) as the motion sensors and a light-weight datalogger (Figure 5.2a). The datalogger has multiple analog input channels and samples at 200Hz. An IMU (Figure 5.2b) consists of a triaxial accelerometer ($X \quad Y \quad Z$) and a dual axial gyroscope ($XR \quad YR$), making up a total of five degree-of-freedom (dof). These IMUs are called IMU-5DOF. They are small and light weight. Each unit of IMU is mounted in an acrylic holder stitched to a flexible strap patched with Velcro. Each unit is wired to the datalogger using detachable plugs and sockets. All IMU-5DOF are pre-calibrated (see Chapter 4) before the trials. The system is powered with a 9VDC battery. When the trial starts, the sensory data will be recorded in a secure digital (SD) card which will be post-processed later. A vest is designed to carry the datalogger and the battery.

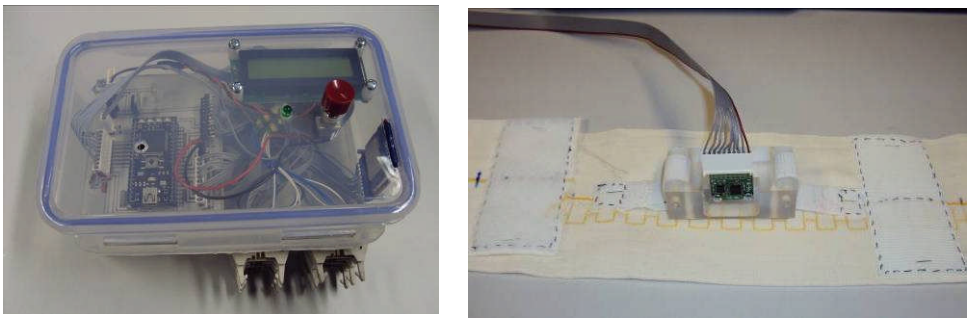

(a) (b)

Figure 5.2: (a) The customized datalogger, (b) An IMU and the Velcro strap

5.4.1 The Body Landmarks

There are five units of IMU-5DOF to be strapped at different body landmarks as shown in Figure 5.3. They are the body centre of mass (BCOM) near sacrum, lateral thighs and lateral shanks. Each IMU-5DOF is labelled accordingly to the location of the body landmarks as listed in Table 5.1.

Figure 5.3: The body landmarks and the IMUs

Table 5.1: The body landmarks and the IMUs

Body Landmark	Label	IMU Type (Components)
Right Shank (lateral)	IMU1	Type-1 (ADXL330/IDG300)
Left Shank (lateral)	IMU2	Type-1 (ADXL330/IDG300)
Right Thigh (lateral)	IMU3	Type-1 (ADXL330/IDG300)
Left Thigh (lateral)	IMU4	Type-2 (ADXL335/IDG500)
BCOM (back)	IMU5	Type-2 (ADXL335/IDG500)

The IMU-5DOF sensory axes are identified. Their sensory axial directions are illustrated in Figure 5.4. At the lower limb segments, they are arranged in such orientations:

1. YZ plane is in the sagittal plane. Y-axis and Z-axis point at the anterior-posterior direction and the vertical direction respectively.

2. X-axis points in the medial lateral direction.
3. XR and YR are aligned accordingly but their output signs are dependant to the type of IMU-5DOF. Their output signs are shown in Figure 5.4.

At BCOM, the IMU-5DOF is arranged in such orientation:

1. The XY plane is in the frontal plane. X-axis and Y-axis point at the vertical direction and the medial-lateral direction respectively.
2. Z-axis points in the anterior posterior (AP) direction.
3. XR and YR axes point at the vertical direction and the medial-lateral direction respectively.

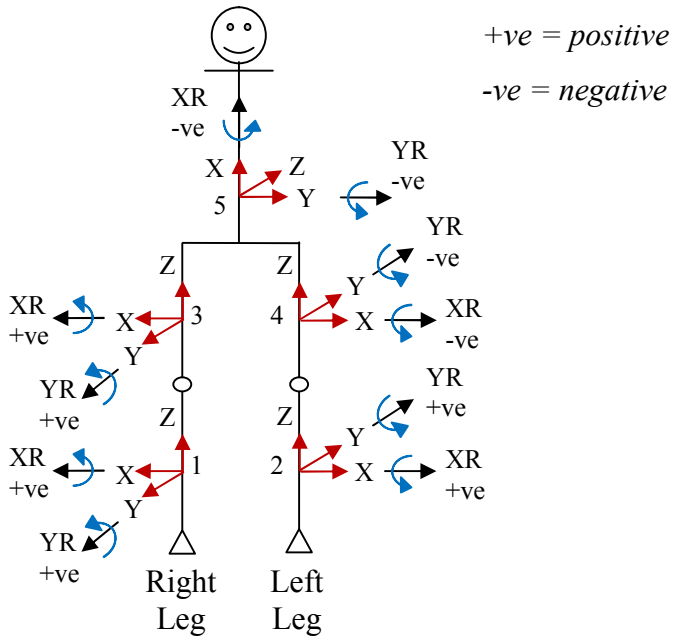

Figure 5.4: IMU-5DOF and their axes at the body landmarks

Original IMU-5DOF axial outputs impose several issues during the interpretation of body movements.

1. Y-axes in the left leg and the right leg are in the opposite direction.
2. XR-axes in the left leg and the right leg are in the opposite turning direction.

A new notation in the body axes is proposed in replacement of the original IMU axes. All gyroscope axes will be positive using the right hand gripping rule. Table 5.2 lists the rules for the conversion. Figure 5.5 shows the new notation of the IMUs after conversion.

Table 5.2: Protocol for the conversion from the IMU axes to the body axes

No	Both legs	BCOM
1	X points laterally.	X points vertically
2	Y points anteriorly.	Y points laterally
3	Z points vertically.	Z points anteriorly
4	XR is +ve when the shank swings anteriorly.	XR is +ve when the body turns from right to left.
5	YR is +ve when the shank swings medially.	YR is +ve when the body leans forward.
+ve = positive		

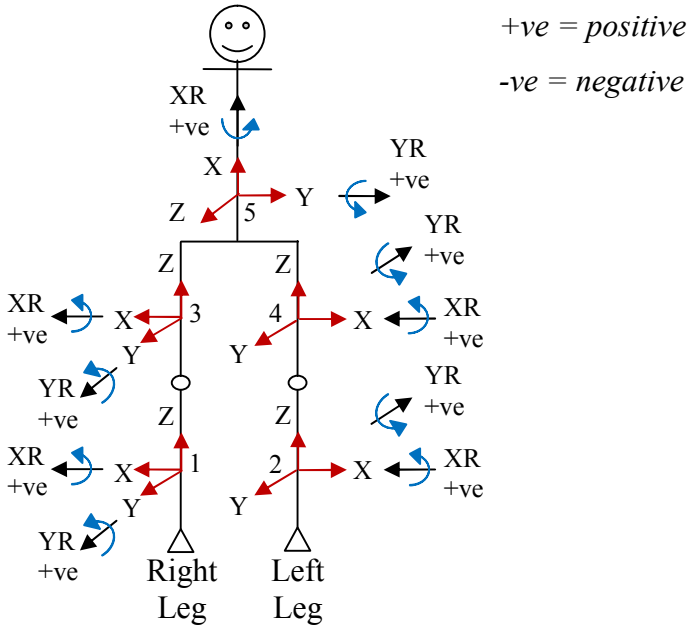

Figure 5.5: Conversion to Body Axes

5.5 Experiment Design

Four different modes of walking trials are cross-designed to investigate two major factors, i.e. the walking level and the ankle alignments. It is decided that two types of walking levels are tested. They are level walking and non-level walking at 5^0 tilt. Before questioning a number of complex gait patterns due to multiple ankle misalignments, the importance of ankles affecting the gait is investigated. Two types of ankle constraints are designed. They are no ankle constraint (ankle-freed) and with ankle constraint (ankle-locked) at the neutral position. The neutral position is

defined as the posture during quiet stance on a flat level where the angle between the insole and the centre line of the shank is approximately at 90^0. The angle could be measured using a protractor. Table 5.3 lists the experiment setup modes. Two pairs of modes, (S1, S2) and (S3, S4), are used to investigate the effect of level changes to the walking performance. Each pair would look into the effect of the ankle to the walking performance. During ankle-freed, a participant is asked to put on his shoes, preferably with little or no heel raised. During ankle-locked, the ankles are immobilized at the neutral position by putting on a pair of foot orthoses which inhibit ankle dorsi/plantar flexions during walking. A manual treadmill tilted at 5^0 is used for non-level walking while an eight metre gangway is used during level walking. These setups are illustrated in Figure 5.6. One of the setups, Level- Ankle-freed (S1), is also known as normal level walking which is the trial of normal human locomotion.

Table 5.3: Experiment setup modes

Mode	Description	Label
S1	Walking on a flat level with ankle freed.	Level – Ankle-freed
S2	Walking on a flat level with ankle locked.	Level – Ankle-locked
S3	Walking on a tilted level with ankle freed.	Tilt – Ankle-freed
S4	Walking on a tilted level with ankle locked.	Tilt – Ankle-locked

Using a statistical test called test-retest reliability, the system is checked for its functionality and reliability. To date, the system is not validated with a benchmark although it is always possible.

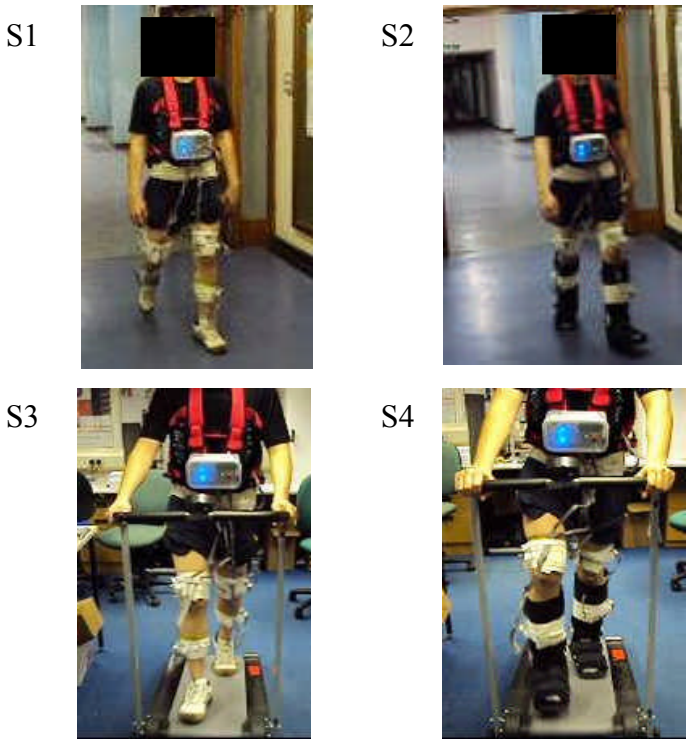

Figure 5.6: Experiment setup modes, S1 to S4
(For S1-S4 details, see Table 5.3)

5.5.1 Test-retest Reliability

It is important to justify the customized ambulatory gait data collection system as a reliable gait measurement instrument. A statistical method [99] called test-retest reliability is adopted for this purpose. This method investigates the consistency of an instrument‘s performances over a duration provided all physical variables are maintained. A coefficient called Cronbach’s Alpha (CA) would justify the reliability of the system. If CA is above 0.7, the system is reliable or vice versa.

5.5.2 Procedures

Figure 5.7 shows the procedure of the gait trials. The bio data of the participants are collected once only before the beginning of the first trial. The data include the age, gender, body weight, height and health status especially walking difficulties if any. The trials work out sequentially according to the modes (S1 to S4). For all modes, a participant will put on the portable monitoring system aided by the investigator. Before the beginning of each mode, the participant will be asked to familiarize with the new installation by walking freely for some times. The gait data collections start

when the participant is confident with the new installation. The participant is asked to remain stand-still for a few seconds at the start of any trials as the datalogger begins recording the gait data. Walking with self-selected speed is advised. The participant is asked to stand still for a few seconds once reaching the end of the gangway during the level walking or sufficient numbers of steps are recorded during non-level walking. Afterward the data logging is stopped. In between each trial, the participant will be asked to rest for a minute. For each participant, at least five trials per modes are collected for post-processing later. The trials are scheduled into two sessions in a week time. Every participant will repeat the same modes of trials as mentioned above in the following week.

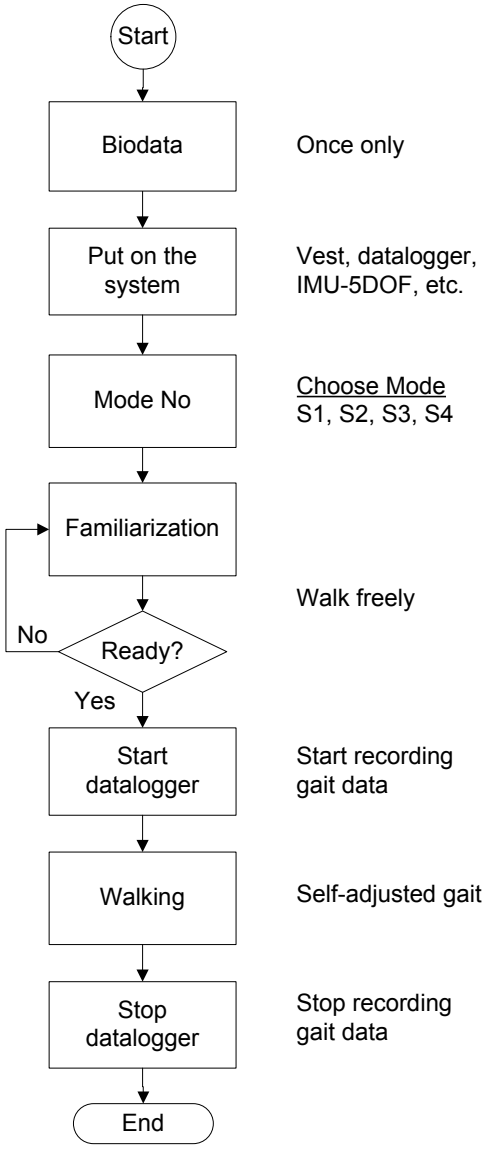

Figure 5.7: The experimental procedure

5.6 Data Analysis

Unprocessed time series gait data could visually provide some qualitative features regarding the walking performance. For further analytical comparisons, the gait data needs to be processed and conditioned. The signal processing and conditioning are as listed below:

1. Spectral analysis
2. Filtering
3. Gait event identification
4. Gait cycle (GC) extraction
5. GC normalization
6. Linear interpolation of the normalized GCs (LiNo GC)
7. Building LiNo GC stacks and data structures with labels

First of all, spectral analysis is performed to identify the frequencies hidden in the gait data. It is expected that normal walking will perform at the low frequency range. Table 5.4 lists the selection of filters and cut-off frequencies used in ambulatory devices. It can be seen that a variety of cut-off frequency selection has been performed. To avoid comparison error due to incompatible time delay after filtering, a Zero Phase low pass filter (ZPLP) at the cut-off frequency, f_c = 3Hz, is proposed.

Table 5.4: Review of the cut-off frequency

No	Author	Devices	Filter	Cut-off (Hz)
1	Moe-Nilssen [72]	*acc*	LPF	55
2	Tong & Granat [33]	*gyro*	LPF Butterworth	4
3	Aminian [32]	*gyro*	LPF	*nm*
4	Moe-Nilssen & Helbostad [73]	*acc*	LPF HPF Zero Phase	55 0.016
5	Auvinet, et al. [74]	*acc*	*nm*	*nm*
6	Mansfield & Lyons [30]	*acc*	anti-aliasing filter LPF	100 2
7	Pappas, et al. [34]	*gyro*	BPF	0.25 - 25
8	Luinge & Veltink [77]	*both*	Kalman Filter	-
9	Henriksen, et al. [76]	*acc*	*nm*	*nm*
10	Jasiewicz, et al. [78]	*both*	*nm*	*nm*
11	Torrealba, et al. [100]	*acc*	*nm*	*nm*
12	Lau & Tong [31]	*both*	2 order Butterworth LPF	10Hz
13	R. Takeda, et al. [80]	*both*	Wave Decomposition	*nm*
14	J. Rueterbories, et al. [83]	*both*	*nm*	*nm*
15	Torrealba, et al. [79]	*acc*	LPF	*nm*
16	R. C. González, et al. [81]	*acc*	11th order FIR filter	2Hz
17	Gouwanda & Senanayake [82]	*both*	*nm*	*nm*

nm = *not mentioned*
BPF = *Band Pass Filter*
LPF = *Low Pass Filter*
HPF = *High Pass Filter*

both = *accelerometer and gyroscope*
acc = *accelerometer*
gyro = *gyroscope*

Gait event identification is the most important step before extracting gait cycles. Successive identification of critical gait events means that steps or strides

could be isolated and hence extracted separately. Two critical gait events, i.e. Heel Contact (HC) and Toe-Off (TO) are criteria to isolate the strides and to discriminate between stance phase and swing phase respectively. Other gait events such as Mid-Stance (MSt), Mid-Swing (MSw) etc. are not the main discriminator during gait cycle extraction but rather important assessment features within a GC. Researchers have attempted to identify critical gait events using accelemetric outputs at the shank and the BCOM. At the same time, some researchers have studied the gait identification using a gyroscope located at the shank or foot. A review of the gait identification strategy in an ambulatory system is listed in Table 5.5. Four of the authors have utilized foot switches to justify the timing of the gait events. Of all gait data, the lateral gyro-output at the shank displays the largest excursion and distinctive swing phase. For normal locomotion, a standard lateral gyro-output (Angular Velocity, ^{0}/s) at the shank will look like Figure 5.8. Mid-Swing (MSw) is identified as the peak excursion of the shank lateral gyro-output.

It is in agreement that Toe-Off is the first valley before the shank goes into swing phase and Heel Contact is the first valley before the heel stamps on the floor or after the swing phase. However to opt to multiple styles of walking performances under different restrictions (S1 to S4), a new gait identification strategy such as the one shown in Figure 5.9 is proposed for decision aids. Figure 5.9 displays two plots of the shank at the same time where the upper plot is the g-forces in the unit of gravity (g) and the lower plot is the angular velocities in the unit of degree per second (^{0}/s). The strategy would make use of the g-forces together with the angular velocities at the shank to identify all criteria gait events. At TO, the g-forces exhibit a steep increase followed by an acute decrease when the shank swings freely in the anterior direction. As the shank accelerates anteriorly (TO to MSw), an increase in the g-forces (especially in the vertical direction) is observed. After the peak of the swing (MSw), the shank de-accelerates (steeper), drop in the g-forces are noticed. At the very moment after HC, the g-forces exhibit a spike of shock wave. These phenomenon provide additional decision aids during gait identification.

Manual gait identification using Matlab plots such as Figure 5.9 is adopted to opt for all experiment designs (S1 to S4). Any selected gait events on the shank lateral gyro-output using the function of 'Data Cursor' (*a function found in a Matlab figure*) could be exported to the Matlab workspace. Their location indexes will be used during gait cycle extraction. These indexes are named as gait cycle indexes

(GCI). This gait event identification process requires great patience from the analyst.

Table 5.5: Review of gait identification methods

no	Author	Method	TO & HC
1	Tong & Granat [33]	Gyroscope at shank	TO ≡ -ve valley before MSw HC ≡ -ve valley after MSw
2	Aminian [32]	Gyroscope at shank Verified with foot switch (FSR)	TO ≡ -ve valley before MSw HC ≡ -ve valley after MSw
3	Pappas, et al. [34]	Gyroscope at back of heel Verified with FSR insole	TO ≡ -ve valley before MSw HC ≡ -ve valley after MSw
4	Jasiewicz, et al. [78]	Gyroscope at shank Verified with foot switch	TO ≡ -ve valley before MSw HC ≡ -ve valley after MSw
5	Lau & Tong [31]	IMU at Thigh and shank and heel Verified with insole FSR	use FSR to validate (HC, TO)
6	Rueterbories, et al. [83]	Review paper of ambulatory system	TO ≡ -ve valley before MSw HC ≡ -ve valley after MSw
7	Gouwanda & Senanayake [82]	Hybrid Multi-resolution Wavelet Decomposition	TO ≡ -ve valley before MSw HC ≡ -ve valley after MSw
-ve = negative *MSw = Mid Swing*			

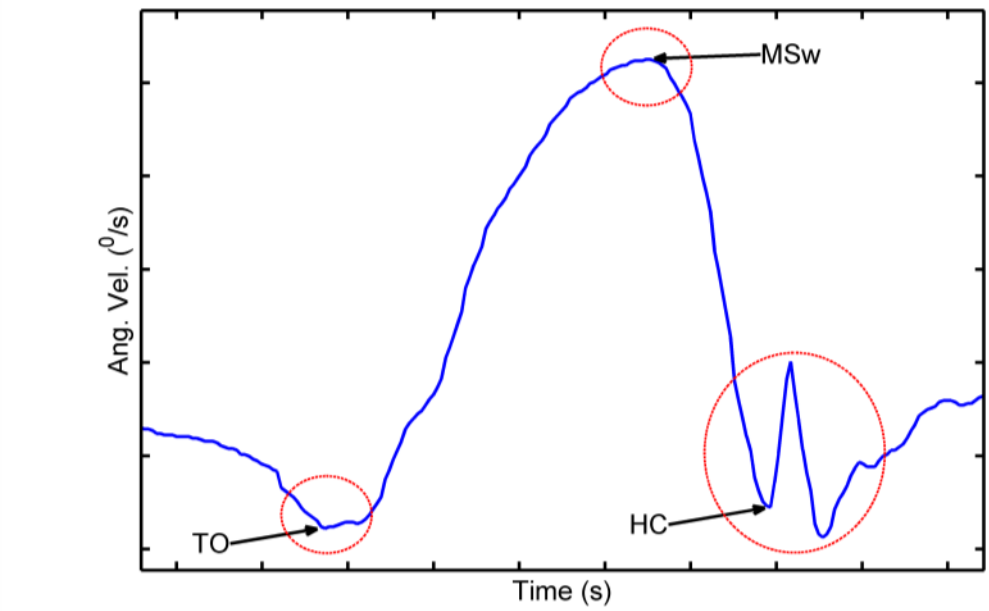

Figure 5.8: Gait event identification using the shank lateral gyro-output (TO = Toe-Off, MSw = Mid-Swing, HC = Heel Contact)

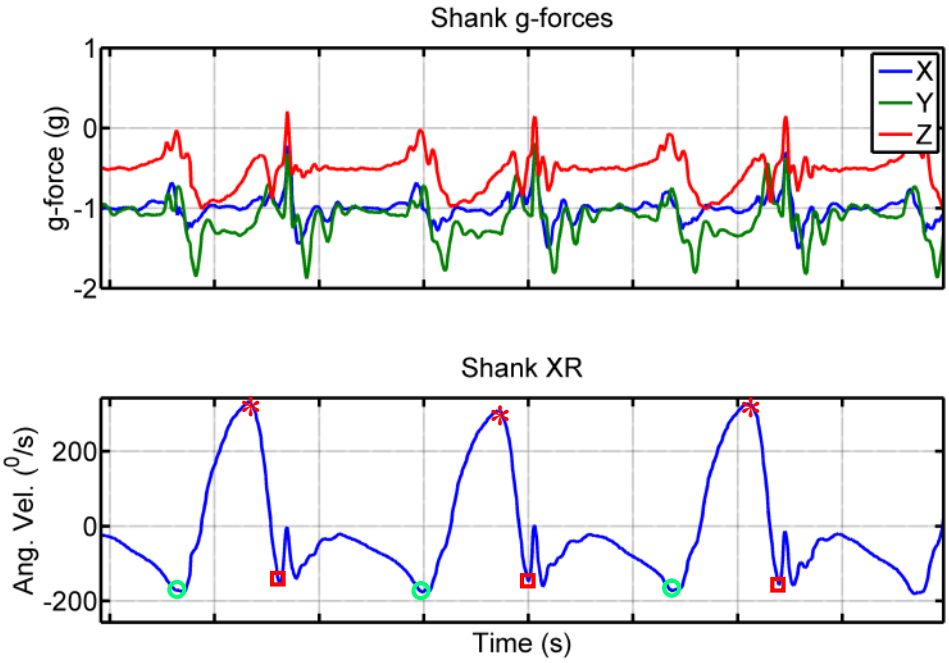

Figure 5.9: A new gait identification strategy (HC, TO, MSw)

GC [20] is defined as the period between two adjacent HC of the same leg. GCs are extracted individually from the time-series data using the gait cycle indexes (GCI). For the sake of comparison, all time axes of extracted GCs are normalized from zero to one. However, they are still not in the same data length and interval.

Normalized GCs are remapped using linear interpolation (LiNo GC). After remapping, their time-axes are in the same range, same length and equal interval.

A data structure is a tree-structure of arrays. Each set of structure is labelled according to the trial (see Table 5.3). The structure is further refined into smaller relevant branches in the term of body segments. Extracted GCs from each sensory axis are stacked. For each participant and each experimental mode, LiNo GC stacks are written and saved in a data structure formatted as shown in Figure 5.10. The data structure is labelled accordingly to the type of experimental modes. New structures are created according to the subjects and trials taken. At this stage, LiNo GC structures are useful for many computational analyses.

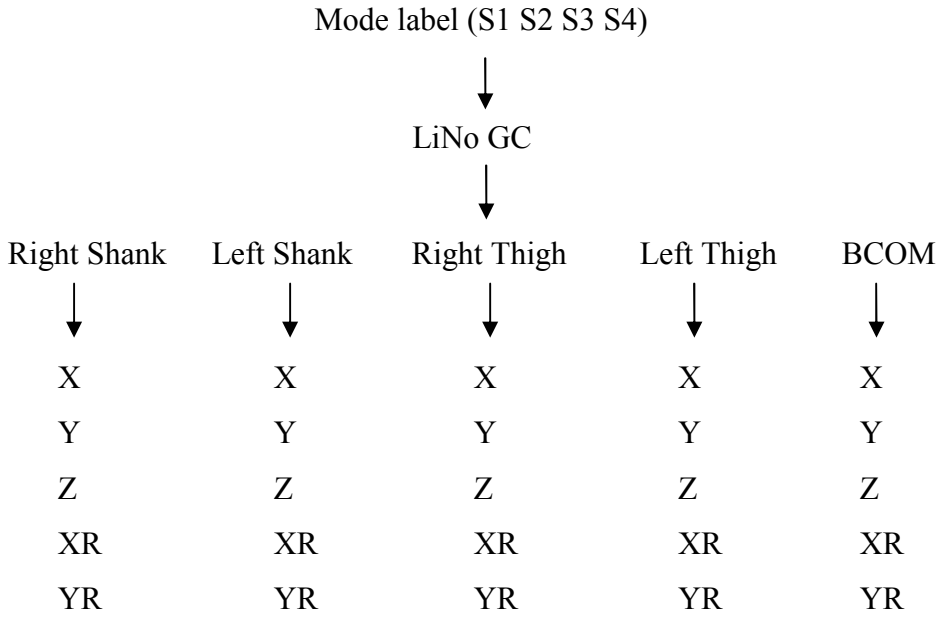

Figure 5.10: GC data structure format

Two Matlab m-files are written to process the gait data into two halves. The first half is semi-automatic gait identification via a Matlab plot (similar to Figure 5.9). The second half will process the gait data as explained above and organize recognized GCs into predefined data structure (similar to Figure 5.10). Another Matlab m-file is written for the test-retest reliability. These m-files could be found in the CD attached.

5.7 Results

The results focus on the first objective that is the basic function of the customized ambulatory gait data collection system as a reliable gait measurement instrument. A series of gait signal processing and conditioning is required before the data is presented statistically or further clustered in groups. The second objective will be achieved by further gait analysis on gait clustering which will be reported on Chapter 6.

Three male participants have volunteered to participate in the study. The bio data of the participants are listed in Table 5.6. They age between 24 to 38 years old. They are healthy and do not have any sorts of walking difficulties.

Table 5.6: Bio data of the participants

Participant	Age	Gender	Height (cm)	Weight	Health
1	38	Male	172	89	Good
2	38	Male	181	86	Good
3	24	Male	175	75	Good

Five units of IMU-5DOF are located at five different body landmarks, making up a total of 25 sets of body kinematic outputs sampled at the same time. The IMU voltage outputs were post-processed. Figure 5.11 to Figure 5.13 illustrate an example of measured kinematic gait data of participant 1 during normal level walking. From these figures, critical gait events and gait phases could be recognized and are labelled. Interpretation of the human walking and relative motions amongst the body segments could be identified according to the gait labels and gait definitions. The kinematic data are the accelerations (g-forces) and angular velocities of each IMU located at the pre-defined body landmarks. From Figure 5.5 (assignments of the sensory axes at predefined body landmarks), body motions could be interpreted in the body axes (ML lateral, AP, vertical) and planes (AP plane and ML plane). These outputs are cyclic. Walking is a series of controlled movements involving multi-linked body segments. The kinematic measurements are localized at the predefined segments. Qualitative observations in different planes could help to develop an overview of the gait before further analysis. Normal human locomotion of all participants is similar. The explanations are based on participant 1.

In the frontal plane, cycles of body bobbing up and down are easily noticed in the vertical axes of the g outputs. BCOM vertical g-output displays the smallest excursion while the shanks display the largest excursion, possibly due to shock absorption [101]. Spikes of g-forces during heel contacts are clearly seen in the vertical axis especially the shanks. Movements in the medial-lateral (ML) direction are less obvious but are still observable. These include cyclic body sways as observed in BCOM lateral axis and the medial-lateral movements in the legs during the highly synchronized inter-changing of stances and swings. The vertical gyro-output at BCOM shows that the body is twisting to the left and right cyclically during walking. The gyro-outputs of the legs in the anterior axis display slightly segments rotations as the legs swing in the medial-lateral direction and the body sways in the medial-lateral direction.

In the sagittal plane, the cyclic body sways in the anterior-posterior (AP) direction are observed. The observations could be seen in both the relevant g-forces in the AP axis and the gyroscope outputs in the lateral axis. In the AP direction, walking is a cyclic ‘pushing’ and ‘braking’ process of the body by the lower limbs as displayed by the AP g-forces in BCOM and the legs. The BCOM gyroscope outputs in the lateral axis indicate that the body swings forward during single limb stance but would appear to lean backward for a short moment during heel contact. Lateral thigh/shank gyro-outputs during swing phase are easily observed as the largest excursions during the swing phase but their outputs fluctuate slightly during stance phase. Significant gait events during normal walking such as Heel Contact (HC) and Toe-Off (TO) could be identified from the shanks outputs especially the vertical g-forces and the lateral gyro-outputs. Successive identification of these gait events are needed for further gait analysis.

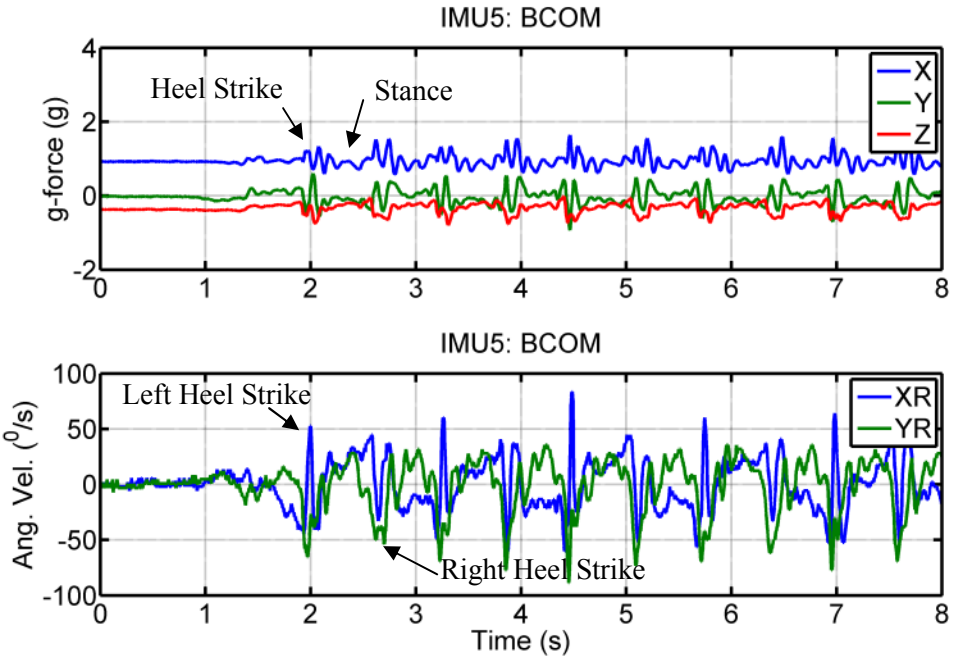

Figure 5.11: Participant 1. BCOM outputs during normal level walking

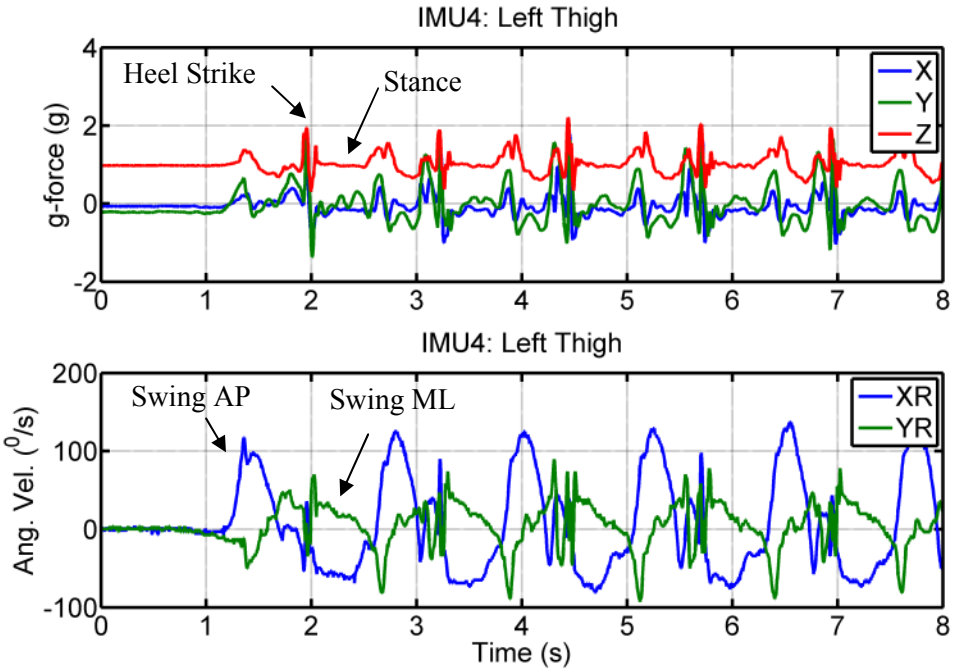

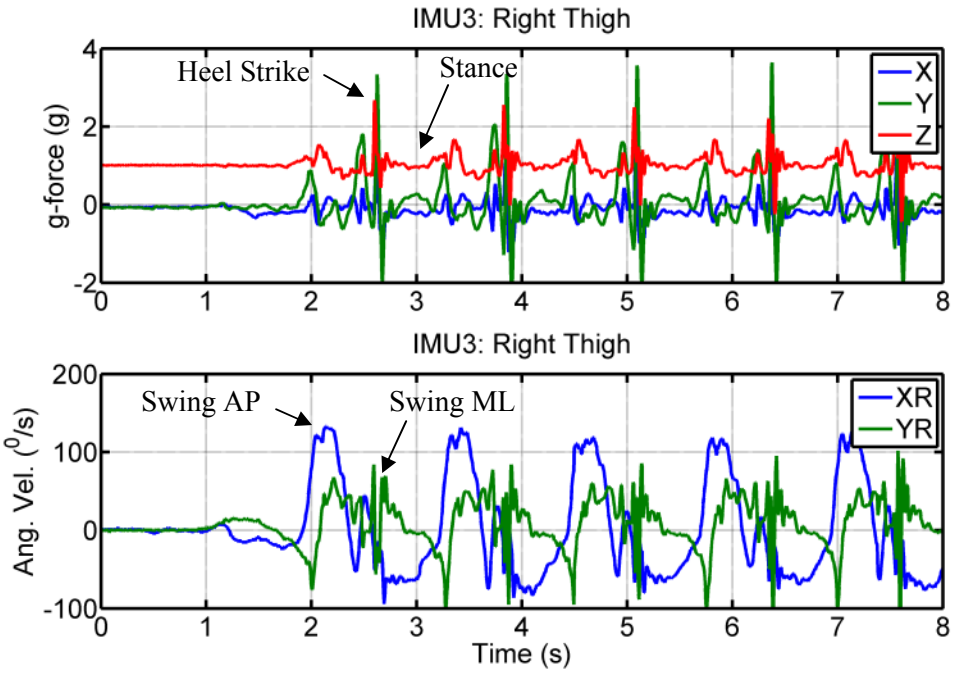

Figure 5.12: Participant 1. Thigh outputs during normal level walking

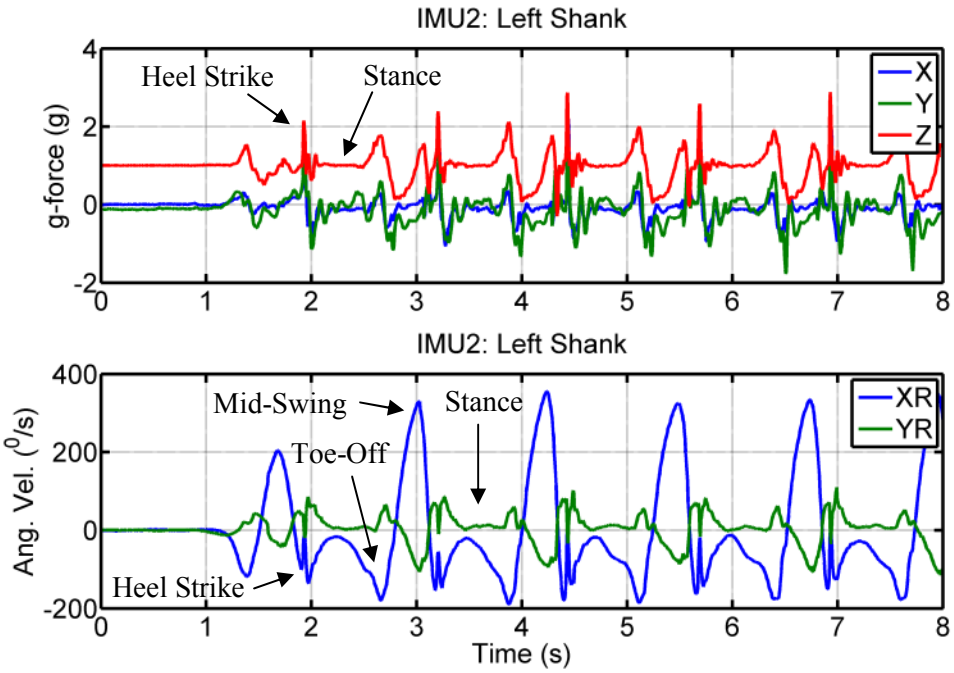

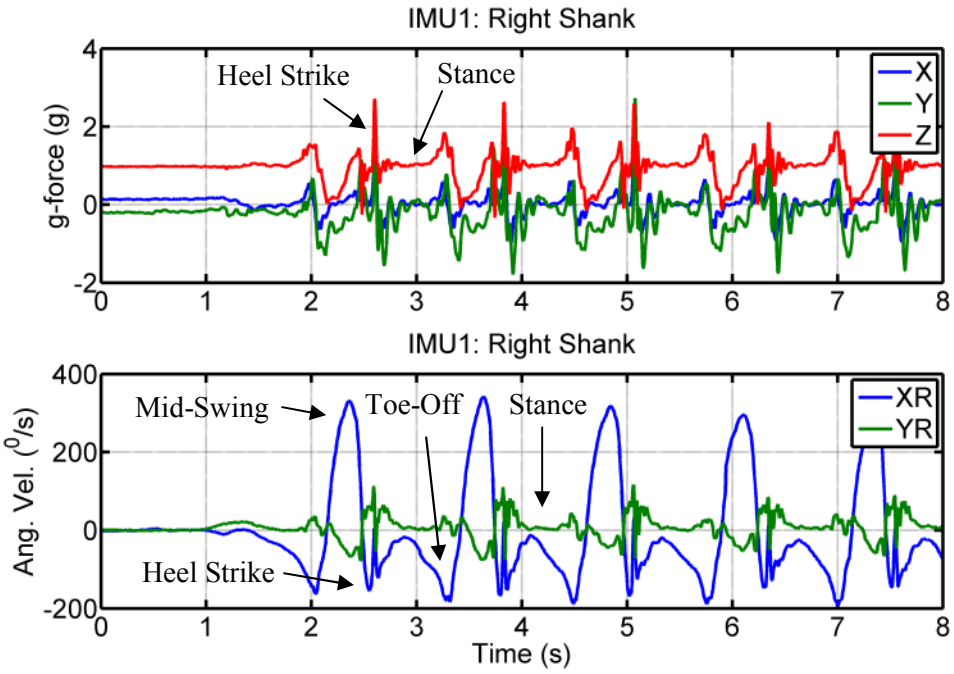

Figure 5.13: Participant 1. Shank outputs during normal level walking

The results of spectral analysis are plotted in the periodogram for every output. An example of the periodogram in the right shank is illustrated in Figure 5.14. From the figure, the first 'mountain' from the left side reveals the fundamental frequency (approximately 1Hz) which is actually the walking frequency. It would be sufficient to select the cut-off frequency near to the walking frequency. A zero phase low pass filter (ZPLP) with the cut-off frequency at 3Hz will eliminate all frequencies beyond that. In further analytical process, ZPLP gait data are presented. An example of the ZPLP right shank outputs is shown in Figure 5.15. As compared with Figure 5.13, it is obvious that the gait data are smoothed.

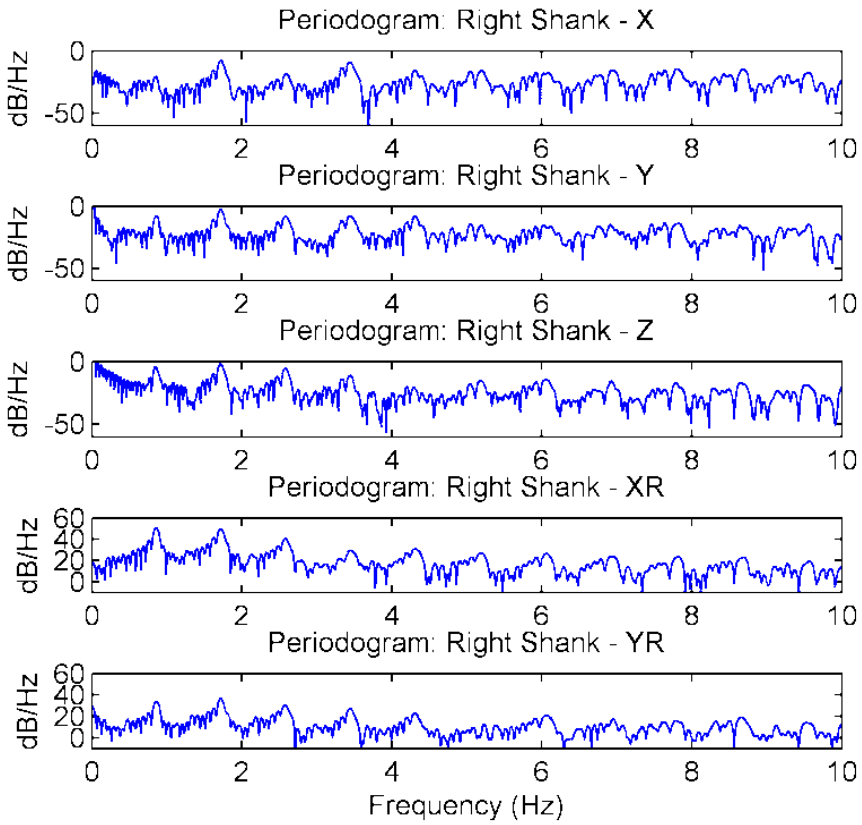

Figure 5.14: Spectral analysis of the IMU outputs at the right shank

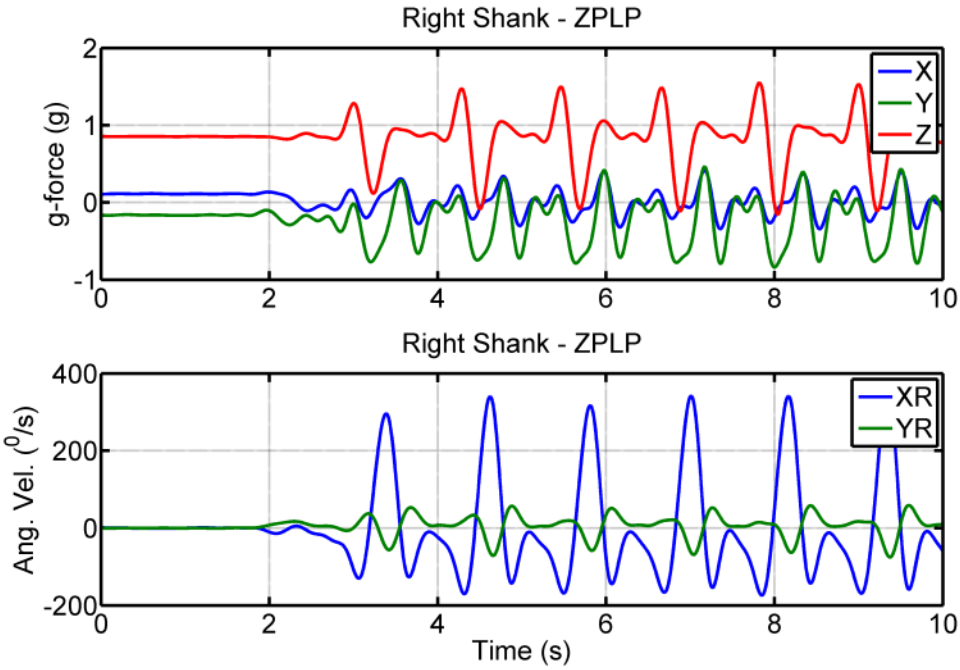

Figure 5.15: ZPLP right shank outputs

Filtered gait data will smooth out the 'peaks' and 'valleys' in the original data. However these 'peaks' and 'valleys' are crucial for the gait identification

process as recommended above (see Figure 5.9). The new gait identification strategy requires manually identifying the gait events (HC, TO and MSw). Chosen gait events are then automatically processed. An example of recognized gait events at the right shank is illustrated in Figure 5.16. Each walking trial will generate two sets of gait cycle index (GCI) for each side of the legs, namely left GCI and right GCI. The gait cycle index are used to allocate the positions of gait cycles in the filtered gait data. Unfiltered gait data are sharing the same time axis with filtered gait data using zero-phase low pass filter (ZPLP). Filtered gait cycles in each side of the legs are extracted according to the gait cycle index (GCI) in each side. For example, the right GCI is projected to all sensory outputs at the right leg and GCs of each sensory axes from the right leg are isolated and structured as defined above (similar to Figure 5.10). So does the left shank. GCs from the BCOM could applied either left GCI or right GCI. In the following analysis, all GCs extracted from the BCOM are extracted using the right GCI. Filtered GCs are used for the rest of gait analysis.

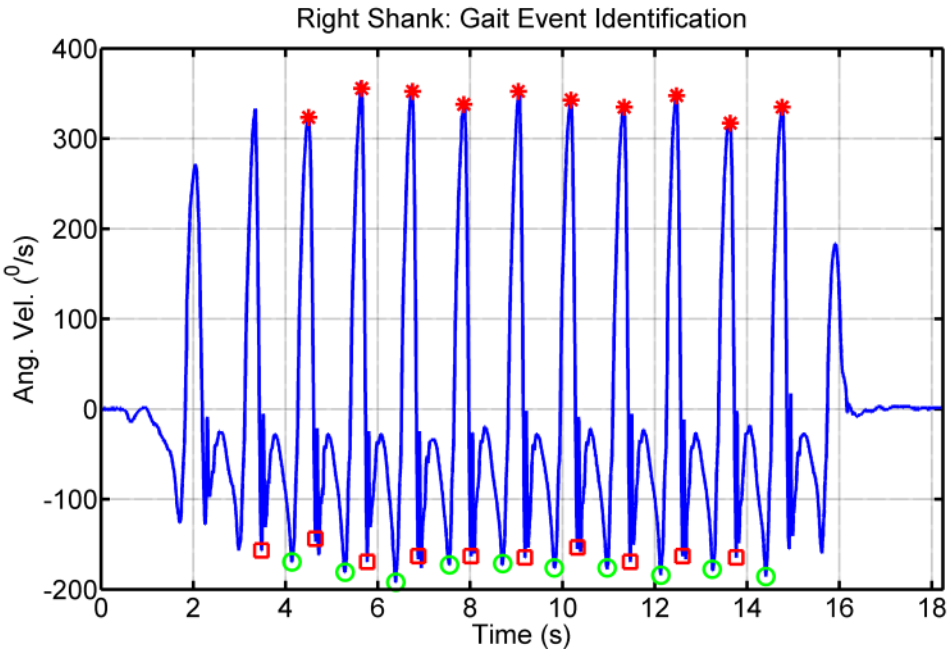

Figure 5.16: Gait identification using the gyro-output (XR) at the right shank (▫ HC, ○ TO, ✳ MSw)

Stacks of gait cycles in strides are extracted. Their time axes are normalized and linearly interpolated for comparison purposes. Filtered gait cycles from normal level walking in two consecutive weeks as shown in Figure 5.17 are used for the purpose of test-retest reliability. Normal level walking displays the most consistent

gait and is used in the test. The test requires all variables to be kept unchanged over a duration (here a week). The figure shows the IMU-5DOF kinematic outputs in eleven strides and the unit is located at the right shank of participant 1 during normal level walking. From the figure, stacks of LiNo GCs appear to be a 'thicken' GC which indicates low statistical variations amongst the GCs. Moreover, pairs of LiNo GCs in a week time appear to be almost identical. The same IMU output axes are paired and are compared statistically. Table 5.7 shows the results of test-retest reliability for every stride extracted from the right shank unit. The means of Cronbach's Alpha are over 0.9 with little variations. The results of test-retest reliability of the system are listed in Table 5.8. The mean CA indexes range from 0.780 to 0.993 and most of CA are above 0.9. Similar results are computed by using other sets of gait data by different participants. CA $\geq$ 0.7 suggests that the customized ambulatory gait data collection system is reliable.

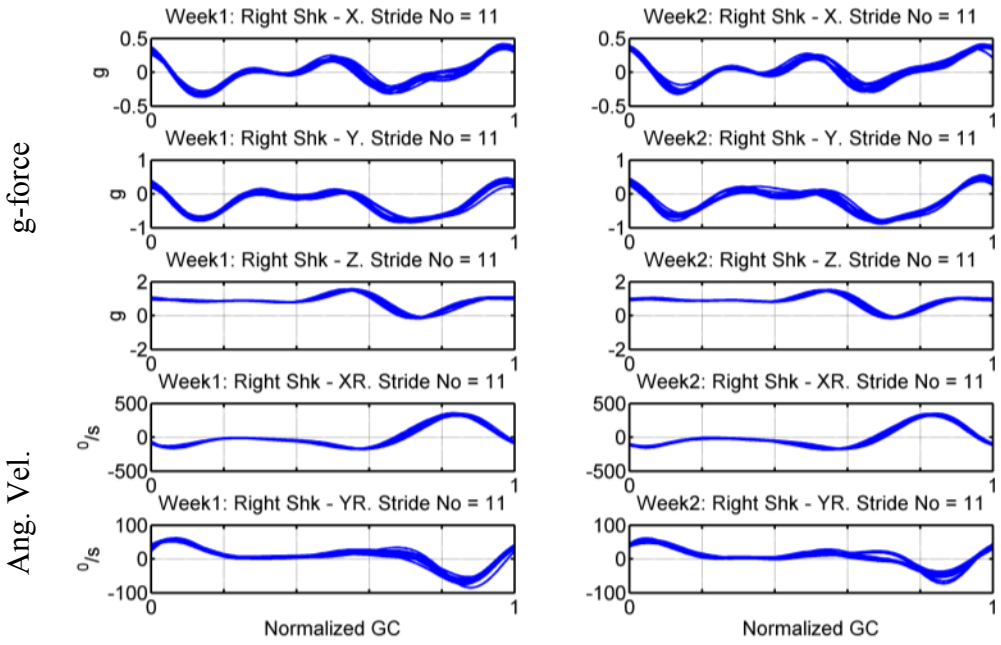

Figure 5.17: Participant 1. GCs of the right shank outputs in Week-1 and Week-2 during normal level walking

Table 5.7: Participant 1. Cronbach's Alpha of the right shank outputs during normal level walking

Stride No	X	Y	Z	XR	YR
1	0.991	0.987	0.998	0.999	0.990
2	0.979	0.976	0.965	0.992	0.975
3	0.965	0.986	0.986	0.994	0.955
4	0.968	0.987	0.983	0.989	0.978
5	0.975	0.990	0.996	0.999	0.992
6	0.964	0.960	0.984	0.997	0.975
7	0.968	0.941	0.917	0.978	0.913
8	0.992	0.979	0.980	0.995	0.963
9	0.981	0.991	0.994	0.996	0.968
10	0.979	0.988	0.992	0.994	0.971
11	0.985	0.986	0.976	0.995	0.927
Mean (CA)	0.977	0.979	0.979	0.993	0.964
s (CA)	0.010	0.016	0.023	0.006	0.025

CA = Cronbach's Alpha
s = standard deviation

Table 5.8: Cronbach's Alpha of the ambulatory system

		X	Y	Z	XR	YR
IMU1	Mean (CA)	0.977	0.979	0.979	0.993	0.964
	s (CA)	0.010	0.016	0.023	0.006	0.025
IMU2	Mean (CA)	0.780	0.970	0.943	0.981	0.811
	s (CA)	0.047	0.010	0.015	0.007	0.024
IMU3	Mean (CA)	0.935	0.985	0.958	0.986	0.951
	s (CA)	0.019	0.010	0.009	0.012	0.022
IMU4	Mean (CA)	0.920	0.930	0.970	0.993	0.834
	s (CA)	0.020	0.019	0.015	0.003	0.026
IMU5	Mean (CA)	0.960	0.970	0.977	0.811	0.935
	s (CA)	0.017	0.011	0.012	0.119	0.023

CA = Cronbach's Alpha
s = standard deviation

5.8 Discussion

The experiment protocol is mainly designed to justify the system using several gait constraints. At this stage, the experiments recruit only healthy subjects. No amputees are involved. Low numbers of participants are required since the primary motive is to justify the functionality and the reliability of the system. Health and safety issues are highlighted. There is no electric shock since a 9VDC battery is used. Tripping is minimized by tidying the wires neatly and removing any obstacles along the path. Moreover, a careful watch during the trials would minimize the hazard.

Several limitations have been identified after the experiments. Due to the constraints of space and cost, a manual treadmill is used to replace a ramp. The treadmill will move according to the user's walking rate. However it has a drawback. It becomes 'slippery' when the tilt angle is increased. The belt needs to be tensioned accordingly to avoid slipping but to a certain extent. During the trials, the customized ambulatory gait data collection system revealed a few minor mechanism defects. The IMU straps at the thighs and the shanks would tend to loosen out due to frequent shocks caused by consistent heel contacts over many trials and muscular movements. Additional adhesive straps are applied temporarily to avoid this issue. Bundle of wires connecting the IMUs to the datalogger imposes a possible tripping issue. The number of wires gets bigger when the IMUs number increases. These wires also distract the subject during the beginning of the trials. The IMU-5DOF locations at the predefined body landmarks are not instrumentally defined. These locations are decided visually or by palpations. Measurement inconsistency could be an issue because the motion sensor locations might not exactly the same for each installation.

The choices of the filter types and the cut-off frequency vary amongst researchers. A typical spectral analysis will reveal the signal spectrum. The noises originate from muscle movements and vibrations caused by the impact during HC and the abrupt posture changes of lower limbs during falling and supporting. In this research, it is highlighted that gait events (HC, TO, MSW) are identified using unfiltered gait data because all high frequency spikes that carry the features are smoothed out in the filtered gait data. To eliminate different time delay, a zero phase low pass filter (ZPLP) is introduced.

Selections of IMU and IMU outputs for the purpose of gait identification have raised a few attentions. Firstly, IMU outputs are attenuated [101] as an IMU position approximates proximally. In this study, the IMU magnitudes at the shanks are the highest and are clearly spotted from a time-series plot. Secondly, the shank IMU outputs provide a number of choices for gait identification. The lateral gyro-output at the shanks exhibits the largest excursion during swing phase and relatively clearer signals. Thirdly, gait events (HC, TO) under the other walking restrictions other than normal level walking are unclear and are not reported so far. Researchers [33, 83] proposed gait identification (HC, TO) using a gyroscope output in the shank lateral axis under normal level walking. However the IMU outputs vary substantially according to different walking restrictions. Gait features as shown in Figure 5.16 might not be clearly noticeable in every steps or strides under other walking restrictions. Assistive decision aids using the shank accelerations [78] during gait event identification provide a secondary suggestion. At HC or TO, the shank g-forces always exhibit relevant spikes at the moment when the foot collides on the ground or the foot leaves the ground. Lastly, it is a tedious and time-consuming process to identify critical gait events manually using a gait plot. However, the rest of the processing can be performed automatically. A fully automatic and robust algorithm is needed to identify critical gait events produced from all walking terraces and restrictions regardless of the subjects.

The gait results collected from the IMUs match with the gait descriptions from a number of literatures [32-34, 74, 78, 83, 101] that report the gait performances using accelemetric or gyroscopic ambulatory systems. The option for gait analysis is numerous. The system could be applied at any axis of interest or a plane or a number of body segments. Above all results, the results of test-retest reliability reassure that the customized gait measurement instrument is reliable and the gait data could be used without query.

5.9 Summary

An experimental protocol for human gait trials was designed, drafted and approved by the Research Support committee. The experiment was aimed at collecting gait data for the system validation. The trials recruited a small number of volunteers and were repeated in a week interval. The system was proved to be functional as a gait

measurement instrument and reliable to be used in future. Further gait analysis needs a lengthy explanation and will be explored in Chapter 6.

CHAPTER 6
A VISUAL AID AND A DECISION GUIDE

6.1 Introduction

This chapter presents a novel method that provides a visual aid and a decision guide to determine the effect of the lower limb prosthetic alignments onto the gait quality. Several sets of human gait data collected under four walking restrictions (Chapter 5) are used to present this method.

Walking is controlled sequences of falling and supporting of the body. It is hypothesized that the gait data should exhibit a set of repetitive events with a statistical centre tendency. Appropriately chosen gait variants should be able to represent this information. However, a typical gait data analysis would generate many variants that are of the researchers' interest. Very often, the numbers of variants swell in high dimension and size. It is hence a challenge to interpret them in an easy-to-understand format.

Gait analysis suffers from two basic challenges, i.e. correlated data and high dimensional data. Researchers have attempted many gait variants for analysis, including temporal, kinematic and kinetic variants. For examples, stride/step time, cycle times, walking speeds, angular displacements and rates of limb segments, insole centre of pressure (COP), ground reaction force (GRF), weight line or load line, joint moments, etc. In most cases, a number of gait variants are selected to look into the quality of gait performance without knowing exactly if the variants are the most appropriate or if the variants are uncorrelated. Correlated variants might cause 'noises' while investigating the gait performance. Handling high dimension data becomes complex as they are not easily interpreted. Visualization of the gait data on a simple plot becomes a difficult task as the data dimension increases.

The proposed algorithm utilizes both Principle Component Analysis (PCA) and Self-Organizing Feature Map (SOFM) to solve the above issues while at the

same time providing a visual aid and a decision guide for the application of lower limb prosthetic alignments. The method is possibly suitable for normal and pathological gait analysis.

6.2 Aims and Objectives

These questions are investigated in this chapter.

1. How to handle correlated or redundant variants?
2. How to 'see' high dimension variants in a simple plot (a visual aid)?
3. How to develop a black box algorithm for future decision guide?

6.3 Principle Component Analysis

PCA [102] is an orthogonal transformation that converts a set of correlated variables $\boldsymbol{X}[\vec{X}_1 \ \vec{X}_2 \cdots \vec{X}_k \cdots \vec{X}_m]$ into another set of uncorrelated variables $\boldsymbol{Z}[\vec{Z}_1 \ \vec{Z}_2 \cdots \vec{Z}_l \cdots \vec{Z}_m]$ called principle components (PCs). The principle components are the linear combination of the input variables such that $Z_l = \beta_{l1}\vec{X}_1 + \beta_{l2}\vec{X}_2 + \cdots + \beta_{lm}\vec{X}_m$ and ${\beta_{l1}}^2 + {\beta_{l2}}^2 + \cdots + {\beta_{lm}}^2 = 1$. These principle components form a basis of linearly independent vectors. Each PC is a unit vector. A covariance matrix, **C** of the input variables **X** is listed in equation (6.1). The PCs are the eigenvectors of the covariance matrix, **C**. The sum of eigenvalues is equal to the diagonal sum of covariance matrix, **C** or equivalent to the total variances of the input variables, X_{kk}. PC1 represents the highest percentage of total variance explained, followed by PC2 and so on. Dimension reduction could be achieved by selecting appropriate numbers of PCs which accumulate to a satisfactory percentage of total variance explained.

$$\boldsymbol{C} = \begin{bmatrix} \boldsymbol{c_{11}} & \boldsymbol{c_{12}} & \cdots & \boldsymbol{c_{1m}} \\ \boldsymbol{c_{21}} & \boldsymbol{c_{22}} & \cdots & \boldsymbol{c_{2m}} \\ \vdots & \vdots & & \vdots \\ \boldsymbol{c_{m1}} & \boldsymbol{c_{m2}} & \cdots & \boldsymbol{c_{mm}} \end{bmatrix} \qquad \textbf{[102]} \quad \textbf{(6.1)}$$

6.4 Self Organizing Feature Map

SOFM [103, 104] is a type of unsupervised artificial neural network, popular for visualization of multi dimensional data into much lower dimension spaces. Figure 6.1 shows the diagram of a SOFM.

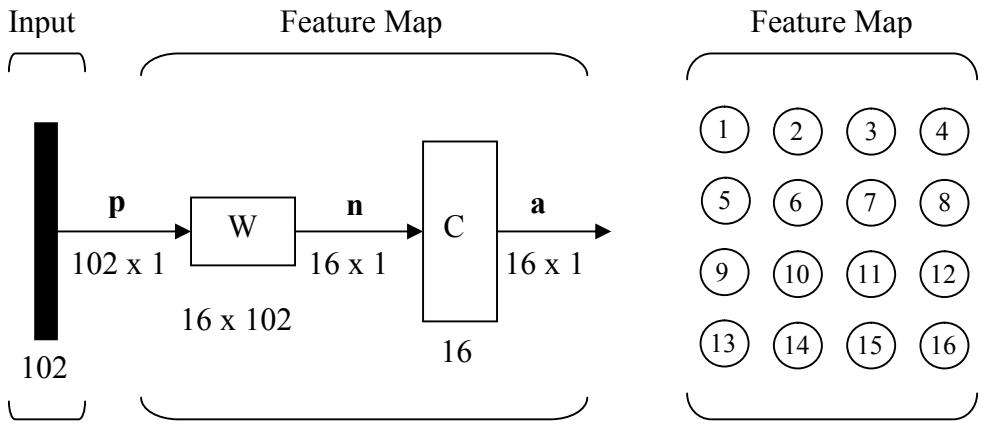

Figure 6.1: Self-Organizing Feature Map. Redrawn from [104]

An input layer (**p**) is fed into a feature map. In the feature map, a grid of neurons called maps is trained via a competitive learning to match closely to the distribution of the input data. Each neuron is linked with a weight vector (**W**) of the same dimension as the input data vectors and a position vector in the map space. During the competitive learning, the shortest squared Euclidean distance between the input vector and the weight vector at *i* neuron will win and the winning neuron is called the Best Matching Unit (BMU). This is a winner-takes-all process. The process updates the neuron weight and the neighbour neurons that lie within a radius, *d* of the winning neuron according to Kohonen rule as shown in equations (6.2) and (6.3) respectively.

$$ {}_{i}\boldsymbol{w}(q) = {}_{i}\boldsymbol{w}(q-1) + \alpha\big(\boldsymbol{p}(q) - {}_{i}\boldsymbol{w}(q-1)\big) \quad \text{for } i \in N_i(d) \qquad \textbf{[104]} \quad \textbf{(6.2)} $$

where,

${}_{i}\boldsymbol{w}$	the weight vector at i neuron
$\boldsymbol{p}$	the input vector
q	the step number
α	the decaying learning rate.

The neighbourhood function at *i*-neuron is represented as below.

$$N_i(d) = \{j, d_{ij} \leq d\} \quad \textbf{[104]} \quad \textbf{(6.3)}$$

6.5 Methodology

Gait data are collected from three participants in four different types of walking restrictions. These walking restrictions are:

1. S1 Level-Ankle-freed (also known as normal level walking)
2. S2 Level-Ankle-locked
3. S3 Tilt-Ankle-freed
4. S4 Tilt-Ankle-locked

Details of gait data collection and basic data processing and conditioning were presented in Chapter 5. The gait data of the body segment kinematic information during walking are measured from the BCOM, the thighs and the shanks. In preparation for gait analysis using PCA and SOFM, further gait data conditioning is needed. The following gait analysis utilizes data structure (see Chapter 5) created before.

There are numerous choices of gait features as input variables. Practically, the choices could be any point within a gait cycle but as long as they are chosen consistently throughout the analysis. For simplicity reasons, four gait events are selected from a gait cycle extracted from the shank lateral gyro-output (Angular Velocity, ^{0}/s) as shown in Figure 6.2. They are Heel Contact (HC), Terminal-Stance (TSt), Toe-Off (TO) and Mid-Swing (MSw). The positions of (HC, TO and MSw) are pre-determined during the process of gait identification recommended in Chapter 5. These gait events are visually identified and marked from the gait plots. Consistency in the manual selection is checked visually with a plot of extracted gait cycles labelled with the previous selected gait events. Large amount of selected features would statistically produce a distribution with a centre tendency. However, for this application, TSt is defined at 0.4 of GC where the heel is raised before toeing-off and the contralateral leg is about to heel strike. Other gait events could possibly be chosen as the input. Besides that, arrays of stride time of the left leg and the right leg are computed and included in the input matrix. There are in total 102

features selected as the input variables, i.e. 5IMU × 5axis × 4 features + 2 Left/Right Stride Time. An input matrix in the format as shown in equation (6.4) is labelled according to the modes of predefined experiments. The matrix rows represent the observations and are labelled accordingly to the experiment setups. Matrix columns represent the selected input variables. All column vectors are standardized before being processed using PCA.

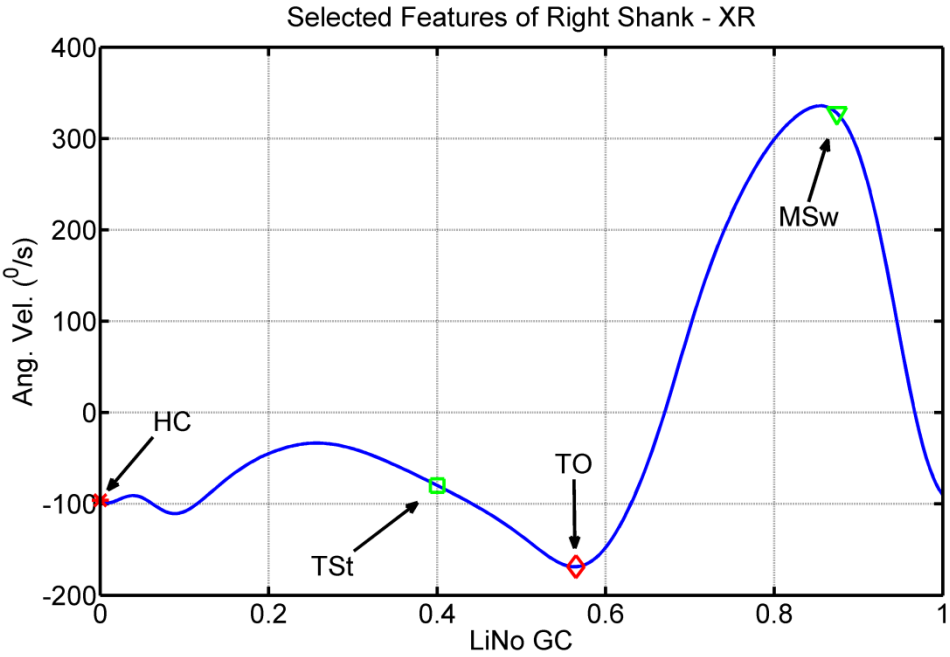

Figure 6.2: Selected features within a gait cycle
[* HC □ TSt ◊ TO ▽ MSw]

$$\begin{bmatrix} \vec{S}_1 \\ \vec{S}_2 \\ \vec{S}_3 \\ \vec{S}_4 \end{bmatrix} \rightarrow \begin{bmatrix} \vec{X}_{11} & \vec{X}_{12} & \cdots & \vec{X}_{1m} \\ \vec{X}_{21} & \vec{X}_{22} & \ldots & \vec{X}_{2m} \\ \vec{X}_{31} & \vec{X}_{32} & \cdots & \vec{X}_{3m} \\ \vec{X}_{41} & \vec{X}_{42} & \cdots & \vec{X}_{4m} \end{bmatrix} \quad \textbf{(6.4)}$$

where,

$\vec{S}_1$ to $\vec{S}_4$ labels of walking restrictions in each observation

$\vec{X}_{im}$ selected feature as the m-input variable at i-observation

After PCA transformation, new variables in term of PCs are uncorrelated and could be selected as the inputs for SOFM training. Input dimension could be reduced by selecting the leading number of PCs that account above 80% of total

variance explained. Training is necessary for SOFM before it can be used to determine any gait patterns. Once trained, the SOFM is ready to determine the location of the recognized clusters if a new set of input variables is fed into the algorithm.

A Matlab m-file is written and could be found in the CD attached.

6.6 Results

Figure 6.3 shows an example of gait features extracted from numerous gait cycles of the shank outputs during normal level walking (S1) from nine strides. Predefine gait features ($HC \quad TSt \quad TO \quad MSw$) are identified and marked in every single GC. Their distributions depend on the gait performance under different gait restrictions. The rest of the sensory outputs are plotted in similar plots of GCs. For all sets of observations, the gait features are identified and the input matrix is generated. The same process is repeated for all trials.

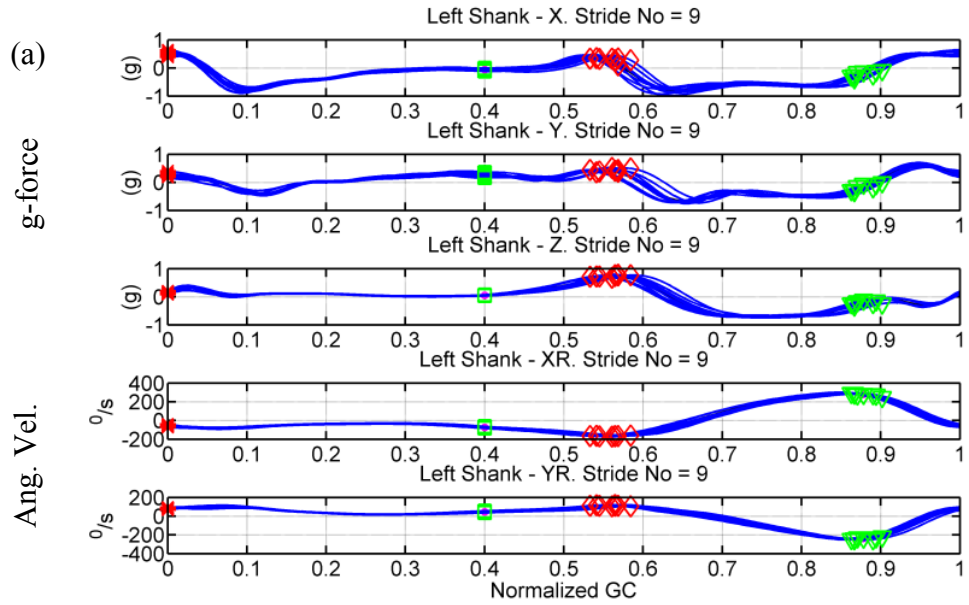

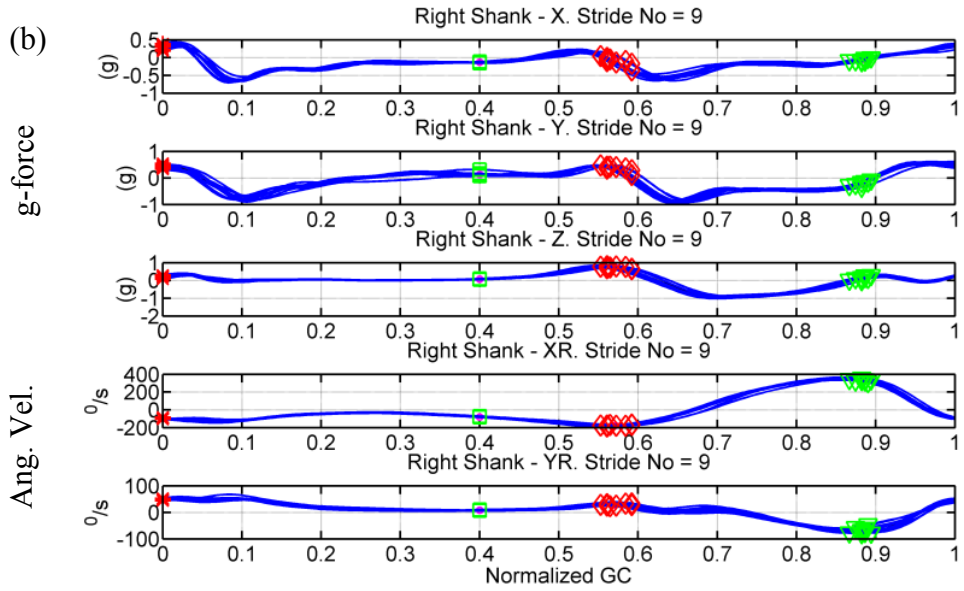

Figure 6.3: Participant 1 at week 1. GC stacks during normal level walking (S1). (a) left shank, (b) right shank
(★ HC □ MST ◊ TO ▽ MSW)

Selected gait features are processed using PCA. The centre tendency of controlled walking could be represented by lumps of PCA data sets or clusters plotted in a 2D or 3D plot. Intra-personal views and inter-personal views are investigated. Corresponding clusters representing different gait restrictions are visually observed from 2D PCA plot or if necessary 3D plot.

In an intra-personal view (gait data comparison within the same subject), the gait data of a participant during a session of trials are checked. Each principle component represents a portion of variance explained in the input data. Figure 6.4 shows the variance explained of the first ten PCs using the data set of participant 1 at week 1. The left vertical axis accounts for the percentage of each PC whereas the right vertical accounts for the accumulated percentages of PCs. The first two PCs represent for nearly 60% of total variance explained. Whereas, the first ten PCs represent for nearly 80% of total variance explained. The rest of PCs contributes to a smaller portion of variance explained. Data dimension could be reduced greatly by selecting the leading PCs which account for a satisfactory percentage of total variance explained. The same procedure is applied to other data sets.

For the intra-personal comparisons, Figure 6.5 shows the results for three participants over trials in a week time with an average of 53% of the total variance explained. Four separated clusters are noticed, corresponding to S1, S2, S3 and S4.

They are clearly separated at four positions. Visually, there are minor variations in two weeks' plots. S1 and S4 are two sets of extreme setups and the distance between them could be visually seen as the farthest. S3 and S4 appeared to be closer to each other as compared to other pairs, probably due to unfamiliar walking restrictions at tilt level. S1 and S2 are more condensed than S3 and S4. Furthermore the effect of restrictions could be classified into two categories, i.e. 'Ground Level' and 'Ankle Alignment'. In the category of 'Ground Level', the group of 'level' (S1, S2) is located at the lower left side while the group of 'tilt' (S3, S4) is located at the upper right side. In the category of 'Ankle Alignment', the group of 'ankle-freed' (S1, S3) is located on the upper left side while the group of 'ankle-locked' (S2, S4) is located on the lower right side.

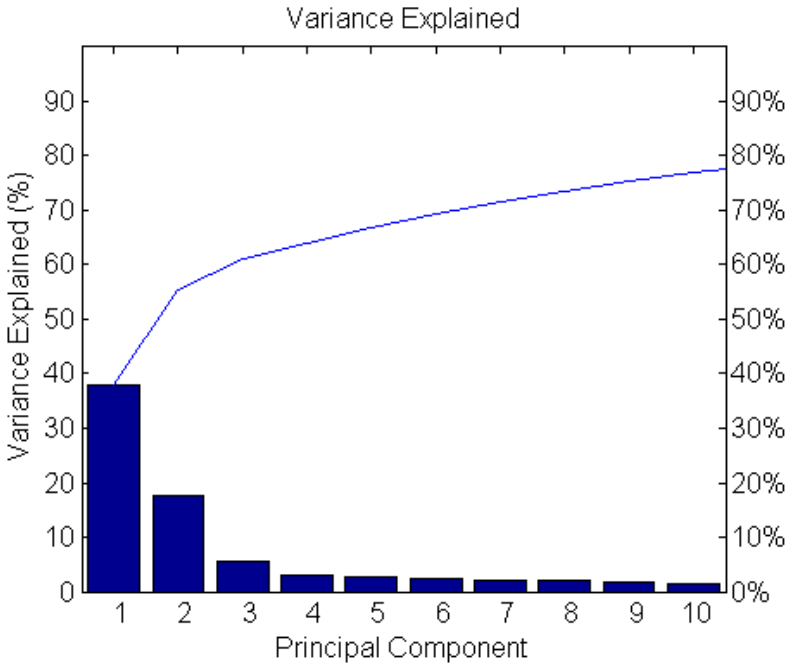

Figure 6.4: Variance explained by each principle component (Intrapersonal)

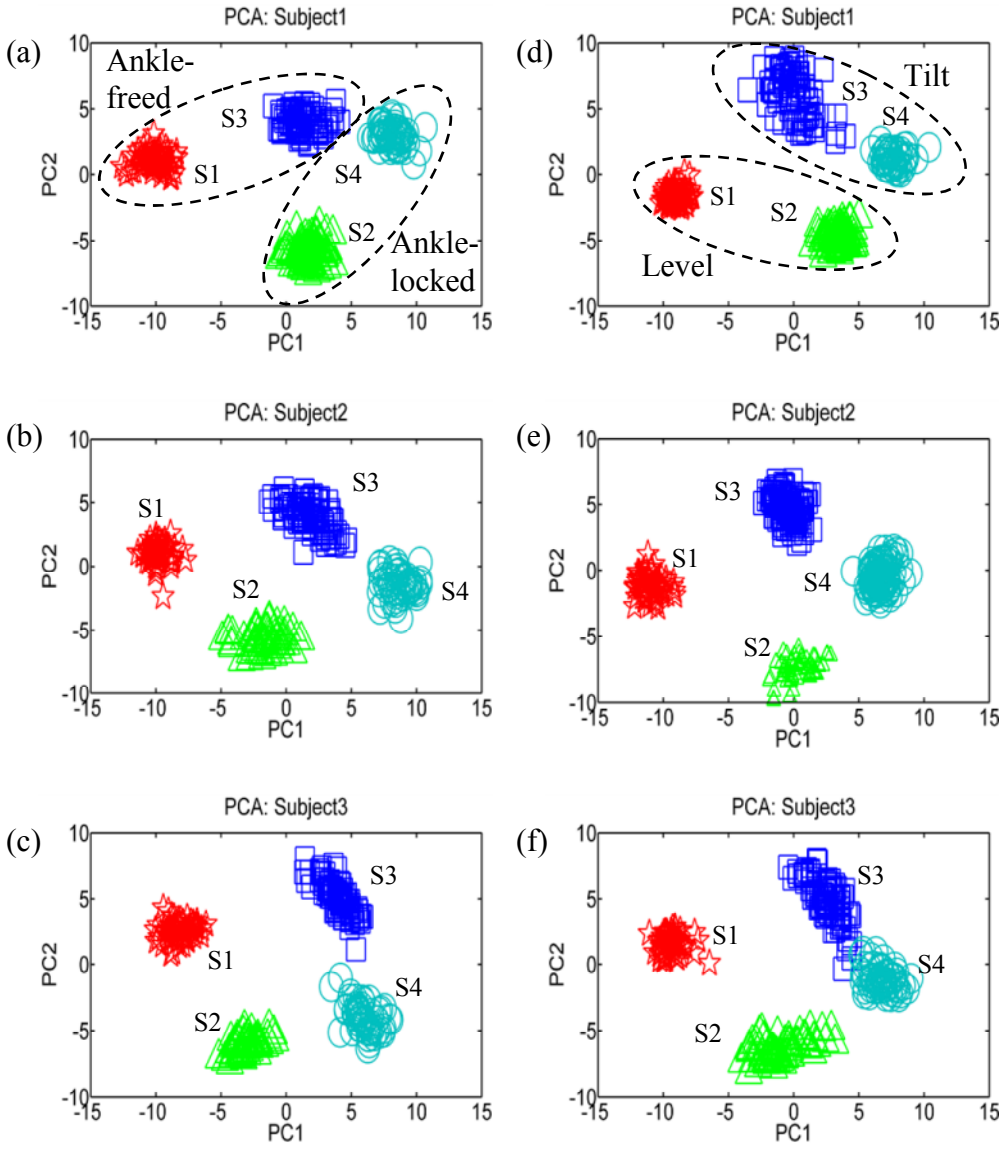

Figure 6.5: Intra-personal view. 2D PCA plots of all participants in week 1 (a, b, c) and week 2 (d, e, f) respectively.
(★ S1 △ S2 ○ S3 □ S4)

In an inter-personal view (comparison amongst subjects), the gait data of all participants in a session are merged together. The merged inputs are labelled accordingly and are processed using PCA. Figure 6.6 shows the percentages of variance explained by each PC. As compared to the intra-personal view, the percentage of the total variance explained represented by the first two PCs drops. The first two PCs represents nearly 40% of the total variance explained whereas the first three PCs represent nearly 50% of the total variance explained. The drop could be possibly due to the increasing variations when all participants' data are merged.

For higher percentages of the total variance explained, the 3D PCA plots are used. Figure 6.7 shows the inter-personal views of three participants at week 1. For each mode of walking restrictions (S1 to S4), the 3D PCA plots shows that the participants own their personal clusters of gait patterns under each walking restriction. The clusters do not coincide. When all modes of experiments are viewed at a 2D PCA plot (low percentage of total variance explained) as shown in Figure 6.8, not all clusters are clearly separable. The mode could be visually classified as labelled. Above all, experiment mode S1 and S4 are clearly apart as they are the most extreme setups. S2 and S3 appear to be slightly overlapped at their borderline. Again, it could be seen that all participants have their own clusters even though the experiment mode is the same. The results in the inter-personal views in week 2 are similar.

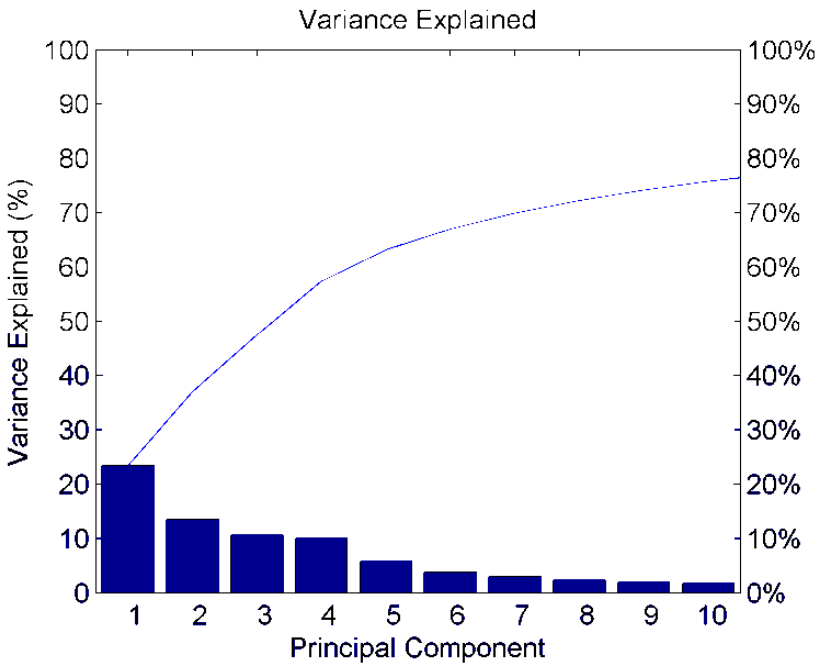

Figure 6.6: Variance explained by principle components (Interpersonal)

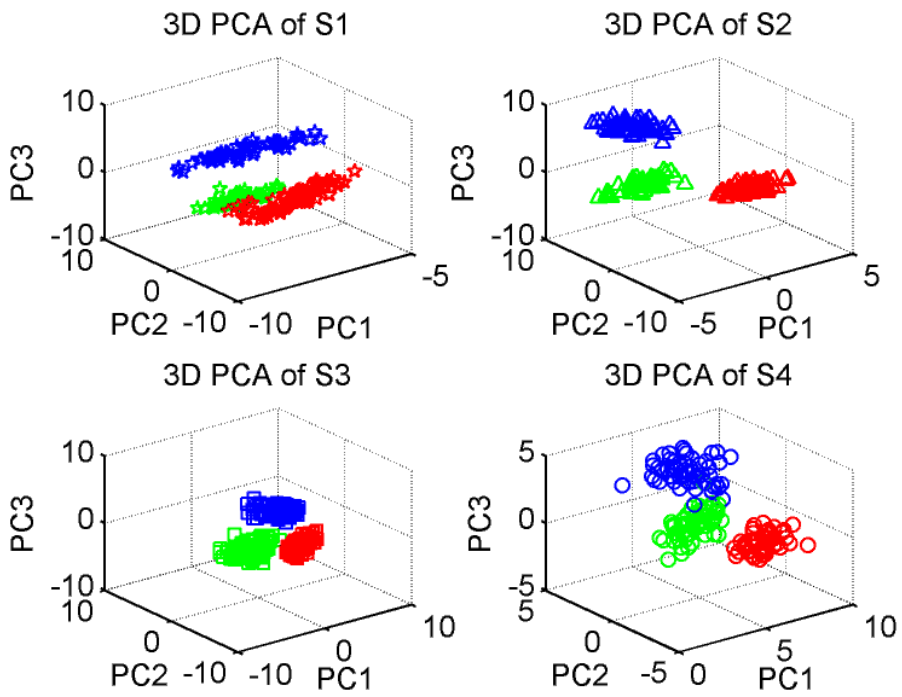

Figure 6.7: Inter-personal view. 3D PCA plots of each mode in week 1 (red = participant 1, green = participant 2, blue = participant 3) (☆ S1 △ S2 □ S3 ○ S4)

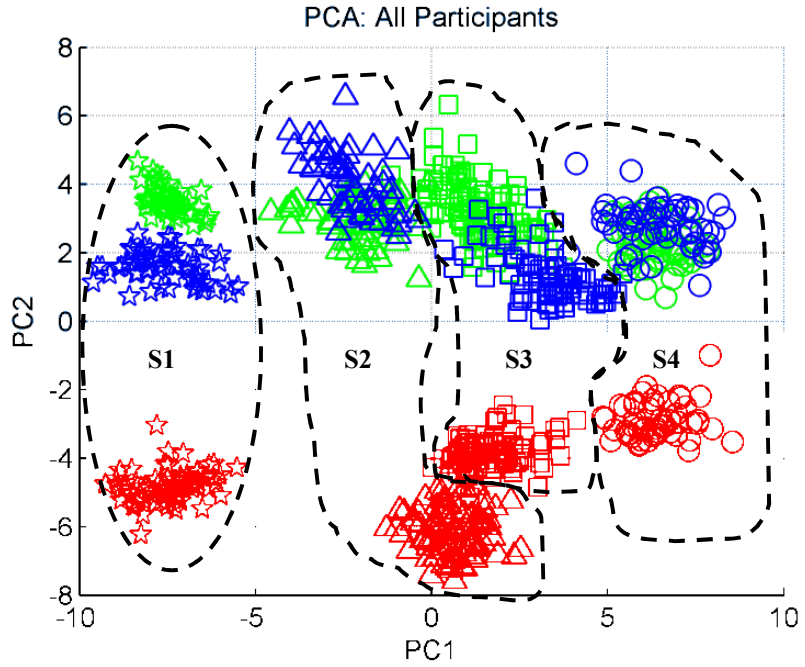

Figure 6.8: Inter-personal view. A 2D PCA plot of all modes in week 1 (red = participant 1, green = participant 2, blue = participant 3) (☆ S1 △ S2 □ S3 ○ S4)

There are numerous choices of SOFM neuron number. But for simplicity while still able to map the gait patterns effectively, a map of 16 neurons is chosen during SOFM training. The results are based on intra-personal data sets. The results of using different inputs for training are shown in Figure 6.9. The first group applies 102 sets of standardized original variables (before processed using PCA) as the training inputs while the second group applies 102 sets of uncorrelated PCA variables as the training inputs. Trained SOFM shows very close and not linearly separable clusters (Figure 6.9a) when the first data group is applied. The neurons appear not to be able to represent the cluster effectively. By using the uncorrelated PCA inputs, the clusters appear to be clearly separated (Figure 6.9b). The neurons are able to represent each cluster and empty spaces effectively.

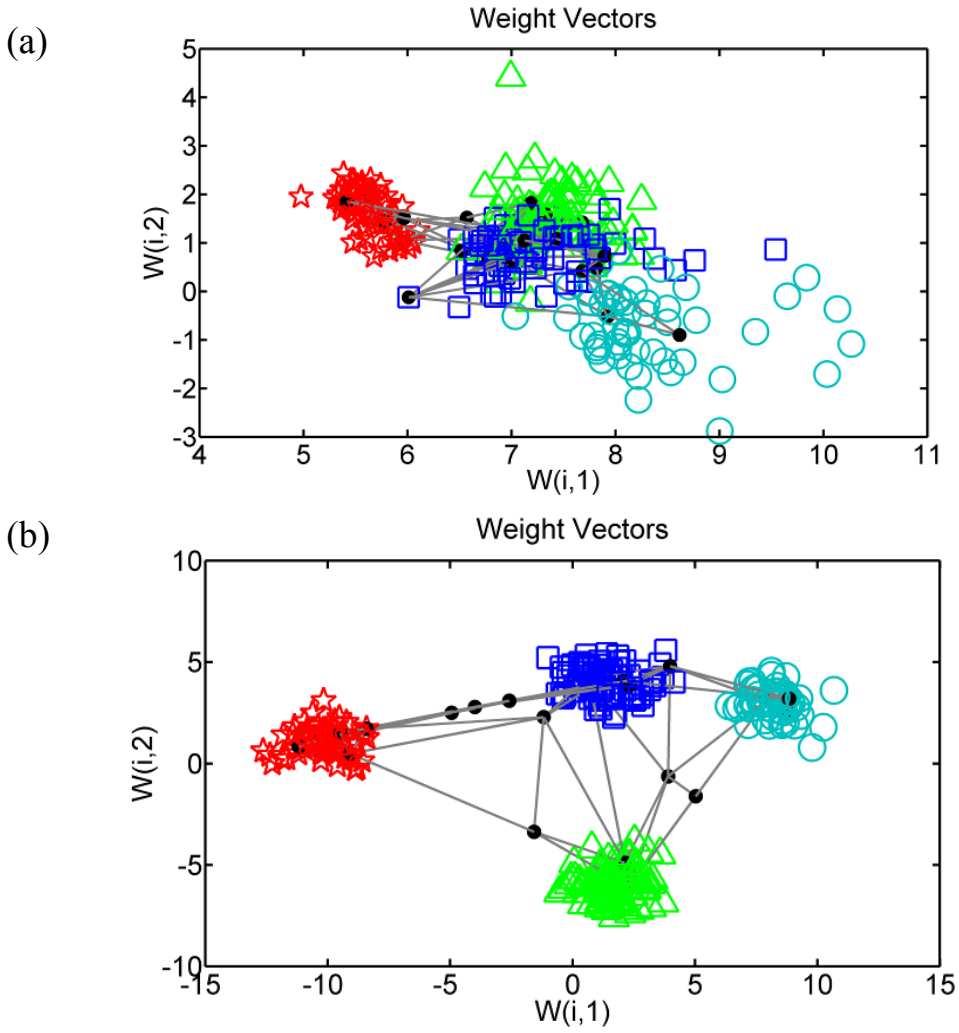

Figure 6.9: (a) Trained SOFM with 102 sets of standardized variables as the inputs. (b) Trained SOFM with 102 sets of uncorrelated PCs as the inputs. (☆ S1 △ S2 □ S3 ○ S4 ● SOFM neurons)

The effect of reducing data dimension is shown in Figure 6.10. The comparison applies intra-personal data sets. There are 102 uncorrelated PCA inputs and a selection of uncorrelated PCA inputs which represent approximately 80% of the total variance explained. It is known from previous results that approximately the first ten PCs would represent the score. Both SOFM maps are able to discriminate the clusters clearly and the neurons are able to map the gait patterns effectively.

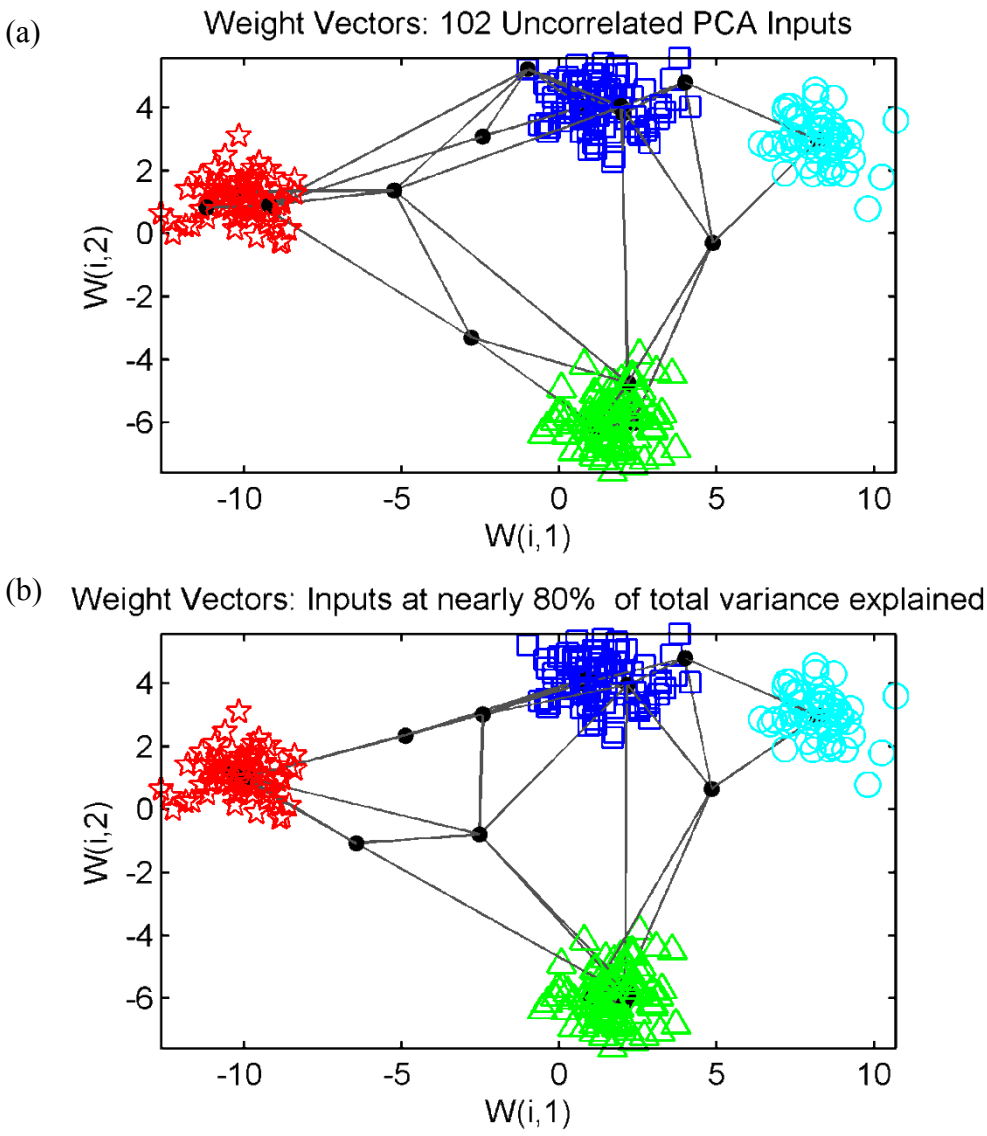

Figure 6.10: Trained SOFM using (a) 102 PCA inputs, (b) PCA inputs nearly 80% of total variance explained
(☆ S1 △ S2 □ S3 ○ S4 ● SOFM neurons)

The rest of the results explain the operation of SOFM and the neuron mapping mechanism. The hit counts per neuron as shown in Figure 6.11 show the number of the inputs that each neuron has classified. Null hit represents the neuron is not able to classify any inputs and would be appeared at the empty space at the SOFM map. A weight plot as shown in Figure 6.12 displays the neighbour weight distances amongst the adjacent neurons highlighted by colours from black to yellow. The weight distance is larger with darker coloured band and vice versa.

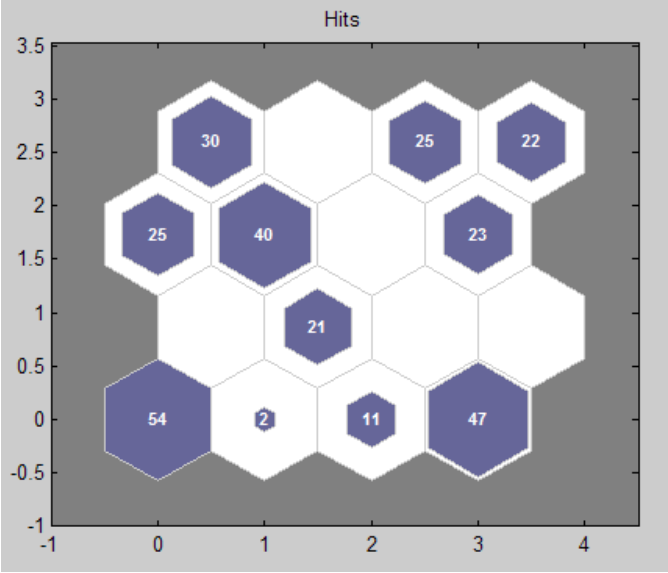

Figure 6.11: SOFM hit counts per neuron

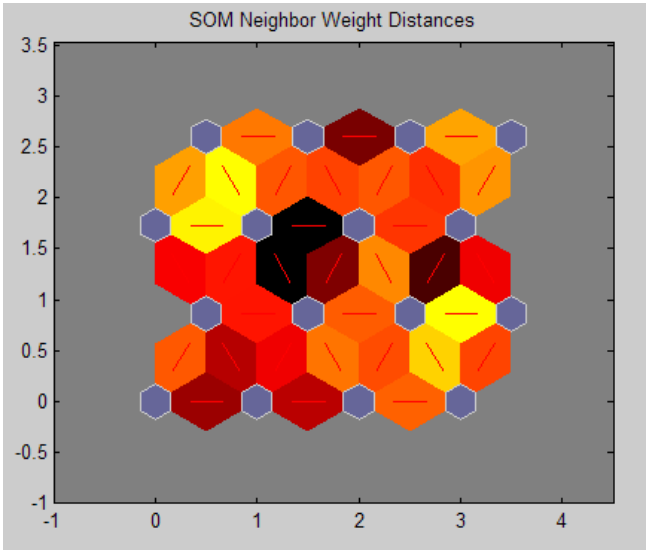

Figure 6.12: SOFM neighbour weight distances amongst adjacent neurons (the neighbour weight distances amongst the adjacent neurons vary from far to closer proportional to the colour changes from black to yellow)

6.7 Discussion

The ultimate objectives of prescribing the lower limb prostheses are to provide comfort and function to the amputees. After prescription, the alignments partially determine if these objectives are optimized. It is an iterative process that requires great patience and careful observations. The amputee gait is affected by many factors, including the alignments, prosthetic types, terrace quality, confidence of walking, age, health and etiological causes. Since walking is controlled sequences of falling and supporting of the body, in this research it has hypothesized that statistically human gait displays a centre tendency which is the result of self-adaptation or voluntary controlled sequences. These centre tendencies could be observed subjectively by the prosthetists via clinical practices, or alternatively observed objectively through an instrumental assessment by a reliable gait measurement instrument and efficient algorithms.

The gait analysis could be expressed in simple parameters such as average walking speed and cadence or other specific terms within a stride or step. Multiple variants of kinematic and kinetic information have enriched the choices of analysis but at the same time confused the analyst. Two important issues are raised here, i.e. correlation or at worse redundancy and 'curse of dimensionality'. The selection of gait features could be subjective. Meanwhile, complexity arises when the number of chosen parameters increases. Visualization of multi dimensional gait parameters becomes a tricky challenge. Multivariate statistical analysis like PCA is the simplest method to eliminate correlation amongst the inputs and at the same time to reduce the dimensionality at a certain extent. The 2D or 3D plots of the principle components could provide a visual aid with satisfactory accuracy.

The spread or distribution of the clusters might serve another guide during the alignments. Although not completely studied in this aspect, it is suspected that larger variation of gait patterns could be seen in a wider spread of cluster. The indication could be either the participant is not familiar with the new setting or simply more time is needed to adapt to the new setting or the restrictions have caused the variations. The study of the adaptation over long hours or days is not performed in this research. Gait patterns in the inter-personal view exhibit larger variability than gait patterns in the intra-personal view. Similar observations are reported by Winter [68]. It is not completely clear whether the intra-personal view

or the inter-personal view is better for the application. Each participant displays different cluster locations of gait patterns under different gait restrictions due to different level of adaptations. Moreover, as stated by Winter [105], amputees tends to develop a new motor mechanism which might not be the same as the original limbs. These observations suggest that the intra-personal view of the gait patterns might be more suitable for the application of lower limb alignments.

Selected gait features pre-processed by PCA are necessary. Uncorrelated inputs for SOFM training reveal better clustering results. Training time is faster when the input dimension is greatly reduced but still maintained a high percentage of total variance explained. While plots of 2D or 3D principle components provide visual aids, a trained SOFM could enhance the visual aids by specifying the label of the clusters defined by weighted neurons. SOFM could serve as a decision guide when the gait patterns become too complex to be visually observed. Visualization on a 2D PCA plot might not always be effective if a new data set collected from a new gait restriction is added in or the clusters are overlapping wholly or marginally in a low dimension plot. Trained SOFM map in the form of 'good' or 'bad' gait patterns under certain walking restrictions might serve a directive guide during the alignments.

The results of different clusters mapped in the PCA and SOFM map might suggest a possible alignment methodology. Two major categories as the results of gait restrictions could be identified. They are the 'Ground Level' and the 'Ankle Alignment'. Each category consists of two different groups of settings. A Venn diagram as shown in Figure 6.13 could possibly provide a directive guide during the alignments. The Venn diagram is used in the logical reduction of two settings using a logical AND if two groups are overlapping. For example, in Venn diagram V1, the optimum zone during 'tilted level' AND 'ankle-freed' would be in S3. The same logical reduction applies to the rest of the Venn diagrams (V2 to V4) to identify the optimum zone. Further combination effects of different prosthetic alignments and ground level onto the gait patterns are not studied in this research.

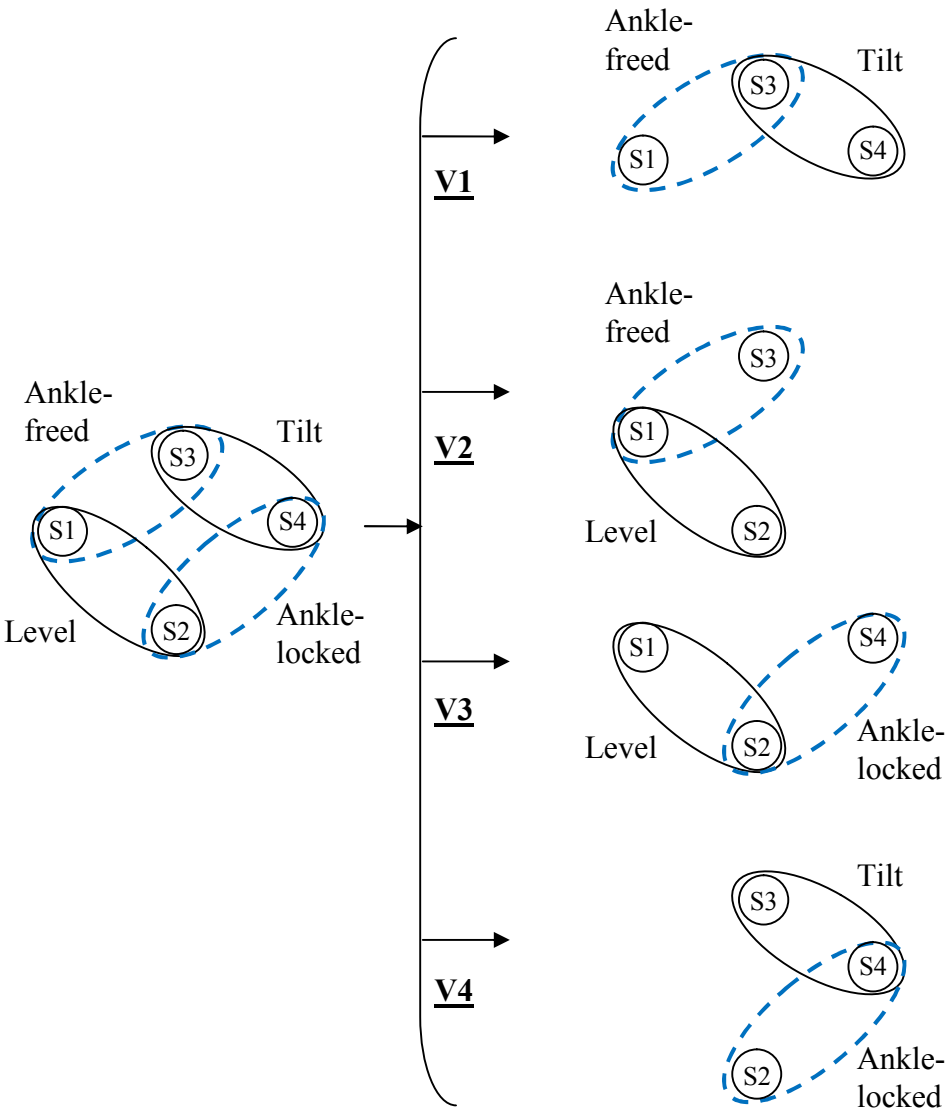

Figure 6.13: The Venn diagrams of the alignments

The method proposed here might suffer from a few challenges. The method could be further refined and validated if amputee gait data are applied and are collected from a number of considerations. These considerations might generate a deeper view regarding the research topic. They include groups of amputation level, gender, types of prosthesis, etiological reasons, multiple combinations of alignment parameters, walking trials on different terraces and levels. Above all, the involvement of medical experts such as the prosthetists is essential to produce significant medical evidences regarding the study. Nevertheless, at this stage, the main objective is the development of a reliable engineering solution for the alignments.

The proposed method is able to provide successfully a visualization of the gait patterns in a low-dimension plot that discriminates different gait patterns effectively. Consistency of intra-personal gait patterns from three subjects could be seen from the plots (see Figure 6.5). Later a trained SOFM with reduced PCA inputs promises a quicker training process (see Figure 6.10) and the neurons could represent each clusters of different gait patterns effectively.

6.8 Summary

A gait pattern clustering method for a novel lower limb prosthetic alignment system is proposed. The method utilizes a multivariate statistical algorithm called PCA to transform original gait variables into uncorrelated gait variables. Clearly separated clusters of gait patterns are observed via a 2D or 3D PCA plot. Greatly reduced dimensional uncorrelated variables are used for SOFM training. Trained SOFM provides an assistive guide to recognize the gait clusters. The method is envisaged to be able to provide both a visual aid and a decision guide to determine the effect of the lower limb prosthetic alignments onto the gait quality.

CHAPTER 7
SUMMARY AND CONCLUSIONS

7.1 Assessment of the Research Objectives

In Chapter 1, a set of research objectives are outlined. This section evaluates the extent to which the objectives were achieved.

1. To develop an ambulatory system for gait data collection. The system should be portable and hazardless.

Chapter 3 demonstrates the development of an ambulatory system for the purpose of portable gait measurement from five predefined body landmarks. Several design considerations are presented. This includes system requirements such as light-weight, cost and number of acquisition channels, sampling rate, data storage, precision and error margin. The customized datalogger is calibrated and is proven to perform reliably and consistently with very low error. System hazard is considered at minimum possible. Preliminary trials reveal that the ambulatory system is able to read and record gait data accordingly.

2. To calibrate the ambulatory system including the datalogger and the sensors. The efforts should provide the specifications of the system and margin of errors.

Chapter 4 demonstrates the techniques of IMU calibrations, i.e. static and dynamic. For static calibration, several methods are innovated and trialled. The results based on different methods of static calibrations differ slightly. Later these methods are justified according to some criteria such as cost, the need of test rig, computation time, static or quasi-static assumption and accuracy. It is found that for the general applications, the 6/12 Known Positions method and the simplest IMU model are

relatively easy and still produce satisfactory results. An innovative dynamic calibration procedure using a pendulous system is presented. The pendulous system could be used to calibrate the gyroscope and validate the dynamic performances of an IMU. Low RMS errors between the theoretical models and the actual measurements suggest that the IMUs are reliable and consistent.

3. To collect gait data using the ambulatory system under several walking restrictions. An ethical approval for the trials is required.

This is reported in Chapter 5. Four cross-designed experiments are drafted according to two walking restriction factors. They are walking on level with the ankles being free, walking on level with the ankles being locked, walking on tilted level with the ankles being free and walking on tilted level with the ankles being locked. The experiments examined the gait performances of three participants under the above walking restrictions. The procedures of drafting the experiment protocol and applying for the ethical approval are reported. The experiments received an ethical approval from the Research Support Unit of the University of Leeds and the consents from the participants.

4. To propose a procedure of gait data processing. The procedure involves multi-stages of signal processing and conditioning.

This is also reported in Chapter 5. Measured IMU gait data are presented in volt over the trial time. These data are converted into kinematic parameters with corresponding models and calibrated coefficients found in Chapter 4. A series of signal processing and conditioning are performed on measured gait data. Spectral analysis is performed to determine the cut-off frequency of the designed Zero Phase Low Pass Filter (ZPLP). Using a new gait identification strategy, critical gait events such as Heel Contact (HC), Toe-Off (TO) and Mid-Swing (MSw) are identified and marked along the gait signals. From HC to consecutive HC, gait cycles (GC) are extracted from the time-series gait data. Later, the time of these GCs are normalized from zero to one. For comparison purposes under the same time axis, linear interpolation is performed to map all the time axis of a GC to the same vector length and equal interval. With a pre-defined data structure, these normalized and linear

interpolated GCs are collected and tagged accordingly. The reliability of the customized ambulatory system is checked with test-retest reliability. A mean Cronbach's Alpha above 0.7 suggests that the system is reliable and consistent.

5. To propose a simple presentation of gait data that could provide essential visual aids and guides during the alignments.

Chapter 6 proposes a potential solution that assesses the gait quality via a visual aid and a decision guide. Principle Component Analysis (PCA) is applied to transform correlated variables into uncorrelated variables. Uncorrelated variables are independent to each others, meaning that changes in a variable would not affect others. A visual aid could be plotted in a low dimension plot using the leading principle components. The plot displays clear clusters of the gait performances under different walking restrictions as explained in Chapter 5. Each cluster reveals a distribution with a concentrated centre. A decision guide is generated by applying SOFM with uncorrelated variables. The trained neurons are weighted and would represent each recognized gait cluster. Trained SOFM assists in recognizing the cluster efficiently via a black box operation. The solution is potentially useful for the lower limb prosthetic alignments as well as normal and pathological gait analysis.

7.2 Conclusions

A summary of the conclusions of the project are listed below:

1. A datalogger was built based on a Mbed microcontroller. It is battery-powered and portable. In addition, it has 32 calibrated analog inputs, 1GB storage memory and 200Hz sampling rate.
2. An ambulatory system was developed to collect gait data from five predefined body landmarks at the BCOM, the lateral shanks and the lateral thighs.
3. The notation of the original IMU axes is revised and a new notation according to the body axes is recommended.
4. Several IMU static calibrations i.e. the rotary table method, the 6/12 known positions method and the in-use calibration are revised and compared. These

methods are justified according to some criteria such as cost, the need of test rig, computation time, static or quasi-static assumption and accuracy. It is found that for the general applications, the 6/12 Known Positions method and the simplest IMU model are relatively easy and still produce satisfactory results.

5. The dynamic calibration of an IMU is demonstrated using a pendulous system. A statistical solution to determine the gyroscopic scale factor is less sensitive to the noises created during the derivation.
6. A pendulous system is used to validate the dynamic performance of an IMU. By applying the principle of circular motion, the theoretical models of an IMU are formulated. Low RMS errors between the models and the actual IMU measurements suggest that the IMUs in the study are reliable and consistent.
7. Human gait trials are cross-designed according to two gait restriction factors i.e. the ankle and the walking level.
8. Gait data were collected from three volunteer participants under the predefined experiments.
9. Based on the gait data collected from the normal level walking, a test-retest reliability is performed and the results suggest that the ambulatory system is performing with high consistency and collecting reliable gait data.
10. A series of gait data processing is recommended. An innovative gait identification strategy using the IMU outputs at the shank is recommended. Filtered, normalized and linear-interpolated gait cycles are extracted from the gait data and are recorded in a structural format.
11. Correlated and multidimensional issues in chosen gait variables could be resolved using PCA. Many gait variables are selected from the GCs. PCA transforms these correlated variables into uncorrelated variables. Clear clusters of different gait patterns are seen from a low dimension plot (2D or 3D) using the leading PC axes.
12. Using uncorrelated variables, trained SOFM displays better cluster distribution of different gait patterns collected from the human walking trials.
13. A potential solution that assesses the gait quality via a visual aid and a decision guide is proposed by applying PCA and SOFM. The solution is potentially useful for the lower limb prosthetic alignments as well as normal and pathological gait analysis.

7.3 Future Works

Future research work is recommended to address the following issues:

1. Redesign the ambulatory system as a wireless system that is much lighter, portable, longer operational time and larger storage memory. No cables and wires will be needed between the datalogger and the IMU. This will enhance the product into actual practices.
2. Further justification of temporal and kinetic properties of gait events by installing insole footswitches such as FSR or miniature load cells.
3. Install additional IMUs at the trunk and the head to investigate the balance and the torso responses during walking.
4. Recruit the amputees and collect gait data using the ambulatory system. The experiment criteria should include the alignment parameters as proposed by Zahedi [1] and the effect of the walking level [16]. The involvement of a medical expert is necessary and will enhance the value of the research.
5. Further enhance the visual aids and guides by justifying the multivariate distribution of each cluster. The degree of variation of the clusters in higher dimension might be a good indicator for the alignment effects.
6. Apply multivariate statistic such as MANOVA, factor analysis etc. to identify key gait variables that are most representative for the change of the gait patterns due to alignments.
7. Validate clinically the proposed visual aids and guides using the amputee data in collaboration with medical experts.
8. Validate the proposed visual aids and guides for normal and pathological gait analysis in collaboration with medical experts.

REFERENCES

[1] Zahedi MS, Spence WD, Solomonidis SE, Paul JP. Alignment of lower-limb prostheses. J Rehabil Res Dev. 1986;23:2-19.

[2] Yang L, Solomonidis SE, Paul JP. The influence of limb alignment on the gait of above-knee amputees. J Biomech. 1991;24:981-97.

[3] Isakov E, Mizrahi J, Susak Z, Ona I, Hakim N. Influence of prosthesis alignment on the standing balance of below-knee amputees. Clin Biomech. 1994;9:258-62.

[4] Levy SW. Skin problems of lower extremity amputee. Artificial Limbs. 1956;3:20 - 35.

[5] Chow DHK, Holmes AD, Lee CKL, Sin SW. The effect of prosthesis alignment on the symmetry of gait in subjects with unilateral transtibial amputation. Prosthet Orthot Int. 2006;30:114-28.

[6] Potter BK, Granville RR, Bagg MR, et al. Special Surgical Considerations for the Combat Casualty With Limb Loss In Pasquina PF, Cooper RA (eds.): Care of the Combat Amputee. Washington, US, Office of the Surgeon General at TMM Publications, 2009.

[7] Levy SW. Skin problems in the amputee. In Smith DG, Michael JW, Bowker JH (eds.): Atlas of Amputations and Limb Deficiencies: Surgical, Prosthetic, and Rehabilitation Principles. 3 ed. Rosemont, IL, American Academy of Orthopaedic Surgeons, 2004, pp. 701-10.

[8] Murnaghan JJ, Bowker JH. Musuloskeletal complications. In Smith DG, Michael JW, Bowker JH (eds.): Atlas of Amputations and Limb Deficiencies: Surgical, Prosthetic, and Rehabilitation Principles. 3 ed. Rosemont, IL, American Academy of Orthopaedic Surgeons, 2004, pp. 683-700.

[9] Hannah RE, Morrison JB, Chapman AE. Prostheses alignment: effect on gait of persons with below-knee amputations. Arch Phys Med Rehabil. 1984;65:159-62.

[10] Zahedi MS, Spence WD, Solomonidis SE, Paul JP. Repeatability of kinetic and kinematic measurements in gait studies of the lower limb amputee. Prosthet Orthot Int. 1987;11:55-64.

[11] Breakey JW. Theory of Integrated Balance: The Lower Limb Amputee. Journal of Prosthetics & Orthotics. 1998;10:42-4.

[12] Blumentritt S. A new biomechanical method for determination of static prosthetic alignment. Prosthet Orthot Int. 1997;21:107-13.

[13] Blumentritt S, Schmalz T, Jarasch R, Schneider M. Effects of sagittal plane prosthetic alignment on standing trans-tibial amputee knee loads. Prosthet Orthot Int. 1999;23:231-8.

[14] Hansen AH, Childress DS, Knox EH. Prosthetic foot roll-over shapes with implications for alignment of trans-tibial prostheses. Prosthet Orthot Int. 2000;24:205-15.
[15] Hansen AH, Meier MR, Sam M, Childress DS, Edwards ML. Alignment of trans-tibial prostheses based on roll-over shape principles. Prosthet Orthot Int. 2003;27:89-99.
[16] Sin SW, Chow DH, Cheng JC. Significance of non-level walking on transtibial prosthesis fitting with particular reference to the effects of anterior-posterior alignment. J Rehabil Res Dev. 2001;38:1-6.
[17] Fridman A, Ona I, Isakov E. The influence of prosthetic foot alignment on trans-tibial amputee gait. Prosthet Orthot Int. 2005;27:17-22.
[18] Zahedi MS, Spence WD, Solomonidis SE. The influence of alignment on prosthetic gait. In Murdoch G, Donovan RG (eds.): Amputation Surgery and Lower Limb Prosthetics. Oxford, Blackwell, 1988, pp. 367-78.
[19] Inman VT, Ralston HJ, Todd F. Human Locomotion. In Rose J, Gamble JG (eds.): Human Walking. 3 ed. Philadelphia, USA, Lippincott Williams & Wilkins, 2006, pp. 1-18.
[20] Perry J. Gait analysis : normal and pathological function. Thorofare, N.J.: SLACK inc 1992.
[21] Whittle MW. Gait analysis: an introduction. 3 ed. Edinburgh: Butterworth-Heinemann 2002.
[22] Kirtley C. Clinical Gait Analysis: Theory and Practice. Edinburgh: Elsevier 2006.
[23] Ayyappa E. Normal human locomotion, part1: Basic concepts and terminology. Journal of Prosthetics & Orthotics. 1997;9:10 - 7.
[24] Ayyappa E. Normal human locomotion, part2: Motion, ground reaction force and muscle activity. Journal of Prosthetics & Orthotics. 1997;9:42 - 57.
[25] Winter D. Biomechanics and motor control of human movement. 3 ed. Hoboken, New Jersey: John Wiley & Sons 2005.
[26] Rose J, Gamble JG. Human Walking. 3 ed. Philadelphia, USA: Lippincott Williams & Wilkins 2006.
[27] Winter D. The Biomechanics and Motor Control of Human Gait: Normal, Elderly and Pathological. 2 ed. Waterloo, Canada: University of Waterloo 1991.
[28] Winter D. Biomechanics and motor control of human movement. 4 ed. Hoboken, New Jersey: John Wiley & Sons 2009.
[29] Hibbeler RC. Engineering Mechanics: Statics & Dynamics. 9 ed. New Jersey: Prentice-Hall, Inc. 2000.
[30] Mansfield A, Lyons GM. The use of accelerometry to detect heel contact events for use as a sensor in FES assisted walking. Med Eng Phys. 2003;25:879-85.
[31] Lau H, Tong K. The reliability of using accelerometer and gyroscope for gait event identification on persons with dropped foot. Gait Posture. 2008;27:248-57.
[32] Aminian K, Najafi B, BulaBula C, Leyvraz PF, Robert P. Spatio-temporal parameters of gait measured by an ambulatory system using miniature gyroscopes. J Biomech. 2002;35:689 - 99.
[33] Tong K, Granat MH. A practical gait analysis system using gyroscopes. Med Eng Phys. 1999;21:87-94.

[34] Pappas IPI, Keller T, Mangold S, Popovic MR, Dietz VM, M. A reliable gyroscope-based gait-phase detection sensor embedded in a shoe insole. Sensors Journal, IEEE. 2004;4:268-74.
[35] Kaufman KR, Sutherland DH. Kinematics of Normal Human Walking. In Rose J, Gamble JG (eds.): Human Walking. 3 ed. Philadelphia, USA, Lippincott Williams & Wilkins, 2006, pp. 33-52.
[36] Saunders J, Inman V, Eberhart H. The major determinants in normal and pathological gait. Journal of Bone & Joint Surgery. 1953;35:543–58.
[37] McGeer T. Passive dynamic walking. International Journal of Robotics Research. 1990;9:68-82.
[38] Childress DS, Gard SA. Commentary on the six determinants of gait. In Rose J, Gamble JG (eds.): Human Walking. 3 ed. Philadelphia, USA, Lippincott Williams & Wilkins, 2006, pp. 19-21.
[39] Gard SA, Childress DS. What Determines the Vertical Displacement of the Body During Normal Walking? Journal of Prosthetics & Orthotics. 2001;13:64-7.
[40] Adamczyk PG, Collins SH, Kuo AD. The advantages of a rolling foot in human walking. Journal of Experimental Biology. 2006;209:3953 - 63. .
[41] Hansen AH, Childress DS, Knox EH. Roll-over shapes of human locomotor systems: effects of walking speed Clin Biomech. 2004;19:407-14.
[42] Miff SC, Hansen AH, Childress DS, Gard SA, Meier MR. Roll-over shapes of the able-bodied knee–ankle–foot system during gait initiation, steady-state walking, and gait termination. Gait Posture. 2008;27:316-22.
[43] Hansen AH, Childress DS, Miff SC. Roll-over characteristics of human walking on inclined surfaces. Human Movement Science. 2004;23:807-21.
[44] Kerrigan DC, Croce UD, Marciello M, Riley PO. A refined view of the determinants of gait: Significance of heel rise. Arch Phys Med Rehabil. 2000;81:1077-80.
[45] Kerrigan DC, Riley PO, Lelas JL, Croce UD. Quantification of pelvic rotation as a determinant of gait. Arch Phys Med Rehabil. 2001;82:217-20.
[46] Croce UD, Riley PO, Lelas JL, Kerrigan DC. A refined view of the determinants of gait. Gait Posture. 2001;14:79-84.
[47] Kuo AD. The six determinants of gait and the inverted pendulum analogy: A dynamic walking perspective Human Movement Science. 2007;26:617-56
[48] Donelan JM, Kram R, Kuo AD. Mechanical work for step-to-step transitions is a major determinant of the metabolic cost of human walking. Journal of Experimental Biology. 2002;205:3717 - 27.
[49] Ortega JD, Farley CT. Minimizing center of mass vertical movement increases metabolic cost in walking. Journal of Applied Physiology. 2005;99:2099 - 107.
[50] Gard SA, Childress DS. The effect of pelvic list on the vertical displacement of the trunk during normal walking. Gait Posture. 1997;5:233-8.
[51] Gard SA, Childress DS. The influence of stance phase knee flexion on the vertical displacement of the trunk during normal walking. American Journal of Physical Medicine & Rehabilitation 1999;80:26-32.
[52] Kuo AD, Donelan JM, Ruina A. Energetic consequences of walking like an inverted pendulum: Step-to-step transitions. Exercise and Sport Sciences Reviews. 2005;33:88-97.
[53] Radcliffe CW. Functional Considerations in the Fitting of Above-Knee Prostheses. Artificial Limbs. 1955;2:35-60.

[54] Quigley MJ. Prosthetic Management: Overview, Methods and Materials. In Bowker JH, Michael JW (eds.): Atlas of Limb Prosthetics: Surgical, Prosthetic and Rehabilitation Principles. 2 ed. Rosemont, IL, American Academy of Orthopedic Surgeons, 1992.
[55] Alignment of Modular Leg Prostheses. Otto Bock HealthCare LP, 2008.
[56] Berme N, Purdey CR, Solomonidis SE. Measurement of prosthetic alignment. Prosthet Orthot Int. 1978;2:73-5.
[57] Sin SW, Chow DHK, Cheng JCY. A new alignment jig for quantification and prescription of three-dimensional alignment for the patellar-tendon-bearing trans-tibial prosthesis. Prosthet Orthot Int. 1999;23:225-30.
[58] Radcliffe CW. Mechanical aids for alignment of lower-extremity prostheses. Artificial Limbs. 1954;1:20 - 8.
[59] Radcliffe CW. Above-knee prosthetics. THE KNUD JANSEN LECTURE. 1977.
[60] Geil MD. Variability among Practitioners in Dynamic Observational Alignment of a Transfemoral Prosthesis. Journal of Prosthetics & Orthotics. 2002;14:159-64.
[61] Uellendahl JE. Bilateral lower limb prostheses. In Smith DG, Michael JW, Bowker JH (eds.): Atlas of Amputations and Limb Deficiencies: Surgical, Prosthetic, and Rehabilitation Principles. 3 ed. Rosemont, IL, American Academy of Orthopaedic Surgeons, 2004, pp. 621-31.
[62] Radcliffe CW. Four-bar linkage prosthetic knee mechanisms: kinematics, alignment and prescription criteria. Prosthet Orthot Int. 1994;18:159-73.
[63] Evans MJ, Evans JH. A new method for the measurement of prosthetic alignment. Proceedings of the International Conference on Biomedical Engineering, Hong Kong. 1994:410-1.
[64] Staros A. Dynamic Alignment of Artificial Legs with the Adjustable Coupling. Artificial Limbs. 1963;7:31-42.
[65] Foort J, Hobson DA. The wedge disc alignment unit. Report of the prosthetics and orthotics research and development unit. Canada, Manitoba Rehabilitation Hospital, 1964.
[66] Schuch CM. Dynamic Alignment Options for the Flex-Foot(TM). Journal of Prosthetics & Orthotics. 1989;1:37-40.
[67] Kohpler P, Lind L, Lind K, Rennerfeldt G, Kreicbergs A. A new in-built device for one-point stepless prosthetic alignment. Prosthet Orthot Int. 1988;12:103-4.
[68] Winter D. Kinematic and kinetic patterns in human gait: Variability and compensating effects Human Movement Science. 1984;3:51-76
[69] Saleh M. Alignment and gait optimization in lower limb amputees. In Murdoch G, Donovan RG (eds.): Amputation Surgery and Lower Limb Prosthetics. Oxford, Blackwell, 1988, pp. 357-66.
[70] Geil MD, Lay A. Plantar foot pressure responses to changes during dynamic trans-tibial prosthetic alignment in a clinical setting Prosthet Orthot Int. 2004;28:105-14.
[71] Radcliffe CW, Foort J. The Patellar-tendon-bearing below-knee prosthesis. 1961.
[72] Moe-Nilssen R. Test-retest reliability of trunk accelerometry during standing and walking. Arch Phys Med Rehabil. 1998;79:1377-85.
[73] Moe-Nilssen R, Helbostad JL. Trunk accelerometry as a measure of balance control during quiet standing. Gait Posture. 2002;16:60-8.

[74] Auvinet B, Berrut G, Touzard C, et al. Reference data for normal subjects obtained with an accelerometric device. Gait Posture. 2002;16:124-34.
[75] Luinge diHJ, Veltink PdiPH. Inclination Measurement of Human Movement Using a 3-D Accelerometer With Autocalibration. IEEE Transactions on Neural Systems and Rehabilitation Engineering. 2004;12:112-21.
[76] Henriksen M, Lund H, Moe-Nilssen R, Bliddal H, Danneskiod-Samsøe B. Test-retest reliability of trunk accelerometric gait analysis. Gait Posture. 2004;19:288-97.
[77] Luinge HJ, Veltink PH. Measuring orientation of human body segments using miniature gyroscopes and accelerometers. Medical & Biological Engineering & Computing. 2005;43.
[78] Jasiewicz JM, Allum JHJ, Middleton JW, et al. Gait event detection using linear accelerometers or angular velocity transducers in able-bodied and spinal-cord injured individuals. Gait Posture. 2006;24:502-9
[79] Torrealba RR, Cappelletto J, Fermin-Leon L, Grieco JC, Fernandex-Lopez G. Statistics-based technique for automated detection of gait events from accelerometer signals. Electronics Letters. 2010;46:1483–5
[80] Takeda R, Tadano S, Todoh M, Morikawa M, Nakayasu M, Yoshinari S. Gait analysis using gravitational acceleration measured by wearable sensors. J Biomech. 2009;42:223-33.
[81] González RC, López AM, Rodriguez-Uría J, Álvarez D, Alvarez JC. Real-time gait event detection for normal subjects from lower trunk accelerations. Gait Posture. 2010;31:322-5.
[82] Gouwanda D, Senanayake SMNA. Identifying gait asymmetry using gyroscopes—A cross-correlation and Normalized Symmetry Index approach. J Biomech. 2011;44:972-8.
[83] Rueterbories J, Spaich EG, Larsen B, Andersen OK. Methods for gait event detection and analysis in ambulatory systems. Med Eng Phys. 2010;32:545-52.
[84] Lötters JC, Schippe J, Veltink PH, Olthuis W, Bergveld P. Procedure for in-use calibration of triaxial accelerometers in medical applications. Sensors and Actuators A: Physical. 1998;68:221-8.
[85] Titterton DH, Weston JL. Strapdown Inertial Navigation Technology. 2 ed, Institution of Engineering and Technology 2004.
[86] Grewal MS, Weill LR, Andrews AP. Global Positioning Systems, Inertial Navigation, and Integration 2ed. New Jersey: John Wiley & Sons 2007.
[87] ADXL330. Accelerometers: Small, Low power, 3-axis ±3g. Analog Device, Inc., 2006.
[88] ADXL335. Accelerometers: Small, Low power, 3-axis ±3g. Analog Devices, Inc. , 2009.
[89] IDG300. Integrated Dual-Axis Gyro. InvenSense, Inc., 2006.
[90] IDG-500. Integrated Dual-Axis Gyro. InvenSense, Inc., 2008.
[91] Fisher CJ. AN-1057: Using an Accelerometer for inclination sensing. In Analog Device I (ed.). Rev 0 ed, 2010.
[92] Rotary Table, 4" H/V. http://littlemachineshop.com/products/product_view.php?ProductID=1927&category=.
[93] Skog I, Handel P. Calibration of a MEMS Inertial Measurement Unit. XVII IMEKO WORLD CONGRESS, Metrology for a Sustainable Development, September, 17-22, 2006 Rio de Janeiro, Brazil, 2006.

[94] Britting KR. Inertial Navigation Systems Analysis: Wiley-Interscience 1971.
[95] Strang G. Introduction to Linear Algebra. 4 ed: Wellesley-Cambridge Press 2009.
[96] Hung JC, Thacher JR, White HV. Calibration of accelerometer triad of an IMU with drifting Z -accelerometer bias. Aerospace and Electronics Conference, 1989 NAECON 1989, Proceedings of the IEEE 1989 National. 1989;1:153 - 8.
[97] Venkataraman P. Applied Optimization with MATLAB Programming. 2 ed. New Jersey: John Wiley & Sons, Inc. 2009.
[98] Matlab. ver.7.9.0.529 [R2009b] ed, The Mathworks, 2009.
[99] Field A. Discovering Statistics Using SPSS. 3 ed. London, UK: Sage Publications Ltd 2009.
[100] Torrealba RR, Castellano JM, Fernandex-Lopez G, Grieco JC. Characterisation of gait cycle from accelerometer data. Electronics Letters. 2007;43:1066-8.
[101] Kavanagh JJ, Menz HB. Accelerometry: A technique for quantifying movement patterns during walking. Gait Posture. 2008;28:1-15.
[102] Manly BFJ. Multivariate statistical methods: a primer. 3 ed. London, UK: Chapman & Hall 2005.
[103] Kohenen T. Self-Organizing Maps. Heidelberg: Springer 1997.
[104] Hagan MT, Demuth HB, Beale M. Neural Network Design. Boston: PWS Publishing Company 1996.
[105] Winter D. Motor patterns in amputee gait: motor adaptions and implications for redesign. Biomedical Engineering, Proceedings of a Special Symposium on Maturing Technologies and Emerging Horizons in. 1988:18-9.

APPENDIX A

Datalogger

The datalogger consists of a microcontroller, analog inputs, data storage, LCD display, a battery, power regulator and connecting cables and ports. Technical information regarding the Mbed microcontroller, Serial Peripheral Interface (SPI), Analog-to-Digital converters and the secure digital (SD) card are presented here.

1.1 Microcontroller

The core of the datalogger is a Mbed microcontroller (Figure 1), NXP LPC1768 with an ARM Cortex-M3 Core running at 96MHz, 512KB flash memory, 64KB RAM and lots of interfaces including Ethernet, USB Device and Host, CAN, SPI, I2C and other I/O. It comes in a small and practical DIP package. It features as a rapid prototyping tool for microcontroller and the supplier (Mbed, http://mbed.org/) offers great online supports on ready to use libraries and various application examples.

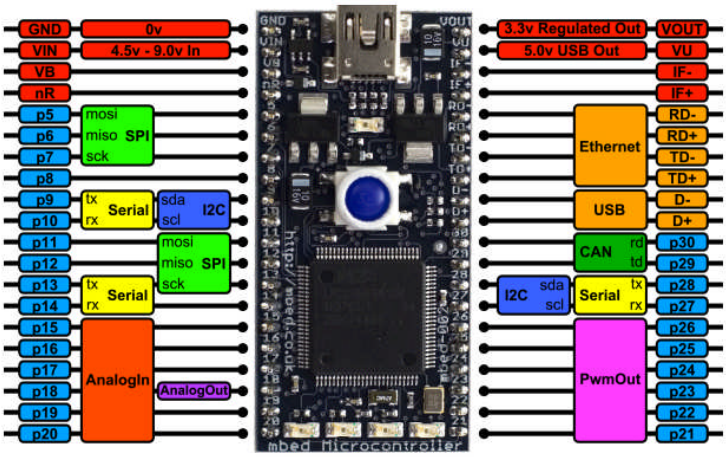

Figure 1: Mbed microcontroller and pin outs descriptions.
(Adopted from http://mbed.org/)

1.2 Serial Peripheral Interface

The datalogger implements serial peripheral interface (SPI) bus to expand the analog input channels and to address a SD card as the data storage. The working principle of the SPI bus is explained as follows. The serial peripheral interface (SPI)[1] is a bidirectional master-slave synchronous interface that is based on an 8-bit shift register. The SPI master generates a baud clock signal that is used by all SPI devices to synchronize full duplex data transmission between the master and its slaves. SPI requires four signals between a master and a slave. These signals are serial clock (SCLK), data signal Master Out Slave In (MOSI), data signal Master In Slave Out (MISO) and Slave Select (SS). A typical SPI structure is shown in Figure 2. The number of slaves could be cascaded as long as the master has sufficient pin outs assigned as SS but at the cost of decreasing sampling rate. In this research, two SPI buses are assigned separately from the same microcontroller (master A and master B) to address four SPI A/D converters (Slave 1A to Slave 4A) and a SD card (Slave 1B).

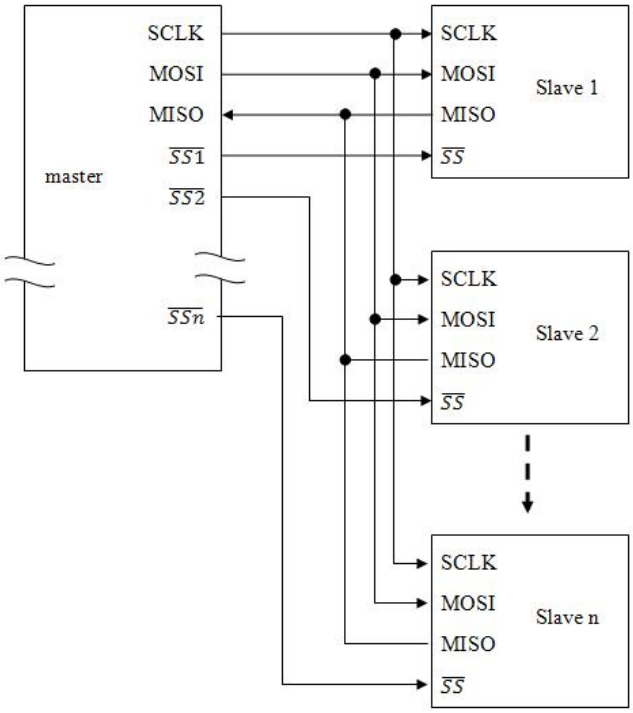

Figure 2: SPI structure

[1] *Barr M, Massa A. Programming embedded systems: with C and GNU development tools. USA: O'Reilly Media, Inc. 2007.*

1.3 Analog-to-Digital converters

Eight channels 10-bits Analog-to-Digital (A/D) converters (MCP3008, Microchip) with SPI bus are used to expand the analog input channels. The pin out assignment of MCP3008 is shown in Figure 3. Detail specification of MCP3008 could be downloaded online. The connection of four units of MCP3008 (named as Slave 1A to Slave 4A) to a Mbed microcontroller via a SPI bus is shown in Figure 4. They share the SPI bus with separated Slave Select (SS) inputs ($\overline{SS1}$ to $\overline{SS4}$). They are cascaded to expand into a maximum of 32 analog input channels. The actual number of active analog input channels could be decided through the program. The SPI expanded analog input channels are assigned as shown in Figure 5. The labels of the pin outs will be used through the design and the program.

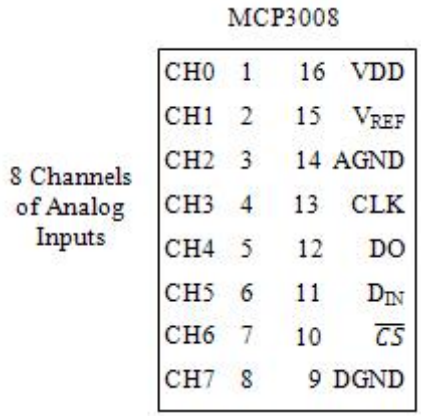

Figure 3: Pin out assignment of MCP3008

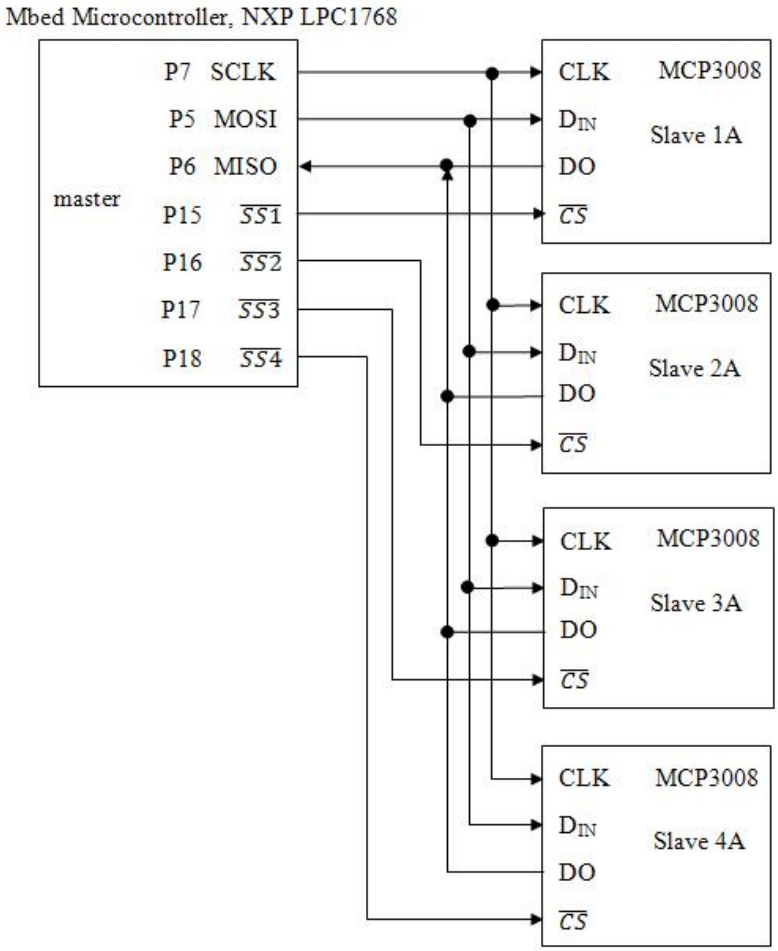

Figure 4: SPI connection between MCP3008 and the Mbed microcontroller

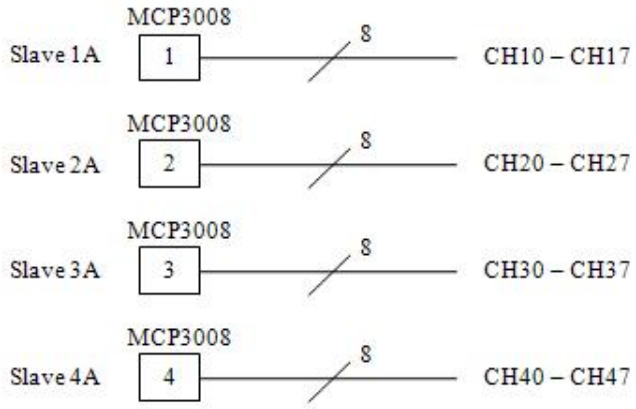

Figure 5: Pin outs of the analog input channels

1.4 Secure Digital Card

A SD card is a popular option for data storage in an embedded system. A SD card of 1GB storage size and a socket in PCB breakout (SparkFun Inc.) as shown in Figure 6 are used in this application. The storage is sufficient for this application. The

stored files are in the format of comma-separated values (CSV) file. The SD card and its socket (named as Slave 1B) as shown in Figure 7 are connected to the Mbed microcontroller via a new SPI bus and a SS output.

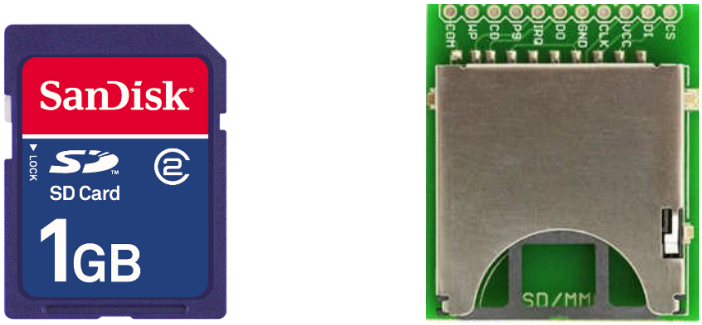

(a) (b)

Figure 6: (a) SD card (b) SD socket

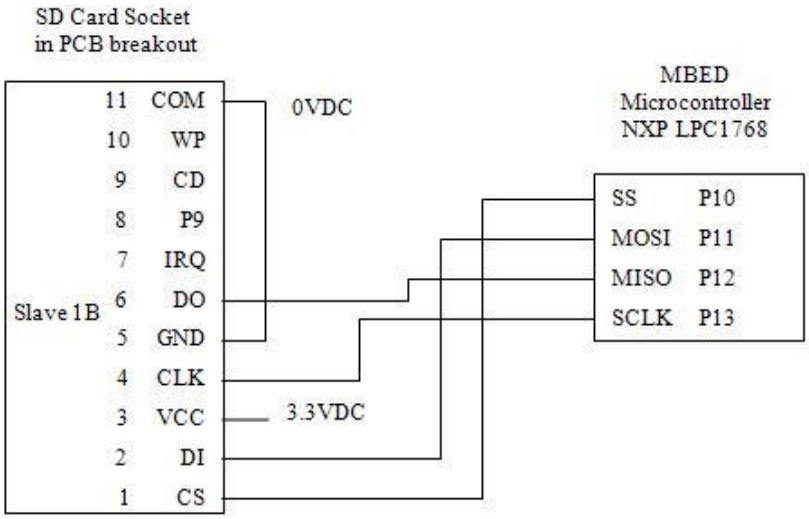

Figure 7: SPI connection between a SD card socket and a Mbed microcontroller

APPENDIX B

MDED C Program for the Datalogger

```
// Program: datalogger_SD_MCPx4_ver1
//scanning 4xMCP3008 and write all inputs channels into file in SD
//SD transfer rate set at 2MHz
//for testing purpose, all inputs channels are pulled high (3.3VDC)
//See circuitry drawing for detail IO assignments
//*****************************************************************

#include "mbed.h"
#include "SDFileSystem.h"
#include "TextLCD.h"

//assign SD IO pins
SDFileSystem sd(p11, p12, p13, p10, "sd");
// rs, rw, e, d0, d1, d2, d3
TextLCD lcd(p24, p25, p26, p27, p28, p29, p30);
DigitalOut led1(LED1);
DigitalOut led2(LED2);
DigitalOut led_button(LED3);
DigitalOut led4(LED4);
DigitalOut led5(p21);
DigitalIn button(p9);
SPI _spi(p5,p6,p7);     //mosi, miso, sck
Timer t;
DigitalOut cs1(p15);     //1st MCP3008 chip select
DigitalOut cs2(p16);     //2nd MCP3008 chip select
DigitalOut cs3(p17);     //3rd MCP3008 chip select
DigitalOut cs4(p18);     //4th MCP3008 chip select

//************************************************
//subroutine to delay input button
//avoid bouncing effect
//not used. Spare

int button_delay(bool b) {
    bool c = false;
    if (b==true) {
        wait(.01);
        c=true;
    } else {
        c=false;
    }
    return c;
}

//subroutine - 1st MCP3008
int MCP_read1(int add) {
    int _data1;
    int _data2;
    cs1=0;
    _spi.write(0x01);
    _data1=_spi.write(add);
    _data2=_spi.write(0x00);
    int ch =(_data1<<8) | _data2;
    ch = ch & 0x03FF;
    cs1=1;
    return ch;
}
```

```
//subroutine - 2nd MCP3008
int MCP_read2(int add) {
    int _data1;
    int _data2;
    cs2=0;
    _spi.write(0x01);
    _data1=_spi.write(add);
    _data2=_spi.write(0x00);
    int ch =(_data1<<8) | _data2;
    ch = ch & 0x03FF;
    cs2=1;
    return ch;
}

//subroutine - 3rd MCP3008
int MCP_read3(int add) {
    int _data1;
    int _data2;
    cs3=0;
    _spi.write(0x01);
    _data1=_spi.write(add);
    _data2=_spi.write(0x00);
    int ch =(_data1<<8) | _data2;
    ch = ch & 0x03FF;
    cs3=1;
    return ch;
}

//subroutine - 4th MCP3008
int MCP_read4(int add) {
    int _data1;
    int _data2;
    cs4=0;
    _spi.write(0x01);
    _data1=_spi.write(add);
    _data2=_spi.write(0x00);
    int ch =(_data1<<8) | _data2;
    ch = ch & 0x03FF;
    cs4=1;
    return ch;
}


//*******************************************************
//main program


char next_file[20];
long loop;
bool st_pb_off;
bool st_pb_on;
int count=1; //initial is 1
float elapse_time;


int main() {
//deselect everything by raise all chip select high

    cs1=1;
    cs2=1;
    cs3=1;
```

```
    cs4=1;

    _spi.format(8,0);           //Set     SPI     transfer     bits
    _spi.frequency(1000000);    //set  SPI  frequency  for  MCP3008


    while (1) {

        if (button==false and st_pb_off==false) {

            //LCD display message when button off

            led_button=0;
            led5=0;
            lcd.locate(0,0);
            lcd.printf("%.8d, %.4f ", loop, elapse_time);
            lcd.locate(0,1);
            lcd.printf("it is %d", count);

            sprintf(next_file, "/sd/temp%d.csv", count);
            count+=1;
            t.reset();
            loop=0;
            elapse_time=0;

            //pb_off status. this rung runs only once        powered
            st_pb_on=false;     //pb_on status.
            st_pb_off=true;             }


//*****************************************************************
//    MCP3008 clock sequence and control bits
//Once cs low, send start bit ==> 0x01  Not expecting any return
//next, send control bits   Expecting return bit9, bit8
//next, send anything, say 0x00, expecting return bit7-bit0
//next shift bit9,bit8 left 8bits
//next merge bit9,bit8 and bit7-bit0 to form 16bits data      (word)
//next, mask off bit15-bit10, to get a clean 10 bit data
//*****************************************************************

//****************** Send registers for MCP3008 ******************
//      1st 8bits         2nd 8bits           3rd 8bits
//ch0      0x01              0x80                0x00
//ch1      0x01              0x90                0x00
//ch2      0x01              0xA0                0x00
//ch3      0x01              0xB0                0x00
//ch4      0x01              0xC0                0x00
//ch5      0x01              0xD0                0x00
//ch6      0x01              0xE0                0x00
//ch7      0x01              0xF0                0x00
//*****************************************************************
**


        if (button==true and st_pb_on==false) {
            //flip while data acquired
            led_button = 1;
           led5=1;

            //open a file to write when button ON
            t.start();
```

```
            FILE *fp = fopen(next_file, "w");
            while (button) {

                loop++;
//ch10 to CH17

                int ch10=MCP_read1(0x80);
                int ch11=MCP_read1(0x90);
                int ch12=MCP_read1(0xA0);
                int ch13=MCP_read1(0xB0);
                int ch14=MCP_read1(0xC0);
                int ch15=MCP_read1(0xD0);
                int ch16=MCP_read1(0xE0);
                int ch17=MCP_read1(0xF0);
 //ch20 to CH27
                int ch20=MCP_read2(0x80);
                int ch21=MCP_read2(0x90);
                int ch22=MCP_read2(0xA0);
                int ch23=MCP_read2(0xB0);
                int ch24=MCP_read2(0xC0);
                int ch25=MCP_read2(0xD0);
                int ch26=MCP_read2(0xE0);
                int ch27=MCP_read2(0xF0);
//ch30 to CH37
                int ch30=MCP_read3(0x80);
                int ch31=MCP_read3(0x90);
                int ch32=MCP_read3(0xA0);
                int ch33=MCP_read3(0xB0);
                int ch34=MCP_read3(0xC0);
                int ch35=MCP_read3(0xD0);
                int ch36=MCP_read3(0xE0);
                int ch37=MCP_read3(0xF0);
 //ch40                                                          only
                int ch40=MCP_read4(0x80);

/*    spare: since only 25 analogue inputs are needed.

                int ch41=MCP_read4(0x90);
                int ch42=MCP_read4(0xA0);
                int ch43=MCP_read4(0xB0);
                int ch44=MCP_read4(0xC0);
                int ch45=MCP_read4(0xD0);
                int ch46=MCP_read4(0xE0);
                int ch47=MCP_read4(0xF0);
                fprintf(fp,"%d,%d,%d,%d,%d,%d,%d,%d,%d,%d,%d,%d,%d,
%d,%d,%d,%d,%d,%d,%d,%d,%d,%d,%d,%d,%d,%d,%d,%d,%d,%d,%d,%d\n",ch10,ch
11,ch12,ch13,ch14,ch15,ch16,ch17,ch20,ch21,ch22,ch23,ch24,ch25,ch26
,ch27,ch30,ch31,ch32,ch33,ch34,ch35,ch36,ch37,ch40,ch41,ch42,ch43,c
h44,ch45,ch46,ch47);
*/
                fprintf(fp,"%d,%d,%d,%d,%d,%d,%d,%d,%d,%d,%d,%d,%d,
%d,%d,%d,%d,%d,%d,%d,%d,%d,%d,%d,%d,%d\n",ch10,ch11,ch12,ch13,ch14,ch1
5,ch16,ch17,ch20,ch21,ch22,ch23,ch24,ch25,ch26,ch27,ch30,ch31,ch32,
ch33,ch34,ch35,ch36,ch37,ch40);

                wait (.003);  // delay to adjust the sampling rate

            }
//write total loops and time for average frequency calculation
            elapse_time=t.read();
            fprintf(fp,"%.8d, %.4f ",loop,elapse_time);
```

```
            fclose(fp);          //close the file when button OFF
            t.stop();
            st_pb_on=true;
            st_pb_off=false;


        }
    }

}
```

APPENDIX C

Documentation for Human Gait Trials

Information Sheet

Research Project Title: Gait patterns at body centre of mass (BCOM) in level and non-level walking under the constraint of multiple ankle angles

Dear Reader,

You are being invited to take part in a research project. Before you decide it is important for you to understand why the research is being done and what it will involve. Please take time to read the following information carefully and discuss it with others if you wish. Ask us if there is anything that is not clear or if you would like more information. Take time to decide whether or not you wish to take part. Thank you for reading this.

What is the project's purpose?

For amputees, practically, lower limb alignment is time consuming and subjective, i.e. it is dependant to the experience of the prosthetists and feedbacks from the amputees. Alignment settings differ from one prosthetist to another. Researchers believe that there is an optimum alignment for each amputee. To date, researchers are not in agreement in an objective yet efficient analytical method to optimize lower limb prosthetic alignment. Alignment is vital to give gait function and comfort for amputees. The aims of the study include:

- to study the gait patterns in level and non-level walking under the constraint of multiple ankle angles.
  The author hypothesises that Body Centre of Mass (BCOM, at waist) gait pattern is a key indicator for optimal gait assessment.

- to propose a solution to optimize the alignment of lower limb prosthetic device.
  The solution could possibly provide an objective aid to the prosthetists during prosthetic alignment.

- to testify and justify if a novel lower limb prosthetic alignment system work.

The author has designed and developed a system for this purpose. The main purpose of this preliminary study is to establish whether or not useful information for lower limb prosthetic alignment can be collected from an analysis of gait data. Meaningful gait information will be used to testify and justify a novel lower limb prosthetic alignment system.

Subjects without walking disability from the School of Mechanical Engineering are invited for the trials. The trials will be conducted in one of the laboratories in School of Mechanical Engineering.

The study will be for two months long [mid-June until mid-August]

.

Why have I been chosen?

You have volunteered for the research and you have met the health requirements.

Do I have to take part?

It is up to you to decide whether or not to take part. If you do decide to take part you will be given this information sheet to keep (and be asked to sign a consent form) and you can still withdraw at any time without it affecting any benefits that you are entitled to in any way. You do not have to give a reason.

What will happen to me if I take part?

You are going to be asked to attend an appointed session in the School of Mechanical Engineering. The session will last approximately two hours. Before the experiment starts, your bio-data such as body weight, height, age and gender will be recorded. You will wear a portable, battery-powered and light weight gait monitoring system under the assistance of the main investigator. A number of gait measurement sensors called Inertial Measurement Units (IMUs), will be positioned at the waist, both thighs, and shanks by using Velcro straps. Once you have put on the system, you are asked to walk freely but carefully to familiarize with the new suit in order to mitigate the risk of stumbling. When you are ready, the trial will be commenced. You are required to walk in three different self-selected walking speeds, i.e. slow, normal and fast, for every new constraints. Ankle angles are measured with a goniometer. The angles are adjusted by inserting light weight wooded spacers under the shoes, bound to the foot by using Velcro straps. The trials will be repeated under these constraints on a flat walkway:

1. Neutral ankle (flat bottom shoe)
2. Heel raise (at 5^0)
3. Heel raise (at 10^0)
4. Forefoot raise (at 5^0)
5. Forefoot raise (at 10^0)

Next, you are asked to repeat the trials on a 10^0 tilted walkway under the same constraints. The trial will be repeated for both incline and decline.

What do I have to do?

You will be putting on a portable gait monitoring system and sensors at pre-designated body landmarks. These devices are battery-powered. You are required to walk with these devices in a short distance repetitively.

What are the possible disadvantages and risks of taking part?

The use of low voltage battery-powered electrical sensors means there is no risk in terms of electric shocks in this investigation. There is a minor risk of stumbling because of new suit and new walking environment but this is mitigated by becoming familiar with the walkway before the experiment.

What are the possible benefits of taking part?

Whilst there are no immediate benefits for those people participating in the project, it is hoped the outcome of the research might benefit the amputees and the prosthetists in the process of lower limb prosthetic alignments.

What happens if the research study stops earlier than expected?

We do not expect the research study stops for any reason as the period of study is very short. However, we might ask you to participate in some and not all of the sessions, if we think that we have collected enough data for the other experiments.

Will my taking part in this project be kept confidential?

All the information that we collect about you during the course of the research will be kept strictly confidential. You will not be identified in any reports or publications.

What type of information will be sought from me and why is the collection of this information relevant for achieving the research project's objectives?

The information that will be gathered about you is your height, weight, age, gender, health status and gait data. The information will only be used during data analysis for statistical purpose.

What will happen to the results of the research project?

The research outcomes will be used to testify and justify a novel lower limb prosthetic alignment system. In addition, the data gathered might be useful for additional research work.

All results will be published in two years time in medical, bioengineering and engineering conferences and journal papers. However, in all our future publication, you are not going to be identified.

Will I be recorded, and how will the recorded media be used?

The audio and/or video recordings of your activities made during this research will be made anonymous by covering the face and will be used only for analysis and for illustration in conference presentations and lectures. No other use will be made of them without your written permission, and no one outside the project will be allowed access to the original recordings.

Who is organising and funding the research?

The research is not funded.

Contact for further information

For further information please contact:
Kian Sek TEE
University of Leeds, School of Mechanical Engineering, Room G52, LS2 9JT
Mobile No. 07527896457

Dr. Abbas A. Dehghani-Sanij
University of Leeds, School of Mechanical Engineering, Room 4.48, LS2 9JT
Tel No. 0113 343 32906

Please keep this information sheet and if you are willing to take place in this project, please sign the consent form.

Many thanks for your time to read this information sheet. If you are going to take part in this project, many thanks for your participation

Participant Consent Form

Title of Research Project:
Gait pattern analysis at body centre of mass (BCOM) in level and non-level walking under the constraint of multiple ankle angles

Name of Researcher: Kian Sek TEE

Please initial box

1. I confirm that I have read and understand the instrument sheet, especially the section of safety information. ☐

2. I understand that my participation is voluntary and that I am free to withdraw at any time without giving any reason and without there being any negative consequences. In addition, should I not wish to answer any particular question or questions, I am free to decline. ☐

3. I understand that my responses will be kept confidential.
I give permission for members of the research team to have access to my anonymised responses. I understand that my name will not be linked with the research materials, and I will not be identified or identifiable in the report or reports that result from the research. ☐

4. I agree for the data collected from me to be used in future subsequent research. ☐

5. I agree to take part in the above research project. ☐

6. I have had the opportunity to ask any questions I have regarding the research. ☐

_____	_____	_____
Name of Participant (*or legal representative*)	Date	Signature
_____	_____	_____
Lead Researcher	Date	Signature

To be signed and dated in presence of the participant

Copies:
Once this has been signed by all parties the participant should receive a copy of the signed and dated participant consent form, the letter/pre-written script/information sheet and any other written information provided to the participants. A copy of the signed and dated consent form should be kept with the project's main documents which must be kept in a secure location.

Agreement to Photographic and Video Records

I agree that the photographic images (where your identity will not be shown through face blackout) taken during this experiment (Gait analysis using a portable gait monitoring system: feasibility, acceptability and initial results) may be used for the following purposes (please circle all that apply):

a) Can be used in publications
(i.e. journals, conference paper, thesis which are the part of this PhD)

b) Can be used in a presentation
(i.e. conferences and societies)

c) Can be used for educational purposes (i.e. lectures)

d) All of the above

If in the future you wish to change your mind, you have the right to do so at any time by contacting the main investigator [Mr. Kian Sek Tee].

Name of Participant	Date	Signature
Main Investigator	Date	Signature

To be signed and dated in presence of the participant

Research Support
3 Cavendish Road
University of Leeds
Leeds LS2 9JT

Tel: 0113 343 4873
e-mail: j.m.blaikie@adm.leeds.ac.uk

MEEC Faculty Research Ethics Committee
University of Leeds

21 May 2010

Kian Sek Tee
Room G52
Advanced Mechatronics Lab
School of Mechanical Engineering
University of Leeds

Dear Kian Sek Tee

Title of study:	**Gait pattern analysis at body centre of mass (BCOM) in level and non-level walking under the constraint of multiple ankle angles**
Ethics reference number:	**MEEC 09-022**
Amendment Number:	**1**
Amendment Date:	**06/05/10**
Amendment description	**Further clarification/ explanations**

The above amendment was reviewed by the MEEC Faculty Research Ethics Committee at its meeting of 20th May 2010.

The following documentation was considered:

Document	*Version*	*Date*
MEEC 09-022 Committee Provisional_100419_reply_100506.doc	1	06/05/10
MEEC 09-022 Ethical Review Form KSTee_100128_ver4.doc	1	06/05/10

On the basis of the information provided, the Committee is happy to approve this project with the following condition and advice.

1. The Committee felt that the revised information sheet did not contain sufficient information and requests that sufficient detail, in lay terms, is added. In particular the section 'what is the purpose of the project' and "what will happen to me if I take part' need to be rewritten in sufficient detail and a manner understandable by a lay person. For example, the section on the project's purpose should give details of the background, aim and duration of the project.

2. Committee members also felt that the information was not very clear for the man in the street, but recognised that if participants are mechanical engineering students they will be sufficiently familiar with this type of research. Perhaps the issue could be resolved

by adding something along the lines of *"I have had the opportunity to ask any questions I have regarding the research"* to the consent form so that if people need further clarification it is clear to them that they can ask for it.

Please could you provide a copy of the amended information sheet for our records.

Yours sincerely

JBlaikie

Jennifer Blaikie
Research Ethics Administrator
Research Support
On Behalf of
Professor Richard Hall
Chair, MEEC FREC.

APPENDIX D
List of Publications

1. K. S. Tee, M. Awad, A. Dehghani, D. Moser, and S. Zahedi, "Comparison of Two Static Calibration Methods of an Inertial Measurement Unit," in *The Eighth IASTED International Conference on Biomedical Engineering, February 16 – 18*, Innsbruck, Austria, 2011.
2. K. S. Tee, M. Awad, A. Dehghani, D. Moser, and S. Zahedi, "Triaxial Accelerometer Static Calibration," in *The 2011 International Conference of Mechanical Engineering, July 6-8*, London, UK, 2011.
3. K. S. Tee, M. Awad, A. Dehghani, D. Moser, and S. Zahedi, "A portable gait monitoring system for lower limb prosthetic alignment," in *The 2011 International Conference of Mechanical Engineering, July 6-8*, London, UK, 2011.
4. K. S. Tee, M. Awad, A. Dehghani, D. Moser, and S. Zahedi, "Dynamic calibration of a gyroscope using a compound pendulum," in *The 14th International Conference on Climbing and Walking Robots and the Support Technologies for Mobile Machines (CLAWAR2011), September 6-8*, Paris, France, 2011.
5. *Preparation.* K. S. Tee, A. Dehghani, D. Moser, and S. Zahedi, "A Visual Guide for Lower Limb Prosthetic Alignment," *Gait and Posture*.